RESIDUAL STRESS IN ALL CERAMIC ZIRCONIA-PORCELAIN DENTAL SYSTEM BY SIMULATION AND NANOINDENTATION

By

YANLI ZHANG

Bachelor of Science in Mechanical Engineering
Technology
Oklahoma State University
Stillwater, OK
December, 2004

Master of Science in Mechanical Engineering
Oklahoma State University
Stillwater, OK
May, 2007

Submitted to the Faculty of the
Graduate College of the
Oklahoma State University
in partial fulfillment of
the requirements for
the Degree of
DOCTOR OF PHILOSOPHY
July, 2012

RESIDUAL STRESS IN ALL CERAMIC ZIRCONIA-PORCELAIN DENTAL SYSTEM BY SIMULATION AND NANOINDENTATION

Dissertation Approved:

Dr. Jay C. Hanan

Dissertation Adviser

Dr. Sandip P. Harimkar

Dr. A. Kaan Kalkan

Dr. James E. Smay

Dr. Sheryl Tucker

Dean of the Graduate College

TABLE OF CONTENTS

LIST OF TABLES

LIST OF FIGURES

Figure Page

Figure Page

Figure Page

Figure Page

CHAPTER I

1 INTRODUCTION

All-ceramic dental crowns have become increasingly popular over the past two decades due to better aesthetics and biocompatibility than crowns with metal core structure (Denry and Kelly, 2009). Yttria partially stabilized tetragonal zirconia polycrystalline(Y-TZP) based frameworks have exceeded alumina based crowns as a better choice in recent years because of higher strength and toughness. However, in the past several years, the reported failure rate of all-ceramic crowns is much larger than the crowns with metal core structure (Larsson et al., 2006; Raigrodski, 2006; Von, 2005; Von et al., 2005). The reason for the failure and its mechanism has not been fully understood because of challenges associated with the complex geometry and firing procedure used to manufacture dental crowns. One Hypothesis is that residual stress formed during manufacturing affected the failure. The source of residual stress could be from mismatch of coefficient of thermal expansion (CTE) between the core and the veneered materials, thermal tempering, grain anisotropy, polishing, and others. So far, there is not a mature method to measure residual stress in crowns and no work has been published to predict the residual stress of zirconia-porcelain crowns due to the effects of both mismatch of CTE and thermal tempering with 3D model. This work will concentrate on analyzing residual stress in zirconia-porcelain frameworks formed due to concentrate

on analyzing residual stress in zirconia-porcelain frameworks formed due to both mismatch of CTE and thermal tempering using a two-dimensional (2D) analytical model, three-dimensional (3D) finite element simulation, and nanoindentation measuring technique. Different design options are also compared to reduce residual stress. Furthermore, manufacture and processing flaws could also be the origin of crown failures. Microstructure and flaw distribution was examined with micro X-Ray computed tomography (μCT) and secondary electron microscope (SEM) imaging. Detailed procedures are described in chapter III to chapter VII.

To be familiar with the background of this work, Chapter II generally reviews the history of dental crowns, the current technology in terms of materials and the challenges that face us today. Detailed literature review is presented in the chapter where specific characterization techniques are used.

To get a perspective of the problem, first in Chapter III the residual stress developed at different tempering rates for two framework systems with different porcelain and zirconia thickness was analyzed using a 2D bilayer model. The effects of tempering rate and porcelain thickness were examined. A 2D model allows researchers to study the impact of the core parameters, though limited when predicting the residual stress in 3D, especially for such complex 3D geometries as found in dental crowns. Predicting residual stress in 3D for complex geometry is very challenging due to lack of analytical models. 3D finite element analysis is carried out to predict 3D stress distribution in crowns. The details are in chapter VI. A detailed 3D dental crown model, formed from μCT scan data is used to simulate the residual stress developed at different tempering rates. The goal was to observe how tempering rates affect residual stress

magnitude and distribution, and whether the effects were correlated with other factor effects, such as porcelain thickness effect. Simulation results were also used to compare with nanoindentation experiment results in chapter IV.

Because 2D flat samples are not able to capture all the behavior of 3D crowns, measurement on 3D samples is desperately needed. Chapter IV discusses a nanoindentation technique used to measure residual stress. Measurements were carried out at different location along the cross section of a clinically relevant crown. X-ray diffraction (XRD) was used to validate the measurement on zirconia.

Manufacture and processing flaw is also an important factor contributing to crown failures. Chapter V describes a procedure to evaluate flaws formed in dental crowns using laboratory scale μCT scanned data. Flaws in three crowns formed at different cooling rates were examined and the relation between flaws and fracture strength was also studied.

Chapter VII explores the option to modify designs of crowns based on a simple shape that is similar to the shape of the crown cusp. The results from the simple shape and a detailed crown were compared. Three different cusp designs were compared for residual stress and stress distribution under loading.

Chapter VIII discusses the findings of this work and future work.

CHAPTER II

2 BACKGROUND

2.1 Historic perspectives

Dental restorative technology existed as early as 700 BC, but remained literally undeveloped until the eighteenth century. During the 18th century, the most used artificial teeth materials were: human teeth, animal teeth carved to the size and shape of human teeth, ivory and porcelain teeth (Kelley *et al*., 1996). The development of porcelain dentures helped to end the use of human and animal teeth. About 1774, a Parisian apothecary, Alexis Duchateau, with the assistance of a Parisian dentist, Nicholos Dubois de Chemant, made the first successful porcelain denture (Ring 1985; Jones 1985). Translucency and color of dental porcelain had been improved over the years through improved formulation and firing protocols. In 1886, Land introduced the first fused feldspathic porcelain inlays and crowns (Jones, 1985; Sproull, 1978). All-ceramic dental porcelain was not widely used until the 1950s with the introduction of alumina and lucite to the formulation to improve thermal and mechanical properties of crowns and fixed partial dentures (McLean, 1967; Freese, 1959). Over the past few decades, since the development of porcelain-fused to metal procedure in the early sixties, refinements in metal ceramic dominated dental ceramic research that resulted in improved alloys,

bonding and porcelains. Metal-ceramic restoration had been the "gold standard" for years in prosthetic dentistry due to good mechanical properties, reliability, and reasonable esthetics (Zarone *et al.,* 2011). The patient's growing demand for highly esthetic and natural-appearing artificial crowns lead to the development of new all-ceramic materials. Zirconia and its composites are the most popular ones due to their relative high strength, fracture toughness, color and biocompatibility. Because of the high strength of these core materials, the failure of crowns shifted to the veneer layer. Most failure modes of zirconia frame crowns involved porcelain veneer layer chipping or cohesive failure, and rarely did cracks extend to the zirconia core. Porcelain chipping was a failure phenomena associated to zirconia frame crowns, which had not been fully understood by the dental community. It has been a research interest over the past two decades.

2.2 All-ceramic crown performance

Routine use of ceramics in restorative dentistry is only a recent phenomenon. All-ceramic dental crowns have better esthetics and biocompatibility than metal-ceramic crowns, but have not achieve the "gold standard" set by metal-ceramic crowns in terms of longevity and reliability. Clinical survival has been the interest and focus of many reviews. However, comparing survival rate is not straightforward and data were not always consistent among studies. A variety of factors including crown manufacture procedure, tooth position, patient factors, dentist factors were not always controlled and reported (Burke & Lucarotti, 2009, malament & Socransky, 2010). Pjetursson *et al*. (2007) analyzed restorations from different types of materials and found out that densely sintered alumina crowns had a five-year survival rate of 96.4%, Lucite-reinforced glass

ceramic had a survival rate of 95.4% and infiltrated glass ceramic survived at 94.5%. Tetrasilicic fluormica glass ceramic had a survival rate of 87.5% for 10 years while 95.5% lithium disilicate crowns survived. Survival of posterior crowns was lower than anterior. The five-year survival rate of metal crowns was 95.6% (Pjetursson *et al*. 2007). Wittneben *et al.* (2009) reviewed 5-year survival rates of single crown restorations made with CAD/CAM by examining the papers published between 1985 and 2007. With the CAD/CAM systems, survival rate of different types of ceramics differed dramatically. The survival rate of Glass-ceramic restorations were at 82.82% and feldspathic porcelain and alumina restorations were at 98.81%. For zirconia-porcelain crowns, especially Y-TZP frames, most failures occurred in the veneer layer, and rarely happened in the zirconia core due to its high strength and toughness (Cehreli *et al.,* 2009; Ortorp *et al*., 2009). It was very difficult to quantify this type of failure in part due to inconsistent reports in the literature as fracture and chipping. The degree of chipping was rarely provided. Some chipping could be severe enough to need a replacement; some may only need a polish or minor repair (Rekow *et al*., 2011).

Few studies had focused on the performance of single zirconia crown restorations, but on the survival rate of zirconia based bridges. Zirconia has become the top choice when it comes to framework of all-ceramic bridges. Its failure rate was much lower than glass-infiltrated alumina frameworks, with zirconia frameworks at 0-6% (Edelhoff *et al.*, 2008; Molin and KArlsson, 2008; Tinschert *et al*., 2008; Silva *et al*., 2010a) comparing to infiltrated alumina frameworks at 10-12% (Vult von Steyern *et al.,* 2001; Olsson *et al*., 2003) for 3-5 years.

2.3 Zirconia

Zirconia can exist in three crystallographic forms based on sintering temperature at ambient pressure. From room temperature to 1170 ^{o}C, the phase would be monoclinic, tetragonal at 1170 to 2370 °C, and cubic at 2370 °C to the melting point. Phase transformation from tetragonal to monoclinic during cooling is accompanied by a 4.5% volume increase in crystal structure. The transformation process is reversible and starts at 950 °C. Adding sufficient stabilizing agent CaO, MgO, Y_2O_3, or CeO_2 to pure zirconia retains the tetragonal phase at room temperature and controls cracks induced due to phase transformation (Garvie *et al*., 1975; Garvie & Nicholson, 1972; Heuer *et al*., 1986). There are many types of zirconia, but only three have been used in dental crowns. They are Y-TZP, magnesium partially stabilized zirconia, and zirconia toughened alumina. 3mol% Y-TZP is the most widely used because of higher mechanical properties. Mechanical strength of zirconia strongly depends on grain size, which is determined by the sintering condition. Above a certain size, Y-TZP is subject to a significant tetragonal to monoclinic phase transformation. Lower transformation rates could be achieved for grain sizes less than 1 µm. However, if too small, such as less than 200 nm, phase transformation is not possible leading to reduced fracture toughness (Heuer, 1982; Cottom and Mayo, 1996). The grain size of Y-TZP for dental applications ranges from 0.2 to 0.5 µmin diameter, with a flexural strength in the 800 to 1000 MPa, and fracture toughness from 6 to 8 MPa $m^{0.5}$ (Guazzato *et al.*, 2004).

2.4 Porcelain Veneer

Porcelain veneer is applied on zirconia and alumina dental crowns or fixed partial

dentures to improve esthetics and to protect zirconia core from oral environment. Zirconia showed degradation under water. The thickness of the porcelain layer, marginal discrepancy, and microstructure all affect strength. Flexural strength of veneering porcelain ranges from 60 to 120 MPa (Fischer *et al*., 2008; Thompson and Rekow 2008, Bottino *et al*., 2009). However, porcelain is vulnerable to slow crack growth. At low continuous or cyclic loads, especially in humid conditions, a crack could keep growing at a slow pace and degrade strength of the ceramic material. In some cases, cracks propagated at less than 50% of the material strength (Rekow, *et al.*, 2011; Lawn, 1993; Salazar Marocho *et al*., 2010).

2.5 Residual Stress

Dental practice normally put a porcelain veneer on top of a high strength core to achieve strength, esthetics and protection for the restoration. Experience from metal-ceramic-restorations (MCRs) showed porcelain with a slightly lower CTE than the core material would produce favorable compressive stress in the veneered layer to suppress crack growth and strengthen the restoration (Aboushelib *et al*., 2008). Normally the CTE of porcelain was 1 ppm lower than its core material. However this strategy did not work on porcelain-zirconia restorations, evidenced by porcelain chipping. The hypothesis was that more residual stress formed in zirconia-porcelain restorations than MCRs due to poor thermal diffusivity of ziconia (Swain, 2009).

Mismatch of CTE is not the only factor causing residual stress. Lab analysis with flat samples had found that chipping behavior was similar for both MCRs and zirconia-ceramics-restorations (ZCRs) (Quinn *et al*., 2010). However, in clinical practice, ZCRs

showed more porcelain chipping than MCRS. This suggested that the residual stress was greater than just what would be caused by a CTE mismatch. Swain (2009) presented a theoretical explanation of the effect of CTE mismatch, thermal tempering, and veneer thickness on residual stress using a 2D analytical model. It mentioned that higher thermal gradient and thermal stress in zirconia could due to its low thermal diffusivity. Also it suggested the predominant driving force for cracks was cooling rate, CTE, and the thickness of the veneering porcelain.

In summary, zirconia core all-ceramic single dental crown and fixed partial denture were very popular because of its esthetics, biocompatibility and high toughness. However, zirconia core crowns exhibited a unique failure phenomenon, which was chipping of porcelain veneer. This failure behavior was different from metal and alumina core crowns and had not been fully understood. Residual stress formed during cooling was thought having played an important role. This work will concentrate on analyzing residual stress in zirconia-porcelain frameworks formed due to concentrate on analyzing residual stress in zirconia-porcelain frameworks formed due to both mismatch of CTE and thermal tempering using a two-dimensional (2D) analytical model, three-dimensional (3D) finite element simulation, and nanoindentation measuring technique. Different design options are also compared to reduce residual stress. Furthermore, manufacture and processing flaws could also be the origin of crown failures. Microstructure and flaw distribution were examined with micro X-Ray computed tomography (μCT) and secondary electron microscope (SEM) imaging.

CHAPTER III

3 A BILAYER DENTAL SYSTEM TO ANALYZE RESIDUAL STRESS DUE TO BOTH MISMATCH OF CTE AND THERMAL TEMPERING

A bilayer 2D analytical model was used to analyze residual stress caused by CTE mismatch and thermal tempering in zirconia-porcelain dental systems. Results showed that the tempering rate and porcelain zirconia thickness have significant impacts on residual stress, and the effects are interrelated. A larger thickness and tempering rate will result in a larger tensile stress. The higher the tempering rate, the more tensile stress will develop in porcelain and the more compressive stress will be in zirconia. This is more apparent on thicker plates. At a tempering rate of 5 ºC/s, residual stress due to mismatch of CTE dominate. At 50 ºC/s, mismatch of CTE and thermal tempering contribute equally to the final residual stress.

3.1 Introduction

Contemporary dental crowns often use different materials as the core or veneered surface layer to meet the demands of durability and esthetics. Manufacturing dental crowns often requires several firing cycles. During the final cooling process, residual stress will form due to a mismatch of CTE between the core and the veneered layer, also a thermal temperature gradient. When cooling rate and crown thickness are

large enough, the tempering stress can be equally important as residual stress caused by the mismatch of CTE between the core and the veneered surface. Many researchers have used two-dimensional bilayer models and bilayer samples to analyze residual stress in dental systems. Analytical models for bilayer system residual stress by mismatch of CTE are readily available. Timoshenco (1925) has analyzed the problem and Roark and Young (1986) also showed it in detail. Most recently Hsueh *et al*. (2005-2008) extended the solution to multi-layers and applied it on a dental crown with an alumina core and porcelain veneer. Good agreement between the analytical and finite element method was obtained. Swain (2009) used a bilayer model to analyze the key parameters to cause unstable chipping of veneered porcelain on an all ceramic dental crown system and fixed partial dentures. Most of the work involves modeling the residual stress from the mismatch of CTE between the core and its veneering porcelain. With the aid of computer simulation, tempering stress had been studied before, mostly for metal-porcelain or porcelain-porcelain dental systems. The ability to understand the tempering stress has been limited by a lack of analytical models. Dehoff and Anusavice (1991) studied tempering stress using a porcelain-porcelain bilayer system, computer simulated temperature files were used. Dehoff *et al*. (1996) simulated the tempering stress of a metal ceramic disk with an ANSYS program. Only Recently, Swain (2009) proposed a way in 2D to estimate the tempering stress analytically.

Because of the complex nature associated with dental crown geometry, 2D analysis will not be sufficient to capture the whole picture. However it can serve as an initial foundation which will lead a better understanding of the problem and the role of key parameters. It also helps to understand the difference between 2D and 3D results by

comparing with 3D simulation and experimental results. This work will use a bilayer model to estimate the effect of tempering rate and thickness on the residual stress of the dental system.

3.2 Theory

3.2.1 Mismatch of CTE

A bilayer plate, as shown in Fig. 3-1, was used to study the residual stress formed due to the mismatch of CTE and thermal tempering. While acknowledging this simple model will not fully represent the response of the complex nature of the real crown, it will give an initial understanding of roles played by key parameters in term of contributing to residual stress.

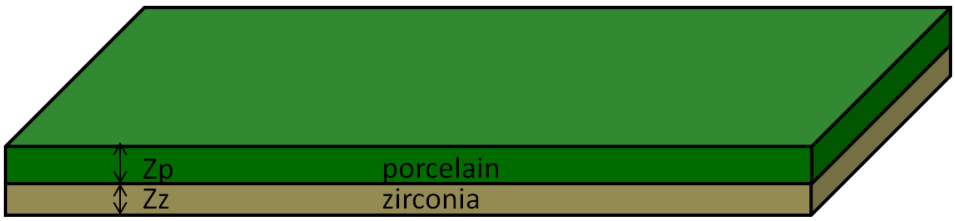

Fig. 3-1 Schematic drawing of the bilayer zirconia porcelain plate bonded together

The model used here consists of two materials bonded together with different material properties, such as: CTE, α; thermal conductivity, K; density, ρ; specific heat, c; Young's modulus, E; and Poisson's ratio, υ. The material properties used here are listed in Table 3-1. The model was designed to let the thickness of zirconia be 0.5 mm and the

thickness of porcelain be 0.5 mm and 3 mm, considering the thickness of porcelain in real crowns is normally between this range.

Normally, porcelain is veneered to zirconia at about 900 ºC, and then cooled to room temperature. However, residual stress will not develop until the temperature reaches porcelain's glass transition temperature. Therefore a heat soak temperature of 500 ºC and heat sink temperature of 25 ºC was assumed for the analysis. Two different tempering conditions were used to examine the effect of tempering rate on residual stress, one is 5 ºC/s and the other is 50 ºC/s.

Table 3-1 Thermal-mechanical properties used for residual stress analysis (Swain 2009 and Dehoff *et al.* 2008)

Materials	CTE α (10-6/K)	Thermal Conductivity K (W/m-K)	Specific heat c (J/K-Kg)	density (g/cc)	Modulus E (GPa)	Poisson's ratio υ
porcelain	10	2	840	2.4	205	0.25
zirconia	11	2	450	6	70	0.25

Bending of two plates with dissimilar materials bonded together has been considered by Timoshenko (1925), Roak and Young (1986), and Hsueh *et al.* (2008). The biaxial in plane residual stress due to mismatch of CTE in the bilayer system are shown by Hsueh (2008) as

$$\sigma_z = E'_z \left\{ \frac{E'_p z_p (\alpha_p - \alpha_z)\Delta T}{E'_z\, z_z + E'_p\, z_p} + p\left[z - \frac{E'_z z_z^2 + E'_p z_p^2 + 2E'_p z_z z_p}{2(E'_z z_z + E'_p z_p)} \right] \right\} \quad (1)$$

$0 \leq z \leq z_z$

$$\sigma_p = E'_p \left\{ \frac{E'_z z_z (\alpha_z - \alpha_p)\Delta T}{E'_z\, z_z + E'_p\, z_p} + p\left[z - \frac{E'_z z_z^2 + E'_p z_p^2 + 2E'_p z_z z_p}{2(E'_z z_z + E'_p z_p)} \right] \right\} \quad (2)$$

$z_z \leq z \leq z_z + z_p$

$$p = \frac{6E'_z E'_p z_z z_p\ (z_z + z_p\ )(\alpha_p - \alpha_z)\Delta T}{E'^2_z z_z^4 + E'^2_z z_z^4 + 2E'_z E'_p z_z z_p (2z_z^2 + 2z_p^2 + 3z_z z_p)} \quad (3)$$

Where p is curvature of the bilayer plate, α_z and α_p are CTE of zirconia and porcelain, and z_z and z_p are thickness of zirconia and porcelain layer, and z is position along the thickness. Also σ_z and σ_p are in plane biaxial residual stress in zirconia and porcelain layer, and $E'=E/(1-\nu)$, with E and ν the Young's modulus and Poisson's ratio.

3.2.2 Thermal tempering

Thermal tempering is a heat treatment process widely used in the glass industry for strength toughening. It is a process in which glass was heated to a temperature well above its glass transition and then cooled rapidly, so that compressive stress was formed on the surface. The process has been adopted by the dental community to treat dental ceramics for the same strength toughening purpose.

A linear cooling model for thin slab was used to obtain the temperature distribution. The plate was assumed to have an uniform temperature T_i. At t = 0, the temperature $T-T_i$ is 0; and must approaching a limiting steady state as t increases, in which the whole body temperature change uniformly at the rate of C degrees per second. When cool down from a heat soak temperature, temperature distribution for an infinite plate with a 2h thickness at a cooling rate C for t > 0 with a surface temperature of Ct is shown by Williamson and Adams (1919).

$$T = T_i + Ct + \frac{C(z^2 - h^2)}{2k} + \frac{16Ch^2}{k\pi^3}\sum_{n=0}^{\infty}\frac{(-1)^n}{(2n+1)^3}e^{-k(2n+1)^2\pi^2 t/4h^2}\cos\frac{(2n+1)\pi z}{2h} \quad (4)$$

Where *Ti* are the heat soak temperature, *C* is cooling rate at the limiting steady state, *h* is half thickness of the plate, *t* is time and *z* is the position on the plate, *k* is the thermal diffusivity of the material. When k*t* become large respected to h^2, the last term in equation (4) will vanish, and temperature gradient will reach a so called steady state, and the temperature distribution is represented by a parabola. The temperature difference between the center and the surface was

$$\Delta T = Ch^2/2k \quad (5)$$

This temperature difference was found to be the most important factor in determining the residual stress at room temperature by Asaoka and Tesk (1989). The magnitude of the tensile stress at the center was

$$\sigma_t = E'\alpha h^2 C/3k \quad (6)$$

Also note the compressive stress at the surface is twice the tensile stress at the center.

3.3 Results

Residual stress due to mismatch of CTE and thermal tempering between the core and the veneering porcelain was obtained separately and then superimposed on each other to get the final residual stress. Residual stress caused by mismatch of CTE for dental systems with porcelain zirconia thickness of 1:1 and 6:1 was shown in Fig. 3-2. Larger porcelain and zirconia thickness ratio resulted in larger residual stress. This is in agreement with the results reported by Allahkarami *et al.* (2010).

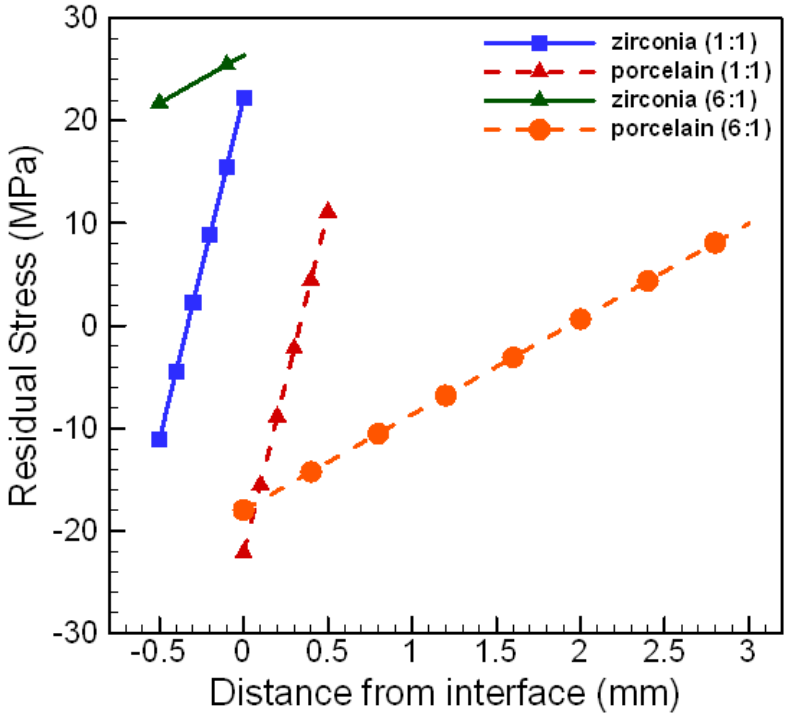

Fig. 3-2 Residual stress due to mismatch of CTE for porcelain and zirconia with thickness ratio 1:1 and 6:1.

Temperature profiles at two different tempering rates, 5 ºC/s and 50 ºC/s, and the two porcelain zirconia thickness is shown in Fig. 3-3 and Fig. 3-4. These are temperature difference across the plate thickness in reference to surface temperature. The temperature

gradient is lager for larger thickness and larger tempering rates. If the total thickness of both porcelain and zirconia is 1mm, at cooling rate 5 ºC/s, the temperature gradient in minimal. It is less than 10 °C at cooling rate 50 ºC/s. If the total thickness of both porcelain and zirconia is 3.5 mm, at cooling rate 50 ºC/s, the maximum temperature gradient can reach 75 °C. These temperature gradients will form tempering stress. Fig. 3-5 and Fig. 3-6 shows tempering stress at two different tempering rates and thicknesses. At 50 ºC/s the maximum tensile residual stress for thickness 3.5 mm doubled that of 1 mm.

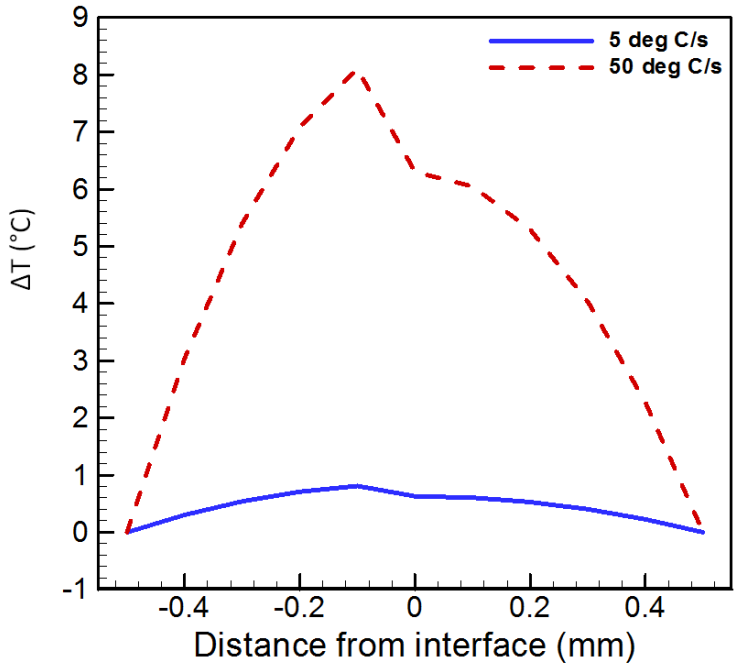

Fig. 3-3 Temperature distribution at two tempering rates for thickness 1 mm.

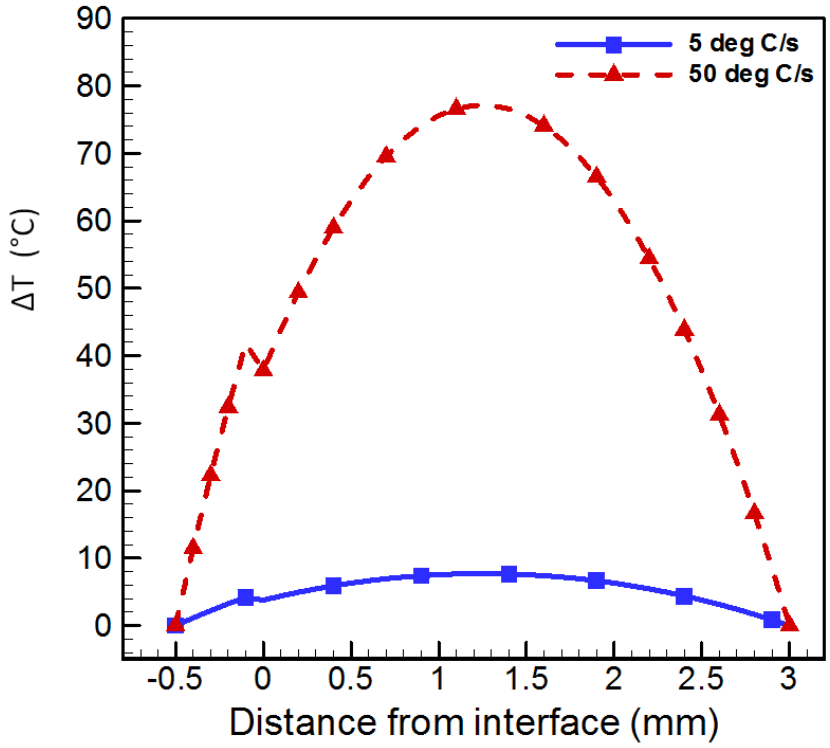

Fig. 3-4 Temperature distribution at two tempering rates for thickness 3.5 mm.

The final residual stress was arrived by adding residual stress from mismatch of CTE and thermal tempering, and the results were shown in Fig. 3-7 and Fig. 3-8. The effects of thickness and tempering rate on residual stress are interrelated. When tempering rate is at 5 ºC/s, the residual stress is a little different for thickness 1 mm and 3 mm. The difference becomes very significant at 50 ºC/s, with the difference in tensile stress is 40 MPa in porcelain. At a tempering rate of 5 ºC/s, residual stress due to mismatch of CTE dominates, while at 50 ºC/s, mismatch of CTE and thermal gradient contribute equally to the final residual stress. The higher the tempering rate, the more tensile stress will develop in porcelain and the more compressive stress in zirconia. This is more apparent in thicker plates.

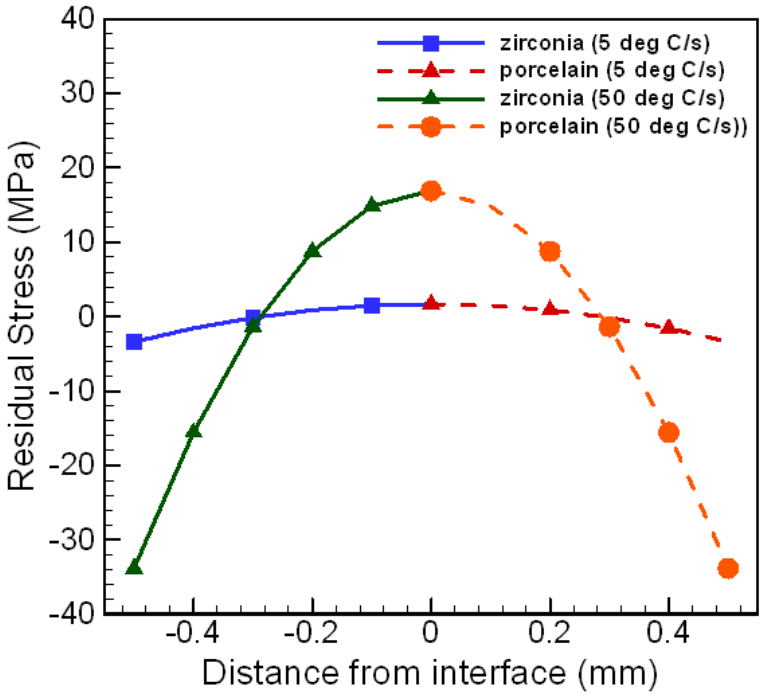

Fig. 3-5 Tempering stress at tempering rates 5 °C/s and 50 °C/s for porcelain zirconia thickness 1.0 mm.

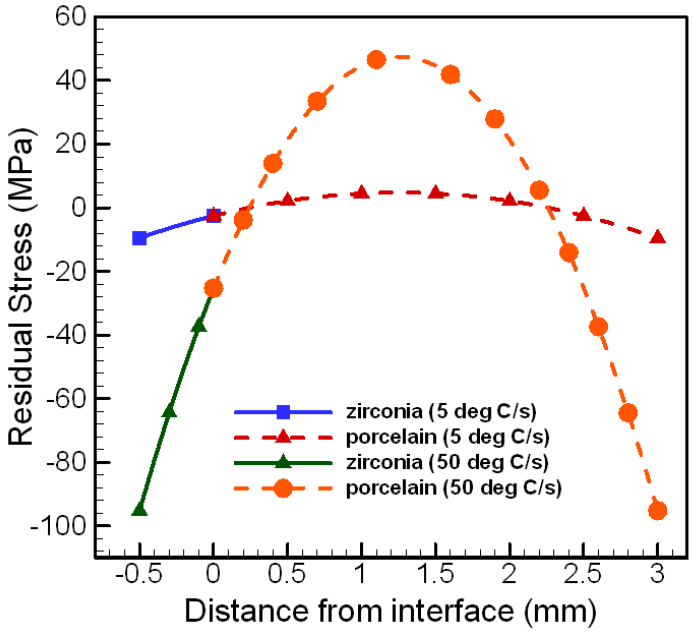

Fig. 3-6 Tempering stress at tempering rates 5 °C/s and 50 °C/s for porcelain zirconia thickness 3.5 mm.

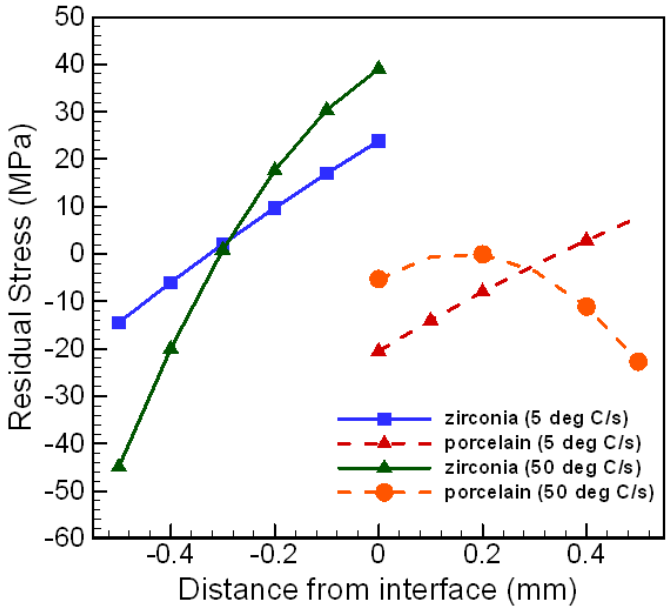

Fig. 3-7 Residual stress at tempering rates 5 °C/s and 50 °C/s for porcelain zirconia thickness 1.0 mm.

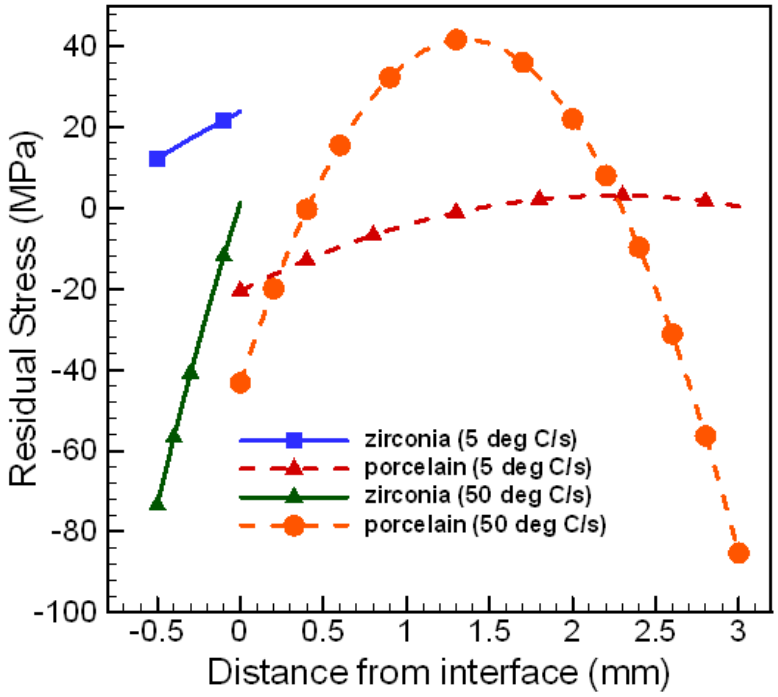

Fig. 3-8 Residual stress at tempering rates 5 °C/s and 50 °C/s for porcelain zirconia thickness 3.5 mm.

3.4 Conclusion

A bilayer system was used to analyze residual stress caused by mismatch of CTE and thermal tempering. Two porcelain zirconia dental frames with different thickness underwent two different tempering processes. Results showed that tempering rate and porcelain zirconia thickness have effects on residual stress and are interrelated. Tempering effects on residual stress for locations with smaller thickness are less relative to locations with larger thickness. The higher the tempering rate, the more tensile stress will develop in porcelain and the more compressive stress in zirconia. This is more apparent in thicker locations. Porcelain thickness gradient on residual stress should be considered carefully in crown and fixed partial denture design.

CHAPTER IV

4 MEASURING RESIDUAL STRESS IN CERAMIC ZIRCONIA-PORCELAIN DENTAL CROWNS BY NANOINDENTATION

Residual stress could play a critical role in failure of ceramic dental crowns. The magnitude and distribution of residual stress in the crown system are largely unknown. Determining the residual stress quantitatively is challenging since the crown has such complex contours and shapes. This work explored the feasibility and validity of measuring residual stress of zirconia and porcelain in ceramic crowns by nanoindentation. Nanoindentation tests were performed on the cross-section of a crown for both porcelain and zirconia along four critical locations which includes the thickest, thinnest and medium porcelain thickness. Zirconia and porcelain pieces, chipped off from the crown and annealed at 400 °C, were used as reference samples. The residual stress was determined by comparing the measured hardness of the stressed sample with that of the reference sample. Nanoindentation impression images were acquired through Scanning Probe Microscope (SPM) equipped with a Hysitron Triboindenter. Zirconia showed large pile-up. Residual stress is determined along the thickness of crowns at the chosen locations for both porcelain and zirconia. The measured results were compared with the results from X-ray diffraction (XRD) and finite element method (FEM). Results show large residual stresses in the dental crown and their magnitude differs

from locations due to the complex shape of the crown. The average residual stress reading is -637 MPa and 323 MPa for zirconia and porcelain respectively.

4.1 Introduction

Demand on all-ceramic dental crowns has been increasing over the years, but reliability and longevity are still concerns. Many efforts have been taken to reduce the brittleness of ceramic dental crowns, including veneering porcelain on stronger core materials, such as zirconia and alumina (Raigrodski, 2004; Tsalouchou *et al.*, 2008). Zirconia has a very high flexural strength of 900-1200 MPa and a fracture toughness (Christel *et al.*, 1989) of 9-10 $MPa/m^{1/2}$. The phase transformation (from tetragonal to monoclinic) behavior of zirconia contributes to its high toughness, but brings other issues like low temperature degradation and sub-cracking (Coelho *et al.*, 2009; Denry and Kelly, 2008). Even with such a strong and tough material as zirconia, fracture of the veneer or sometimes the core is still the dominant clinical complication (Pjetursson *et al.*, 2008). In three published reports, up to 50% of crowns developed crazing or cracking with loss of material after 1 to 2 years of in service (Larsson *et al.*, 2006; Raigrodski, 2006; Von, 2005; Von *et al.*, 2005). Crazing and chipping often indicates the presence of tensile stress. Stronger core materials could not bring down the failure rate, suggesting other factors than mechanical strength played an important role in failure. Residual stress can be caused by the mismatch of coefficients of thermal expansion, tempering or grain anisotropy (Bale and Hanan, 2008). Preexisting stress will amplify the applied cycling stress and induce cracks in the region that has preexisting tensile stress, but our understanding of magnitude and distribution of residual stress in the crown system is very

limited. Some researchers (Hsueh *et al*., 2008; Swain, 2009) were able to estimate the residual stress in a bilayered system from mismatch of coefficient of thermal expansion (CTE) and tempering using an analytical model. Recently, Mainjot *et al.* (2011) measured residual stress by hole-drilling in veneered porcelain using a bilayered sample. However, it is well known that the crown geometry will affect residual stress, along with mismatch of CTE, tempering, core and the veneer thickness ratio. Bilayer models and measurements will not capture the situation in real crowns, given the complex geometry. Experimental measurements using real crown samples are necessary. Bale (Bale, 2010) did measurements on the zirconia core of crown systems using XRD and found that the magnitude of residual stress in zirconia can be as large as 1 GPa locally with an increase after veneering with porcelain. But XRD cannot provide the same information in the amorphous porcelain layer and the hole drilling method is hard to carry out in crown samples being limited by spatial locations. The magnitude and distribution of residual stress in porcelain in real crown samples had never been measured, until Zhang and Hanan (2011) explored the method of measuring the residual stress by nanoindentation for both porcelain and zirconia. This showed nanoindentation was capable to detect the residual stress difference, but the absolute value was still in question due to the selection of the strain reference. This work improves the technique of measuring residual stress by nanoindentation by adopting a better procedure for strain reference samples. Also it improves the understanding of residual stress distribution across all ceramic dental crowns by performing residual stress measurements at many locations across the crown. Results are compared with those from XRD and FEM. Nanoindentation can be a very powerful technique, when proved feasible, due to the relatively simple data analysis,

sample preparation, spatial resolution, and limited safety requirements. Measuring residual stress with nanoindentation is a new field. The mechanism of the problem was not explored until Tsui *et al.*(1996) pioneered studying the effect of residual stress on nanoindentation hardness using a sharp berkovich indenter. They found that preexisting tensile stress decreases hardness, while compressive residual stress increases hardness. A later numerical simulation (Bolshakov *et al.*, 1996) suggested variations in hardness are caused by the inability to include the influence of material pile-up. Swadener *et al.* (2001) proposed a model for a spherical indenter based on the onset of yielding and the contact pressure. Suresh and Giannakopoulos (1998) proposed a model using a sharp berkovich indenter which measures the residual stress through comparing the load-depth curves between the reference sample and the stressed sample. Carlsson and Larsson (2001) formulated the problem for a sharp indenter using Tabor's relation approach.

This work measures residual stress of the zirconia-porcelain crown system by nanoindentation using a berkovich tip. Results are compared with FEM and XRD.

4.2 Theory

Several researchers had shown that residual stress will affect the measured global parameters, such as hardness, indentation depth, or contact area (Tsui *et al.*, 1996; Bolshakov *et al.*, 1996; Swadner *et al.*, 2001; Suresh and Giannakopoulos, 1998; Carlsson and Larsson, 2001). Residual stress acts as an extra force adding to the applied indentation force. Assume the residual stress is biaxial and perpendicular to the direction of indentation. If the residual stress is tensile, it acts the same way as an extra force in the same direction of the indentation force. If the residual stress is compressive, it acts

like an extra force in the opposite direction of the indentation. In result, when applying the same indentation force to the stressed and reference material, the measured depth, contact area or hardness will be different. Material with tensile stress will show less resistance to the indentation force and the one with compressive residual stress will show more resistance. In reverse, by comparing the difference of the global parameters of stressed and reference sample, residual stress can be extracted.

Tabor's relation (Tabor, 1951) as used by Swadener *et al.* (2001) and Larson and Carlsson (2001) was used to compare hardness from stressed and reference sample.

$$H_0 = C\sigma_Y \tag{1}$$

$$H = C(\sigma_Y - \sigma_R) \tag{2}$$

Where H_o and H are hardness of a reference sample and stressed sample, respectively. σ_R is the in plane residual stress. The sign of σ_R is positive for tensile stress and negative for compressive stress. σ_Y is the yield stress. The constrain factor, C, has a value between 0.5 and 3 for elastic-plastic indentation. It was determined using Johnson's "Expanding Cavity" model (Johnson, 1985).

$$C = \frac{2}{3}\left[2 + \ln\frac{\left(\frac{Etan\alpha}{\sigma_Y}\right) + 4(1-2\nu)}{6(1-\nu^2)}\right] \tag{3}$$

E and *v* are Young's Modulus and Poisson's ratio. The angle α, is angel of the berkovich tip. The hardness was defined as the average pressure,

$$P_{ave} = \frac{P}{A} \tag{4}$$

P_{ave} is the average pressure at the maximum load *P*, which is directly obtained from nanoindentation. The contact area *A* is determined based on the classic Oliver and Pharr method (Oliver and Pharr, 1992), which assumed that the indentation process can be modeled as a rigid axisymmetric indenter into an elastic half space, and at peak load, the edge of the contact is vertically displaced relative to the initial position of the surface. The projected area at the contact depth is determined by the area shape function, the relation between contact depth and area was experimentally calibrated using fused silica as,

$$A = \sum_{i=0}^{8} C_i (h_c)^{2-i} \tag{5}$$

where C_i are a series of constants, h_c is contact depth.

4.3 Experiment

4.3.1 Sample preparation

The examined ceramic crown has a zirconia core with 0.5 mm thickness and veneered porcelain with varying thickness (see Fig. 4-1). The zirconia core is 3% yttria stabilized TZP (LAVA, 3M/ESPE, St. Paul, MN) with Young's modulus at 205 MPa and CTE 11×10^{-6}/ ºC. The veneered porcelain is LAVA Ceram (3M/ESPE, St. Paul, MN) with a Young's modulus of 70 MPa and a CTE of approximately 10×10^{-6}/ ºC (Bale, 2010;

Paulo *et al.*, 2009). They were prepared in a dental lab following a typical procedure for zirconia core and porcelain veneer crowns. Several firing cycles are normally involved when making dental crowns, but typically the firing temperature at the final cycle has the greatest influence on residual stress. The crown was cooled down to room temperature from its final firing temperature of 840 ºC following the manufacture's recommended procedures. Here the crowns were cut in half with a diamond saw and subsequently polished to provide a smooth surface. Pieces of zirconia and porcelain, chipped off from the crown and annealed at 400 °C for 5 hours, were used as a reference samples. Both reference and stressed samples were polished the same amount to minimize effects of polishing.

4.3.2 Nanoindentation

Nanoindentation was performed on the cross section of an all-ceramic zirconia-porcelain crown using a MTS nanoindenter XP, which has a resolution of 0.2 nm in displacement and 50 nN in load. Nanoindentation impressions were examined for pile-up and sink-in by a Scanning Probe Microscope (SPM) equipped with the Hysitron Triboindenter. The Hysitron has a resolution of 0.04 nm in displacement and 1 nN in load. Indentation was performed on both stressed and reference samples. On the stressed sample, indentations were performed at four critical locations, marked as a dashed line in Fig. 4-1. The four locations were carefully chosen to include locations having the thickest, thinnest, and medium porcelain thickness. The porcelain thickness along lines 1, 2, 3, and 4 is 1.4 mm, 2.2 mm, 0.5 mm, and 1.2 mm respectively. The maximum load applied on zirconia and porcelain was 200 mN and 30 mN respectively, while the loading

time was 40 s for both materials. Randomly chosen two dozen indents were performed on the reference porcelain and zirconia. The average hardness value of indents on the reference crown was used for residual stress computation.

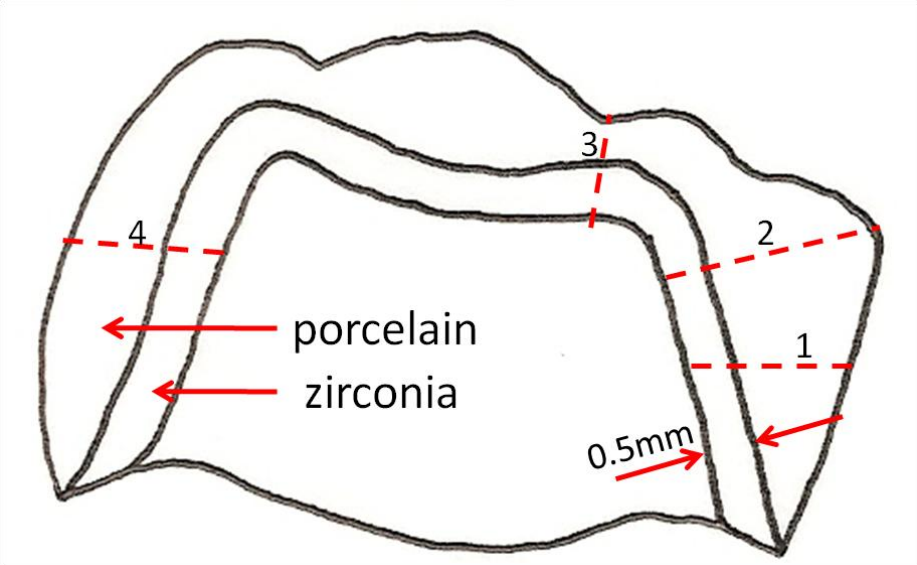

Fig. 4-1 Schematic cut face of crown. Nanoindentation tests were performed in both phases along the four dashed lines.

4.3.3 XRD method

The $\sin^2\psi$ X-ray diffraction method (Krawitz, 2001) was used also to measure residual stress along line 2 in the crown sample shown in Fig. 4-1. A Bruker D8 Discover micro-X-ray diffractometer with a General area Diffraction Detection System (GADDS) and Hi-Star 2D area detector was used for these measurements. The detector to sample distance was kept at 295 mm, which covers the area of 20° in 2θ and 20° in χ directions with 0.02° resolution. An X-ray beam incident angle of θ_1=37° and detector angle of θ_2=37° were used. The particular θ_1 and θ_2 was chosen in such a way that the (004) tetragonal ring had a maximum χ range.

4.4 Simulation

Commercial finite element analysis software ABAQUS (6.9-1) was used to simulate the berkovich nanoindentation response at different residual stresses for zirconia. A 2D axisymmetric model with 30 μm x 50 μm dimension, as shown in Fig. 4-2, was used. A conical tip with a 70.3^{o} including angle was used to simulate the pyramid shaped berkovich indenter. Edge biased meshing was applied so that the area directly under the indenter tip had a much finer mesh to better capture surface deformation. The element size under the tip was less than 30 nm. Displacement history from nanoindentation experiments was used as an input in the FEM. The material was assumed elastic perfectly plastic. Several trial runs were made to find the parameters that will give the best fit between experiment and simulation for the case with zero residual stress. Then residual stress was applied through a surface traction force. Simulation results at different residual stresses were compared to experiment results. The Young's modulus and yield stress for zirconia were assigned 200GPa and 10 GPa.

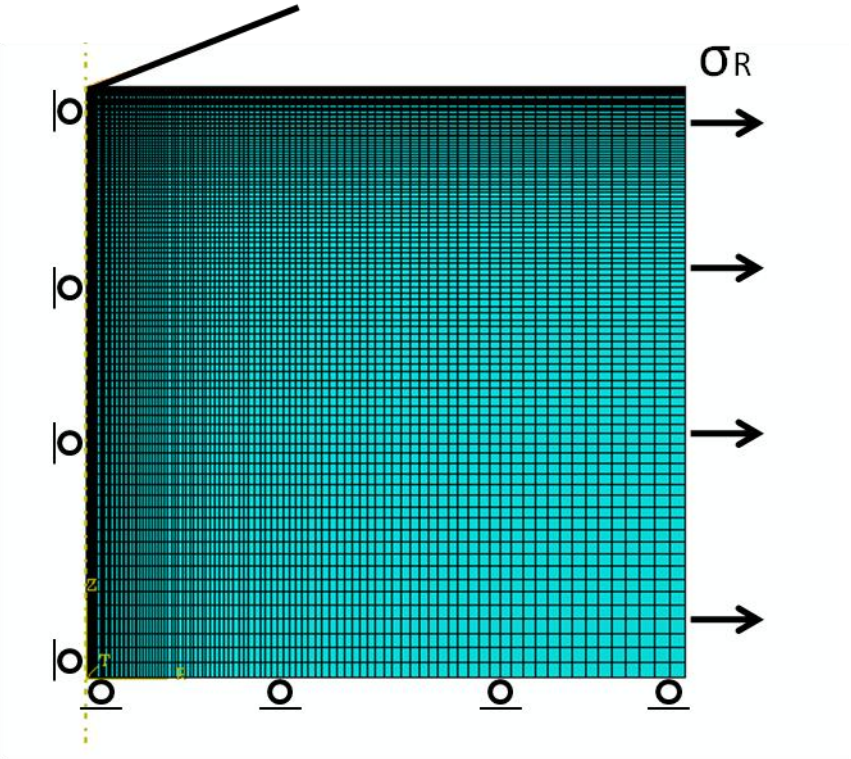

Fig. 4-2 2D axisymmetric finite element model showing, mesh, boundary conditions, and imposed residual stress.

4.5 Results and discussion

4.5.1 Nanoindentation results

Residual stress was extracted by comparing the measured hardness for the reference sample and stressed sample. Hardness was derived from the measured load-depth curve. Fig. 4-3 shows a typical load depth curve of a stressed and reference sample for both porcelain and zirconia in a case of tensile stress. At the same indentation load, the indentation load depth curves for stressed and reference samples will be different because of the effect of the residual stress. If the residual stress is tensile, at the same load, the indentation depth is larger for the stressed sample, resulting smaller hardness. It would be opposite for compressive stress.

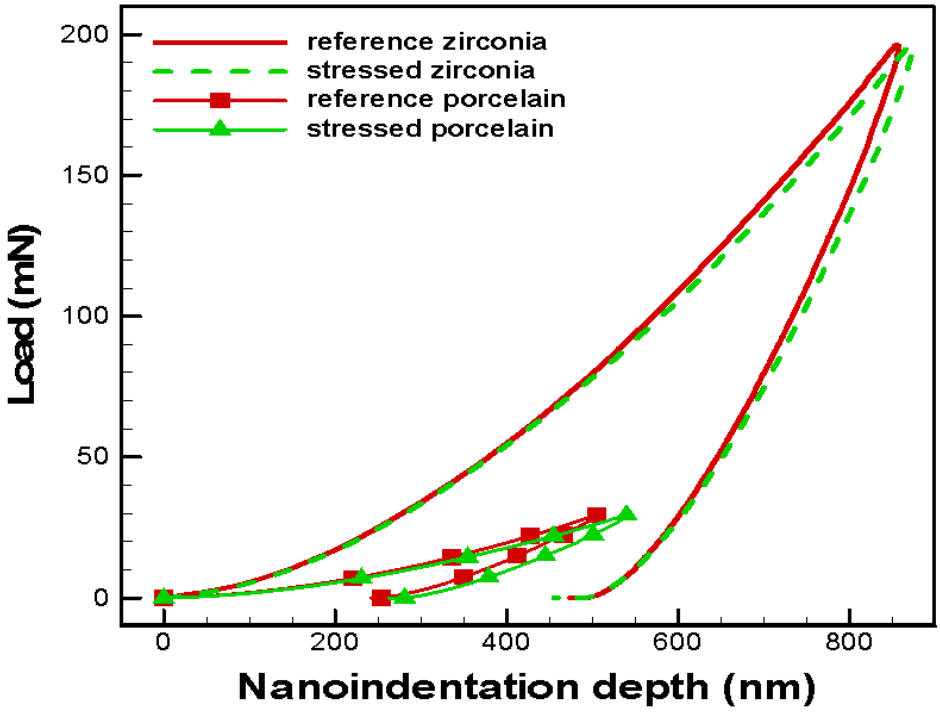

Fig. 4-3 Load depth curves of both reference and stressed porcelain and zirconia.

The average hardness of the reference samples were 6.53±0.41 GPa and 13.94±0.32 GPa for porcelain and zirconia respectively. Residual stress along the four critical locations marked on a crown for both porcelain and zirconia was obtained as shown in Fig. 4-4. Position 0 in Fig. 4-4 is the interface between zirconia and porcelain. Residual stresses at different locations for both porcelain and zirconia are different. The average residual stress along line 1, 2, 3, and 4 for porcelain were 260, 323, 231, and 104 MPa, while the average residual stress along line 1, 2, 3, and 4 for zirconia were -637, -536, -480, and -398 MPa. Not only did crown thickness affect the residual stress state, crown geometry had significant effect. Residual stress along line 2 was more tensile comparing to others, which indicates curvature has an effect. Lines 1 and 4 have

similar thickness, but are located at different parts of the crown. The residual stress trend across the thickness was different.

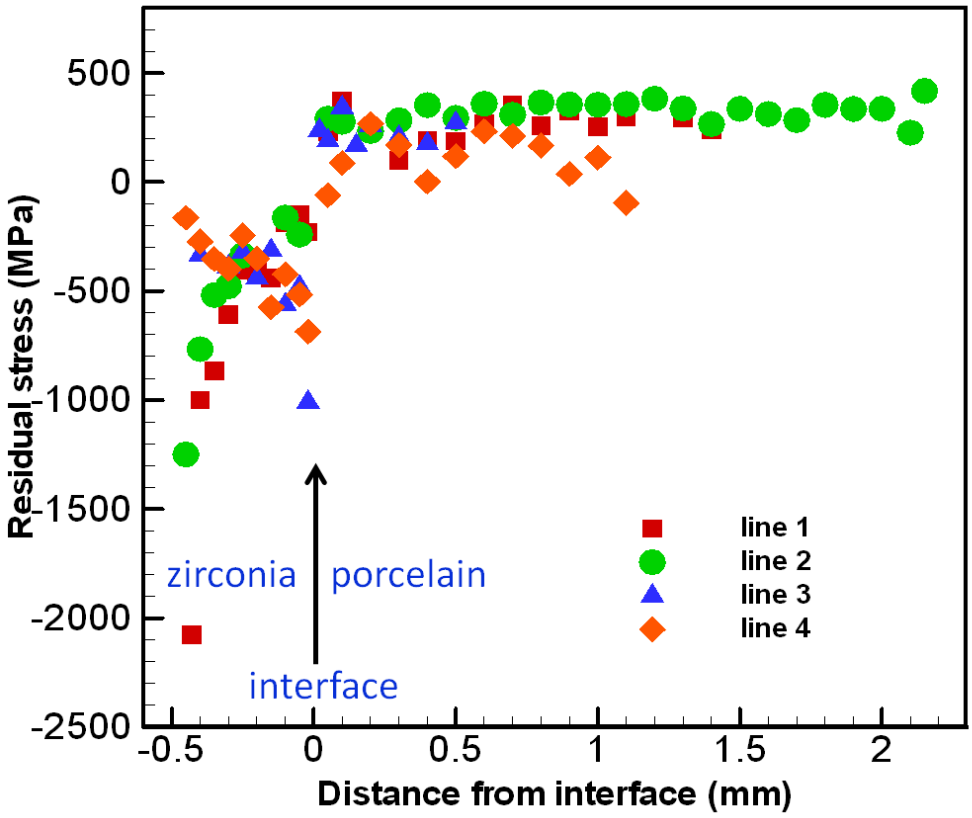

Fig. 4-4 Residual stress along four critical locations on crown for both porcelain and zirconia, lines 1, 2 and 3 have the thickest, thinnest, and medium porcelain thickness. The typical measurement error are ±6.3% and ±2.3% for porcelain and zirconia respectively, based on two dozen measurements on the reference samples.

For zirconia, along line 1, the stress was more tensile getting closer to the interface, while it was more compressive for line 4. The results additionally prove

complexity of the residual stresses in dental crowns. There are large amounts of residual stress in the crown and its magnitude varies from place to place.

Nanoindentation impression images, as shown in Fig. 4-5, indicated a large amount of pile-up in zirconia. This could be duo to high E/Y ratio or phase transformation. Porcelain has almost no pile-up.

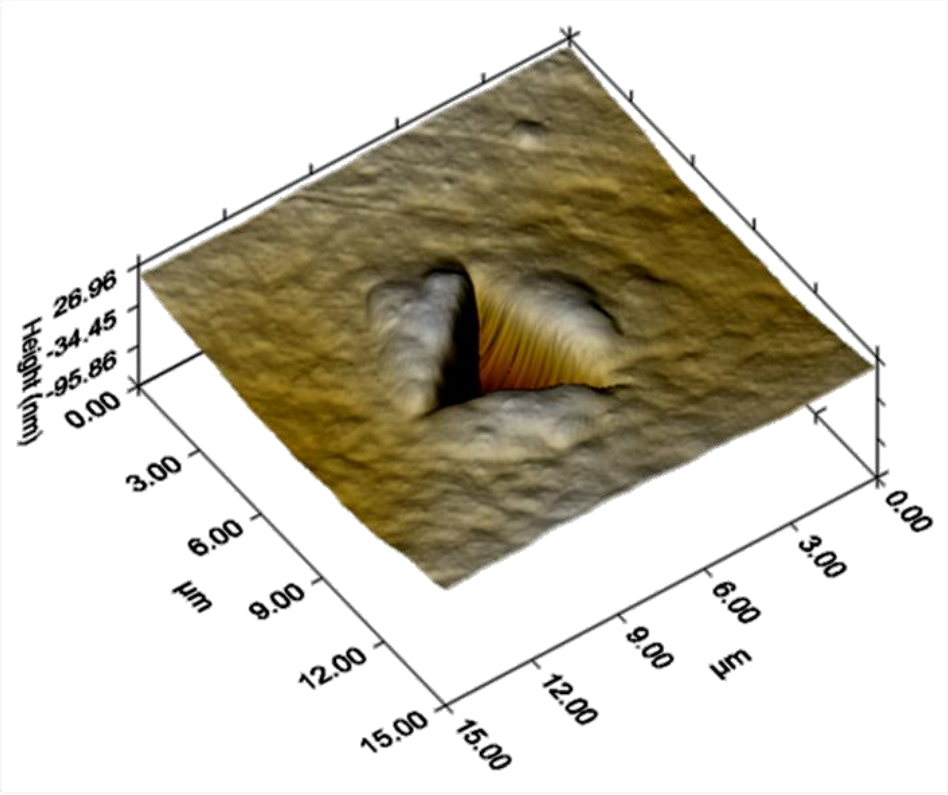

Fig. 4-5 Zirconia nanoindentation impression shows large pile-up

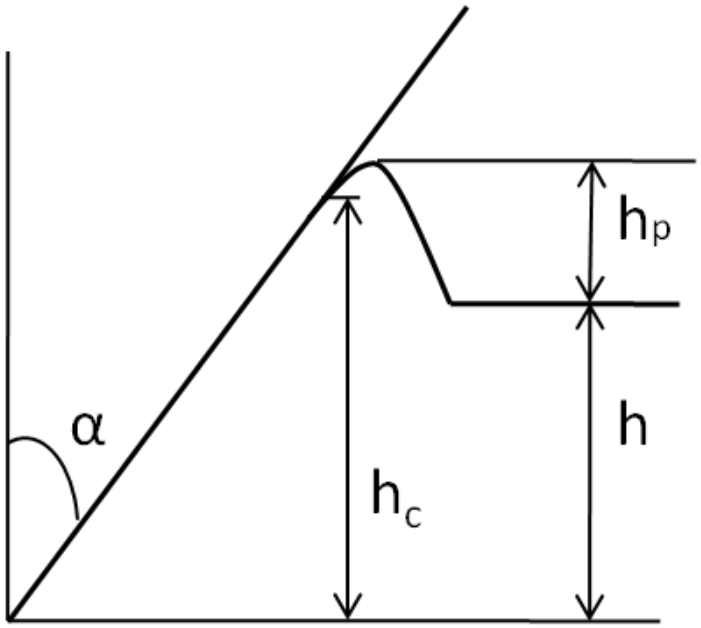

Fig. 4-6 A schematic drawing of nanoindentation half place with pile-up

The traditional Oliver and Pharr[20] method does not include the effect of pile-up. A new parameter h_p shown in Fig. 4-6, similar to the modification used by Choi *et al*. (2004), was used to include the pile-up effects. The resulting maximum indentation depth, $h_{max}=h+ h_p$, was used to calculate the contact area and hardness.

4.5.2 XRD results

Fig. 4-7a illustrates a typical frame with a segmented (004) ring and Fig. 4-7b indicates one of the segments with the integration profile along the 2θ direction. The integrated intensity peak was fitted using Pearson VII using a Matlab program.

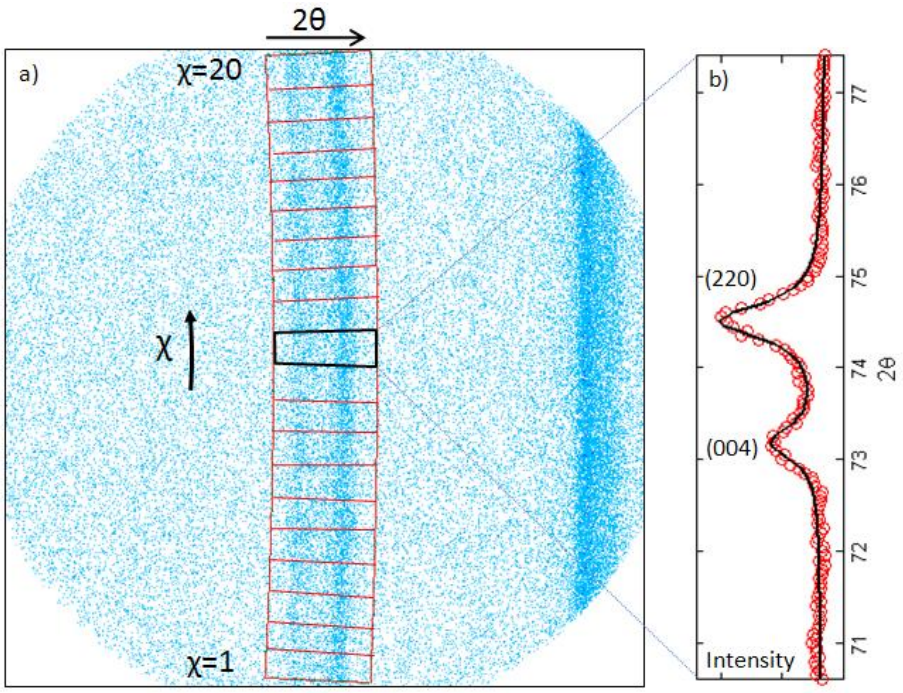

Fig. 4-7 a) Typical segmentation on a diffraction frame b) Integrated intensity profile, fitted by two Person VII functions for a 1° highlighted segment of the (004) ring.

Using equation 6 based on the slope and the intercept, the residual stresses were determined. More details of similar work were explained previously (Bale *et al*., 2011).

$$\sigma_{\phi} = \frac{Slope}{d_{\psi=0}} . \frac{E}{1+\upsilon} \tag{6}$$

These are plotted in Fig. 4-8 along with the results by nanoindentation. The two methods were able to give the same trend, but the magnitudes shows an offset of 1130±485 MPa. Residual stress measured by XRD was more tensile than by nanoindentation. XRD was

performed after nanoindentation. Nanoindentation could have changed the surface residual stress state slightly. However, a much larger spot size is measured by XRD than by nanoindentation. Independent strain free reference methods were used for the two measuring techniques.

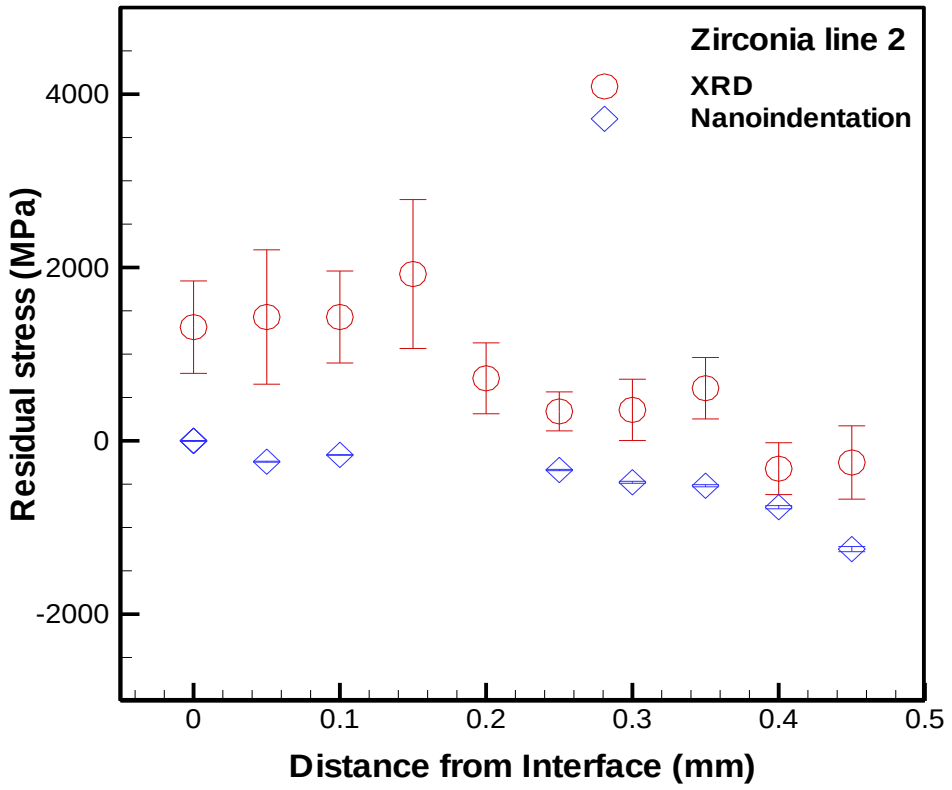

Fig. 4-8 Residual stress measured by XRD and nanoindentation along line 2. In this case, independent strain free reference methods were used for both techniques and their difference gives an offset 1130±485 MPa between the curves above.

4.5.3 Simulation results

To compare the results from nanoindentation experiments and FEM at different residual stresses, first, the material parameters were optimized to obtain the best match

between experiment and simulation at zero residual stress. Load-depth curves from simulation and experiment at zero stress for zirconia and porcelain were plotted in Fig. 4-9. Theses curves are remarkably similar, even a conical tip was used to simulate the berkovich. Once the model to match the experiment results is obtained at zero stress, different residual stresses were applied to the model to simulate the response and compare with experiments. Fig. 4-9 showed experiment and simulation results of zirconia with residual stress at 0 MPa and -518 MPa. The finite element simulation and nanoindentation results agreed very well.

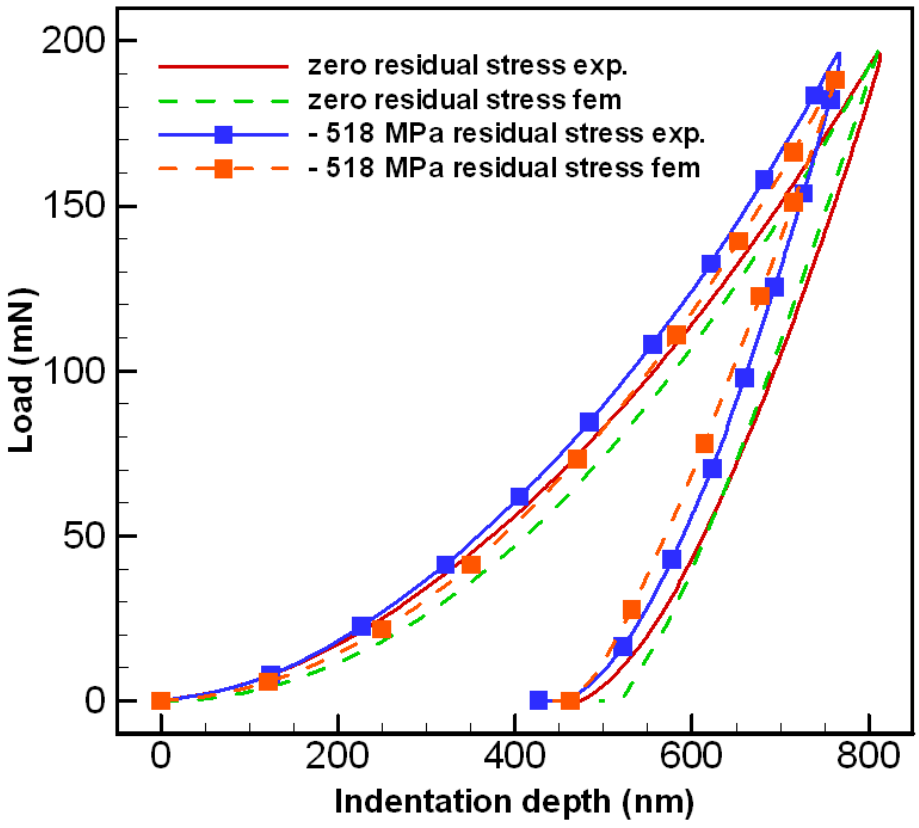

Fig. 4-9 Experimental and FEM results at different residual stress for zirconia.

4.5.4 Discussion

Clearly residual stress is seen in these ceramic crowns. Simply observing the trends in stress through the porcelain, which have not been observed before is useful in understanding potential sources of early failure observed clinically. Stresses are both tensile and compressive when moving away from the interface. The cusp area has the highest average stress at 323 MPa for porcelain, which offers an explanation why chipping is often severe in the cusp area (Tholey *et al.*, 2011; *Pjetursson et al.*, 2008). The residual stress gradient can be strong as well amplifying stress concentration at voids commonly observed in porcelains (Taskonak *et al.*, 2008). The degree of change can be as much as +/-500 MPa over only 0.2 mm. The thinner porcelain layer had stronger stress gradients. The thicker portions were more well behaved. 300 MPa is high since the reported fracture strength of bulk porcelain is between 57 to 149 MPa (Fischer *et al.*, 2008; Kon *et al.*, 2001). It is possible some error is due to uncertainties regarding the reference sample. It is difficult to assure a reference has zero strain, and the condition of the reference sample will affect the final measured residual stress. Another possibility for the observation of high stresses could be the scale of the measurement. Nanoindentation is sensitive to local stress concentrations. It is practical that these local stresses could be sustained at higher values. Bulk measurements are limited by flaw distributions. Even local residual stress concentrations could act like flaws in bulk measurements. Based on what has been observed here, it would be interesting to use nanoindentation to probe residual stress fields in samples used for traditional bulk measurements.

Zirconia is known for its phase transformation behavior (from tetragonal to monoclinic). Examining the load depth curve is one way to look for signs of phase

transformation. The indentation load-depth curves for both porcelain and zirconia shown in Fig. 4-3 are very smooth, and show no abrupt phase transformation. Other researchers had reported tetragonal to monoclinic phase transformation for pyramid–shaped indenter tips (Chintapalli *et al.*, 2012; Gaillard *et al.*, 2009; Gogotsi *et al.*, 1995). However in most cases, the load they employed was much larger than the one used here. Whether the pile-up observed here was caused by phase transformation has not been determined at this point. Surface treatment, grinding and polishing, has been shown to slightly alter the surface stress state of zirconia due to stress induced phase transformation (Ho *et al.*, 2009; Juy and Anglada, 2009). Here, to minimize the effect of polishing, both the reference and stressed samples were polished the same amount.

Finding the appropriate reference sample is always a challenge. A zirconia and porcelain piece, chipped off from the crown, annealed at 400 °C, and slowly cooled down to room temperature, was used as a reference in this case. Fischer *et al.* (2005) showed that annealing at about 100°C below the glass transition temperature of porcelain relaxes residual stress while not changing the microstructure. There are many different kinds of porcelain and their glass transition temperature varies. Choosing the right annealing temperature is not trivial, there is a risk of changing the microstructure if the temperature is set too high, and a risk of not completely relaxing the residual stress if the temperature is set too low. 400 °C is a conservative number for annealing. Microstructure changes are unlikely due to this thermal treatment, but there is a risk residual stresses are not completely relaxed. The average hardness for the reference sample was 6.53±0.41GPa and 13.94±0.32GPa for porcelain and zirconia respectively, which are in agreement with values reported in the literature (Gong *et al.*, 2004; Tanaka, 1999).

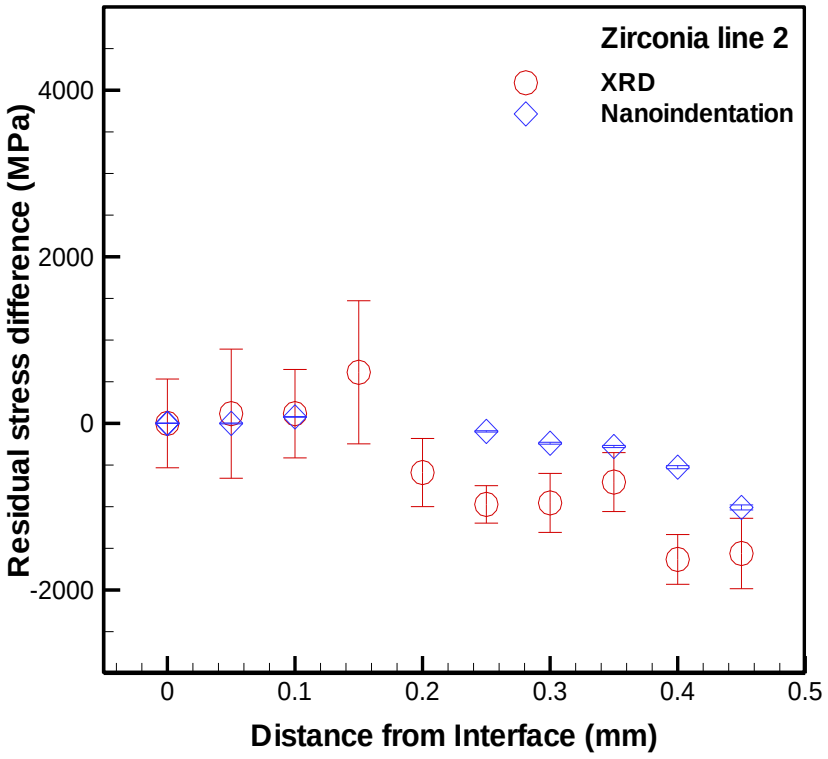

Fig. 4-10 Comparing nanoindentation and XRD results. Error bars are from peak fitting with XRD results and from typical standard deviation of two dozen measurements on annealed sample in nanoindentation.

It is challenging to find the right reference value for both nanoindentation and XRD method when measuring residual stress. From Fig. 4-8 we can see results from both methods had the same trend, more tensile at the interface between zirconia and porcelain, and more compressive at the zirconia surface. However, the absolute value is significantly different, which must be largely due to independent strain free references. If the stress value at a point close to the interface was assume to be zero and used as a reference, we can see the results agree well at location close to the interface and diverges close to surface, as shown in Fig. 4-10.

The stresses measured by these techniques are tensorial. Cutting perpendicular to the layers would relieve stresses in the direction out of the plain of the cut, but the in plane stresses remain and these are the stresses nanoindentation would be most sensitive too. Nanoindentation provides a scalar value sensitive to all in-plane stresses whereas the $\sin^2 y$ XRD provides a stress vector. Here we assumed the principle direction would be aligned with the interface. This may explain the best agreement near the interface where this one direction was dominant and suggests the principle direction of the stress may no longer line up as we move at least 0.2 mm away from the interface. This is not unreasonable, given the curved geometry of the crown. Also, it was only expected that the probed locations by both nanoindentation and XRD were in the same neighborhood, not the exact location. Local stress variation could contribute to the point to point differences too.

4.6 Conclusions

Residual stress can be extracted by comparing hardness of a stressed and reference samples. Residual stress along four critical locations in a crown across the thickness for both zirconia and porcelain was obtained. Results showed large residual stresses existed in the dental crown, and the magnitudes differ from location to location as might be expected from the geometry. Both geometry and thickness have an effect on the residual stress distribution. The cusp area in porcelain has the biggest tensile stress. Results by XRD and nanoindentation were compared and showed agreement in trend, but given the references used here, the magnitudes did not agree. Some of this can be due to sampling volume differences or reference determination, but clearly for unambiguous

application where absolute values are important, the new technique needs further refinement. Finite element analysis was also used to simulate the material response at different residual stress and compared with experimental data, results agreed very well building confidence in these measurements. An examination of the 3D stress state either by FEM or a biaxial XRD analysis would further aid in comparison of the techniques. At this stage, nanoindentation was shown a useful tool to explore the otherwise unseen residual stresses.

CHAPTER V

5 USING MICROFOCUS X-RAY COMPUTED TOMOGRAPHY TO EVALUATE FLAWS IN CERAMIC DENTAL CROWNS

The size and distribution of flaws in ceramic dental crowns are important factors that will affect fatigue and fracture. Microfocus X-ray computed tomography (μCT) was used to characterize flaws in three crowns made at different cooling rates to help determine the best manufacturing process. Results show that there are flaws as big as 220 μm in porcelain, and the faster cooling rate corresponds to more flaws but not necessarily big flaws. The crown with the slowest cooling rate had fewer flaws. The corresponding critical fracture stress was predicted based on the biggest flaw from microtomography.

5.1 Introduction

With improved toughness due to the introduction of materials like zirconia and zirconia composites, all-ceramic crowns have become more practical even as they are popular due to their natural color and biocompatibility (Lawn et al., 2012; Lorenzoni et al., 2010). Ceramics are often very brittle and contain a large number of preexisting flaws which formed during processing due to incomplete densification, anisotropic thermal expansion and modulus between grains, for example. These flaws normally distribute unevenly. One ceramic material often displays a range of fracture properties due to variation of flaw size and distribution. In some Cases, crowns fail unexpectedly due to flaws. Flaw size

and distribution are also the reason for differences between experimentally observed and theoretically predicted critical loads for the initiation of contact-induced radial cracks in brittle coatings on compliant substrates (Kelly and Denry, 2008; Lohbauer et al., 2009; Gonzaga et al., 2009; Taskonak et al., 2008; Maranda et al., 2001). Defects and stress formed during manufacture will accelerate failure. Research has shown there are large residual stresses [Mainjot et al., 2011; Zhang et al., 2012]. Lohbauer *et al.,* (2009) analyzed fractography of a failed zirconia frame work and found that the defect cluster in the veneer layer and preexisting stress are reasons of failure, and defects at 35 μm can induce local veneer chipping. Reliability and longevity of all ceramic crowns have always been a concern.

Knowing the flaw size and distribution will be a huge advantage and can help control the quality of crowns or other dental restorations and reduce the failure rate in clinical practice. μCT can be a powerful tool to evaluate the flaws, since it is nondestructive and can successfully visualize and measure the internal structure with almost no material preparation. μCT is efficient and convenient for 3D evaluation. This gives it an advantage over conventional optical microscopes and Secondary Electron Microscopes (SEM). The latter needs samples physically cut into different two dimensional cross-sections, and some 3D information is lost during the process. The disadvantage of μCT is its working spatial resolution is lower than SEM. μCT operates the same way as a conventional medical scanner, but with much higher spatial resolution. The μCT technique is based on the principle that X-rays attenuate as they pass through the object. Since Hounsfield (1973) introduced microtomography to medical science, its application has been extended to geosciences, such as, paleontology, soil science,

petroleum engineering, and sedimentology (Long et al., 2009). Development of new generations of high resolution μCTs in the last decade (Ferrerra de Paiva, 1995) makes it possible to characterize mineral distribution (Yao et al., 2009; Van Geet et al., 2000) and pore structures (Hanan *et al*., 2006; Cnudde et al., 2004).

This study evaluated the flaw size and distribution in three dental crowns made at different cooling rates using μCT and provided information to help determine the optimal manufacturing procedure.

5.2 Experiment

5.2.1 Material Sample Preparation

Three ceramic crowns with a zirconia core (3M LAVA, St. Paul, MN) and porcelain veneer (Noritake CZR, Japan) made at different cooling rates were used to image flaws. Yttiria stabilized polycrystalline zirconia is a preferable dental core material due to its high fracture toughness and flexural strength. Zirconia is well known for its phase transformation, from tetragonal to monoclinic. A second phase of 3% Yttiria was used to stabilize the tetragonal zirconia phase. Porcelain was veneered to zirconia following the typical procedure used by dental labs for zirconia-porcelain crowns. All the manufacturing procedures were the same for the three crowns, except the hold time at high temperature and furnace cool time in the final step. The detailed schedule for the final firing step is listed in Table 5-1. One crown was processed following normal industry standard cooling procedures, while the other two crowns were made at slower and faster than the normal cooling rates. Fig. 5-1 shows an image of the crown.

Fig. 5-1 Photo of a typical crown sample.

Table 5-1 List of high temperature hold time and furnace cooling time in the final firing step.

final firing procedure	high temperature (°C)	hold time (min)	furnace cool time (min)
slow	930	2	8
normal	930	0.5	4
fast	930	0.5	0

5.2.2 Microtomography

A high resolution desktop Skyscan 1172 (Skyscan, Kontich, Belgium) µCT equipped with a 10x megapixel camera and a 100 kV tungsten source was used to scan the crowns. The nominal resolution was less than 1 µm and spatial resolution was less

than 5 µm. The technique is based on Beer's law that the intensity of X-rays will attenuate as they travel through objects.

$$\frac{I}{I_0} = \exp(-\mu t) \tag{1}$$

Where I_0 is intensity of the incoming X-ray beam, I is the intensity of the attenuated X-ray, μ is the linear attenuation coefficient, and t is the material thickness.

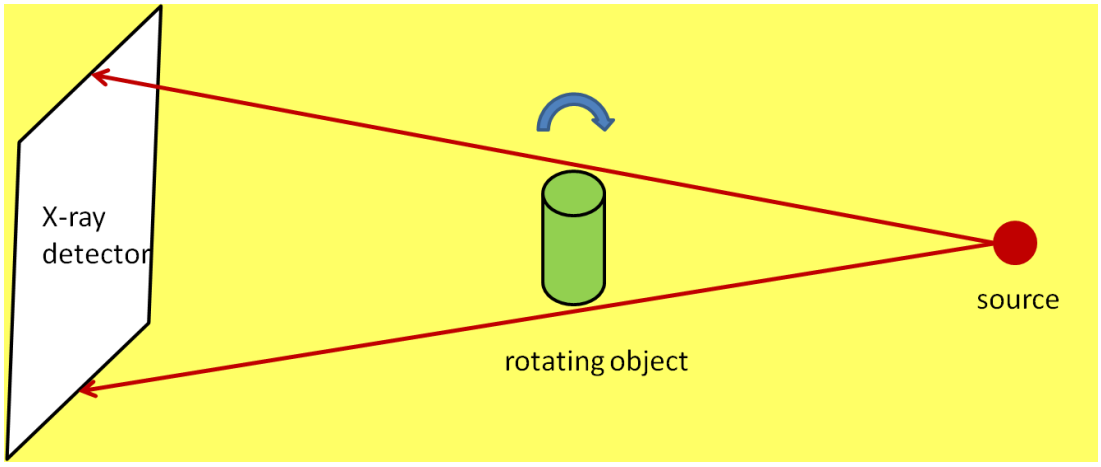

Fig. 5-2 Schematic X-ray µCT setup

The X-ray source was a cone beam. As the crown sample rotates on the high precision stage and X-rays pass through, a series of shadow transmission images were obtained at different angular views. The complete 3D image, representing the internal structure, consists of a stack of 2D cross section images constructed from shadow images using NRecon software (Skyscan, Belgium). A schematic setup of the scanner is shown in Fig. 5-2.

The parameters used for the scan were 100kV power with an exposure time of 474 ms for each frame at a resolution of 14.7 μm. An Al+Cu filter was used to minimize beam hardening. The crowns were scanned at every 1° rotation with four frames for better quality images. It took only 11 minutes to finish scanning one crown at this resolution. 205 radiographs were obtained and were reconstructed into 484 two-dimensional cross section slices. All three crowns were scanned. Three-dimensional rendering software (Amira) was used to visualize the tomographs. Also a small portion of porcelain on top of the cusp, 2.85mm thick, of the slow cooled crown was scanned with a 1.5 μm resolution to quantify the defect size and distribution. Commercial software CTAn (Skyscan, Belgium) was used to analyze the defects.

5.3 Results and discussion

Most ceramics are very poor thermal conductors. It would be natural to think different cooling rates will result in different flaw structures and mechanical behavior. This study examined whether different cooling rates affected the flaw size and distribution. A radiograph and tomography slices in Fig. 5-3 to Fig. 5-5 showed the position and size of flaws in the three crowns. Not all the flaws were shown, but all observed flaws lie between the two green lines marked on the radiographs. Most voids were found on the top one-third portion of the porcelain. There could be some defects in other part of the crown, but they would be harder to detect because of the large attenuation of zirconia. The biggest voids were 220 μm, 162 μm, and 132 μm for crowns with the normal, fast, and slow rates respectively. The fast rate showed 27 flaws larger than 0.75mm, while the slow rate had 6, and the normal cooling rate had 7 locations. The

crown with the fastest cooling rate had more locations with flaws, but the crown with the slower cooling rate had the largest flaw. Additional research on a larger number of samples would provide more conclusive statistics. Fig. 5-6 to Fig. 5-8 showed a typical 2D tomography showing flaws of crows made with different cooling rates.

To quantify the defect size and distribution, a high resolution scan, 1.5 μm, was performed on the top 2.85 mm thickness of the porcelain cusp in the slow cooled crown. Fig. 5-9 showed a 2D tomography of the higher resolution scan. The higher resolution scan produced an image with rich material information and large size digital data. Because of limitations of computation capacity, only a cube area with the size of 1.275x1.275x1.275 mm was considered for defect size and distribution, as shown in Fig. 5-10. The equivalent sphere diameter was used as a parameter to compare the size distribution of defects. The results indicated that most defects were below 30 μm, and there were a couple larger than 50 μm. The higher resolution scan revealed defects at a smaller size which is not obviously seen at lower resolution as shown in Fig. 5-3 to Fig. 5-5.

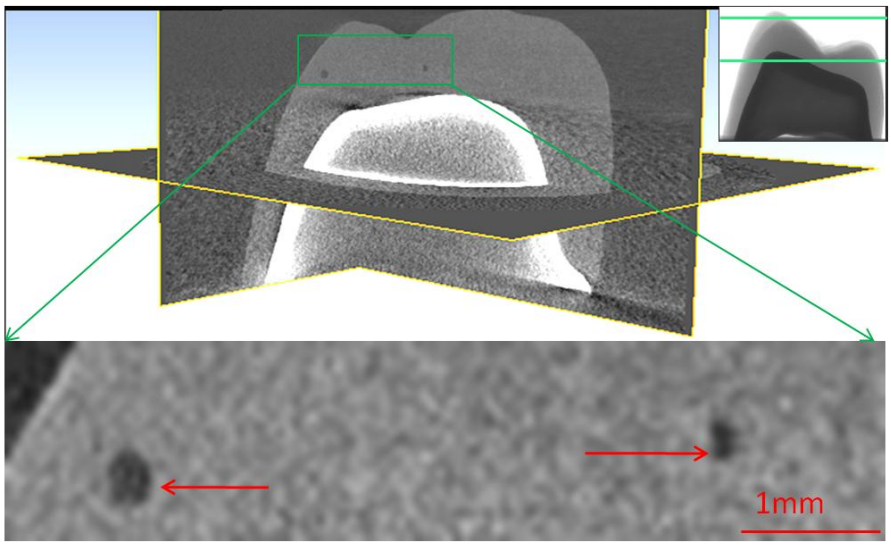

Fig. 5-3 Tomography slices and radiograph (top right corner) of the normal cooling rate crown. Voids as big as 220 µm were observed. All the observed flaws were located between two green lines marked in the inset radiograph.

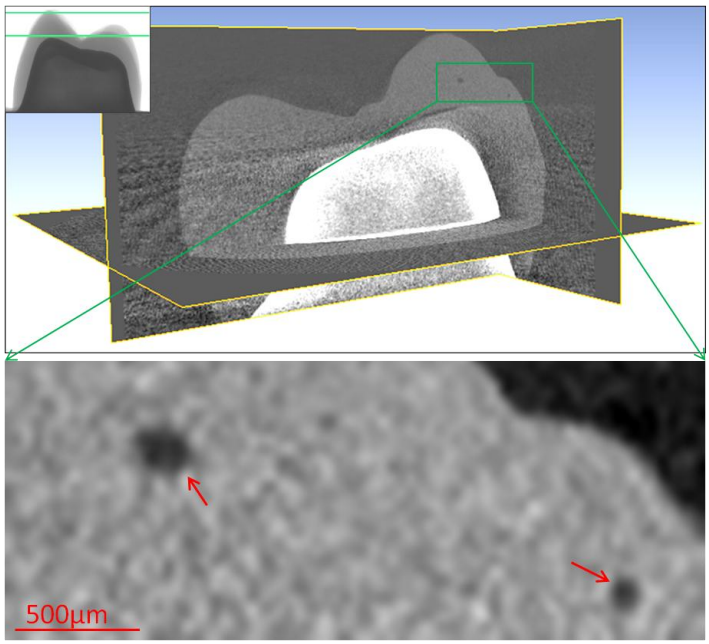

Fig. 5-4 Tomography slices and radiograph (top right corner) of the fast cooling rate crown. Voids as big as 162 µm were observed. All the observed flaws were located between the two green lines marked in the inset radiograph.

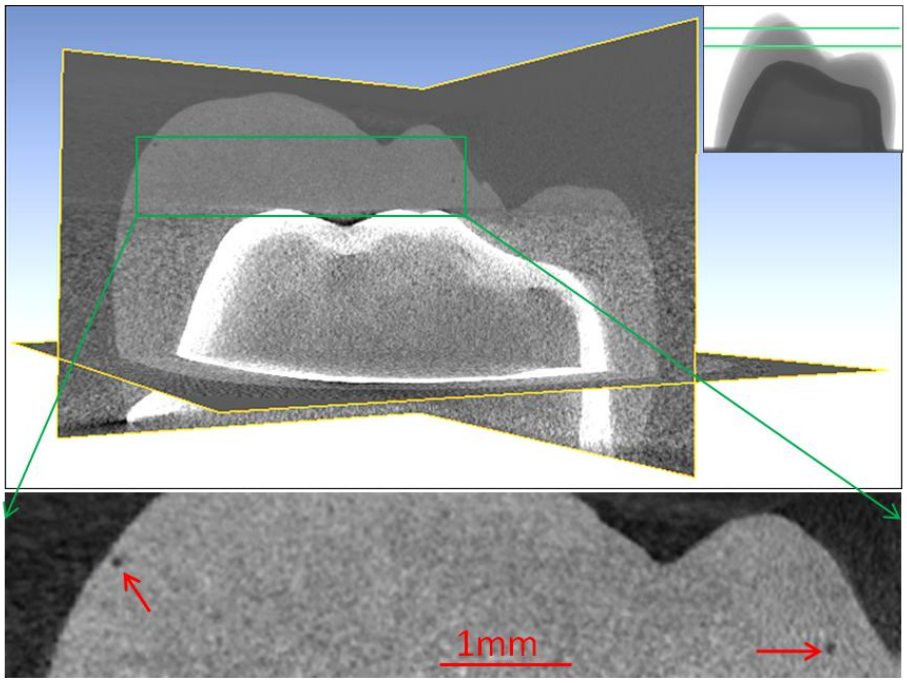

Fig. 5-5 X-ray images from the slow cooled crown similar to the previous figure. Voids as large as 132 µm were observed. All the observed flaws were located between two green lines marked in the inset radiograph.

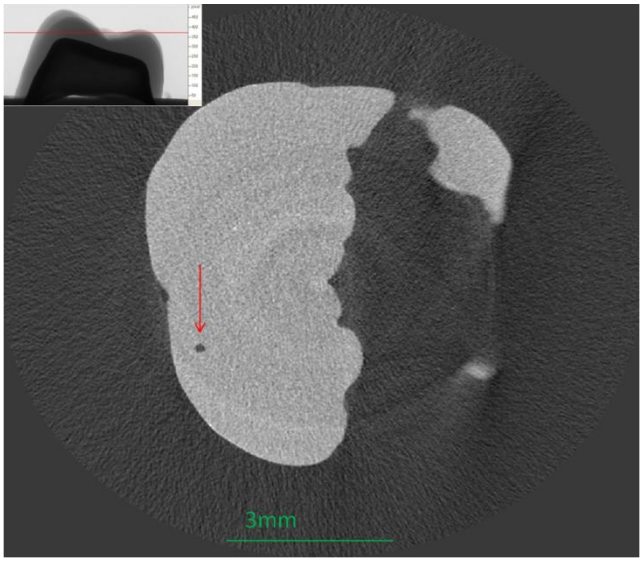

Fig. 5-6 Normal cooling: A 2D tomograph and radiograph to more clearly show the position of one flaw.

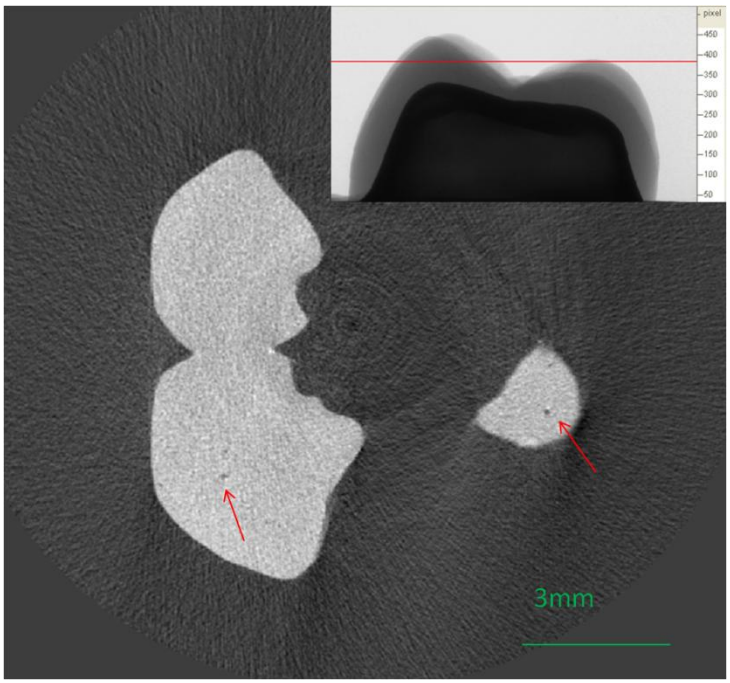

Fig. 5-7 Fast cooling: A 2D tomograph and radiograph more clearly show the position of flaws.

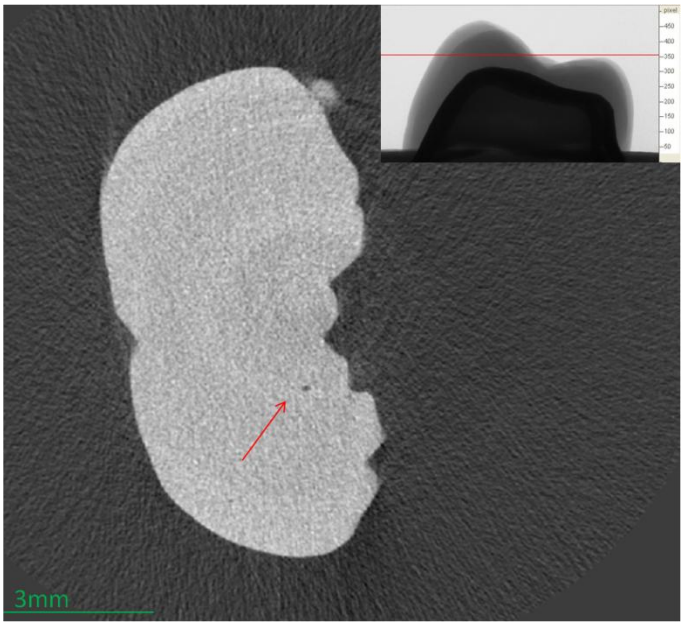

Fig. 5-8 Slow cooling: A 2D tomograph and radiograph to more clearly show the position of one flaw.

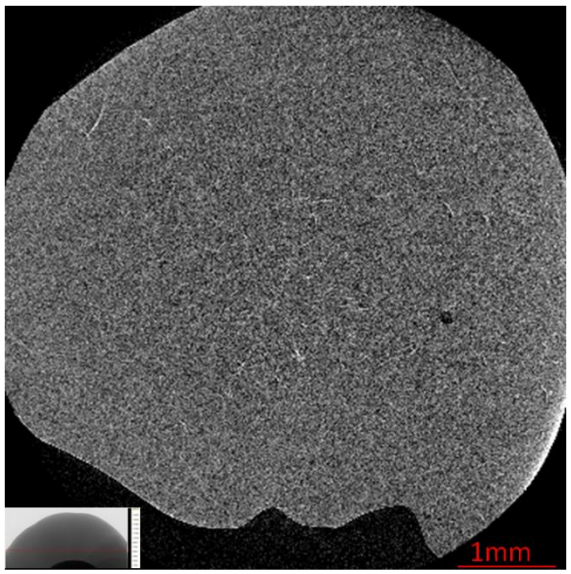

Fig. 5-9 2D tomographs of slow cooled crown with higher resolution scans only on the porcelain cusp.

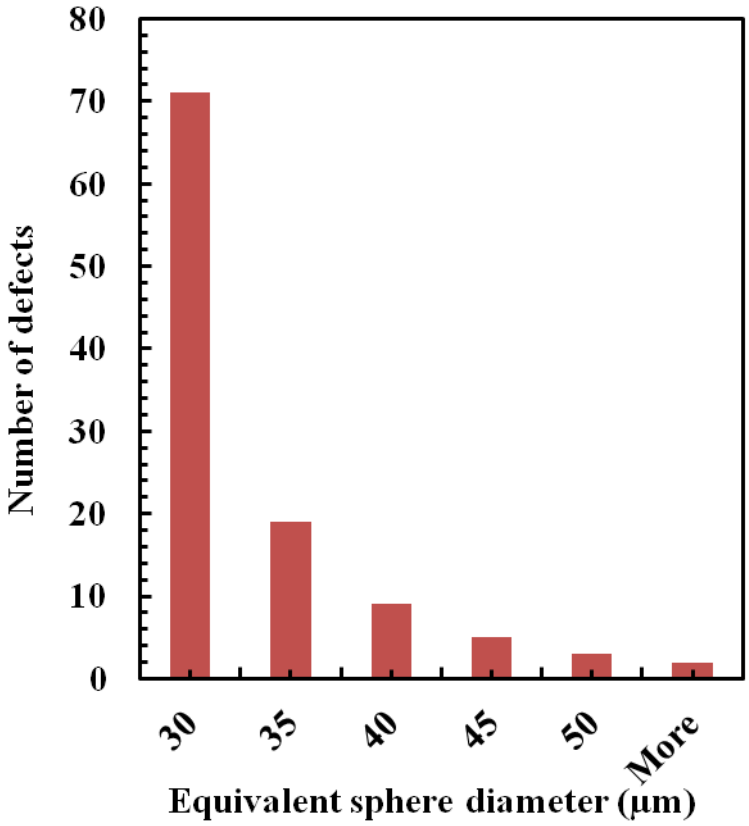

Fig. 5-10 Porcelain defect size distribution in a slow cooled crown scanned at high resolution.

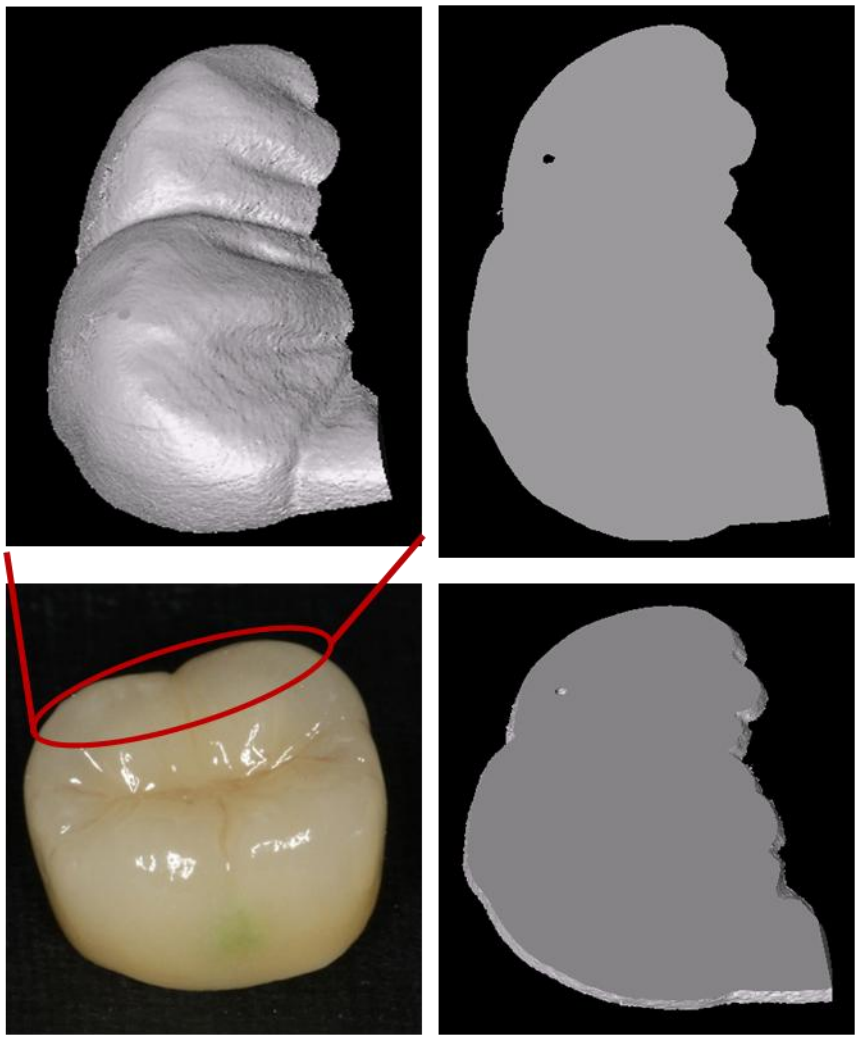

Fig. 5-11 Tomograph formed 3D models showed flaws

Both the number and size of flaws will affect the fracture stress. If the flaw size was the dominant factor for fracture, the critical fracture stress could be predicted based on Griffith Mode I fracture (Lawn, 1993):

$$\sigma_c = \frac{K_{Ic}}{\psi \quad c^{1/2}} \tag{2}$$

Where, σ_c and K_{Ic} are the critical fracture stress and critical stress intensity factor, or fracture toughness, Ψ is a crack geometry related factor, and c is the critical crack length. The flaws were treated as penny-shaped cracks. Porcelain fracture toughness reported in the literature (Taskonak et al., 2008; Morena et al., 1986) are from 0.6~1.5 (MPa.m$^{1/2}$). The value use here was 0.7 MPa.m$^{1/2}$, measured previously on another crown sample. The critical flaws were 220 µm, 162 µm, and 132 µm for the normal, fast, and slow cooled crowns. The predicted critical stress worked out to 42, 49, and 54 MPa, if the crown fails due to the size of its biggest flaws. Typical stresses on the crown in service are caused by a range of geometries. Typical loads can range from 30 to 530 N (Fernandes et al., 2003; Paphangkorakit and Osborn, 1998). Assuming a contact area of 1 mm^2 the above stresses suggested failures at loads as low as 42 N! Using this µCT method, experimental validation could be employed to determine the true load to failure and lifetimes associated with flaws and establish a maximum flaw size or shape safe for use in dentistry.

2D tomography from scanned data could create 3D models to be used for visualization and finite element analysis, as shown in the following chapter. Fig. 5-11 showed a partial crowns model formed from scan data with flaw on it.

5.4 Conclusion

Microtomography was used to evaluate the number and size of the flaws in three crowns made at different cooling rates. The flaws were clearly observed in the tomographs, with the biggest flaw observed at 220 µm. A simplified view suggests such crowns can fail at a stress of 42 MPa, if the flaw size was the dominant factor. The

cooling rate affects the number and size of flaws, with fast cooling produced the more flaws. Additional research on larger number of samples is needed.

CHAPTER VI

6 COOLING RATE EFFECT ON MICROSTRUCTURE AND RESIDUAL STRESS OF ZIRCONIA-PORCELAIN DENTAL CROWNS

This work explained the unique veneered porcelain chipping phenomena of Y-TZP frame crowns by examining the residual stress, microstructure of crowns made with different cooling processes through FEM, SEM. Also the effect of the porcelain's CTE change around the glass transition temperature on residual stress had been studied.

A detailed 3D crown model, created based on μCT data of a real crown, was used to simulate the residual stress formed during the cooling process. The hypothesis was that cooling rate, porcelain's CTE change around glass transition temperature, affected tensile residual stress, microstructure. The residual tensile stress, together with microstructure and flaws change as shown in chapter V, compromised the strength of the crown and resulting early and sometimes unexpected failure. Two different cooling rates and two different porcelain's CTE changes around glass transition temperature were used for the simulation. Residual stress due to only mismatch of constant CTE between zirconia and porcelain was also performed as a comparison. SEM and μCT were used to examine the microstructure and flaw distribution difference of the crowns made at different cooling rate.

Residual stress was obtained for the whole crown. Cooling rate and porcelain's CTE change effects on residual stress are correlated. When porcelain's CTE changed during glass transition, tensile stress existed in the porcelain veneer. This was especially apparent in the cusp with thicker porcelain, there was a tensile stress zone beneath the more compressive surface and above zirconia-porcelain interface, which could explain why chipping was seen in the cusp area, and won't crack all the way to the interface. Cooling rate had effect on residual stress, but its magnitude depended on the porcelain's CTE change during the glass transition region. If the porcelain CTE change was large the residual tensile stress was large. If the porcelain CTE change was small, the cooling rate effect was very small. Matching CTE between zirconia and porcelain veneer should consider the effect of porcelain CTE change during the glass transition. Tempering stress obviously exited, especially apparent in parts with thicker porcelain. Fast cooling resulted in more thermal tempering stress. The SEM showed no apparent microstructure difference at different cooling rate, even though in chapter V μCT showed fast cooling had more random flaws. Slow cooling process showed better performance comparing to fast cooling. It not only reduced residual stress as describe in this chapter, but also reduced processing flaws as shown in chapter V.

6.1 Introduction

All-ceramic dental crowns became more and more popular due to esthetics and biocompatibility. However, most of them had a tendency to fracture easily. With the introduction of the more tough material zirconia, the strength and toughness of the crown had been improved. But a new problem appeared which was chipping of the porcelain

layer over the zirconia, especially in the cusp area (Pjetursson *et al*., 2008; Tholey *et al*., 2011). This was a fracture behavior associated with the zirconia-porcelain framework. Metal crowns and other all-ceramic dental materials did not show the same fracture phenomena. One hypothesis was that residual stress formed during cooling of the crowns attributed this unique fracture behavior because poor thermal diffusivity of the zirconia. Accurately measuring residual stress in the crown was extremely difficult because of phase transformation, zero strain reference and spatial limitations (Zhang *et al*., 2012; Allahkarami and Hanan, 2011). Due to lack of analytical solutions for the complex shape of the crowns and fixed partial dentures, numerical simulation had became an effective way to predict the transient temperature, transient stress, and residual stress.

To optimize dental crown design, Dehoff *et al.* (2006) analyzed the residual stress state in a three unit fixed partial denture and found a large amount of residual stress present. The magnitude was large comparing to the flexural strength of porcelain, and indicated it could jeopardize survival under occlusal loading. Dehoff *et al.* (1996) analyzed the tempering stresses in metal-ceramic disks at different cooling rates, and found that larger cooling rates would result in more tensile stress in porcelain. Asaoka *et al*. (1992) and Asaoka and Tesk (1989) studied the tempering residual stress of porcelain using layered samples. Jager *et al.* (2006) and Sorrentino *et al.* (2007) analyzed the influence of different core materials using FEM determined stress distribution in dental crowns. Rafferty *et al.* (2010) used the FEM method to analyze the maximum principle stress related to different design features of a three dimensional molar crown. Even though there were some studies about the cooling rate effect on the residual stress, most had been limited to disk bilayer samples and crowns with metal or porcelain core.

Geometry effects on residual stress were very important and in some conditions were more profound than mismatch of the CTE. Lenz *et al*. (2002) studied metallic crowns and found curvature would increase the residual stress due to mismatch of the CTE. Bertolotti (1980) found the effect of curvature on residual stress was far more apparent than mismatch of thermal expansion. The need to study the effect of mismatch in CTE, tempering, and geometry on residual stress with detail 3D model were imminent. Choi *et al* (2011) evaluated experimentally the cooling rate effect on the residual stress with disk Y-TZP samples and conclude cooling rate affect the residual stress and recommend slow cooling for the last cycle. However the demand on the dental lab encourages minimizing cooling time. Tholey *et al* (2011) experimentally studied two crown designs to evaluate the temperature gradient and residual stress. They showed that a large temperature gradient exists and slow cooling would decrease the temperature gradient and eventually minimize the residual stress. Even though many studies have been done on Y-TZP crowns, transient residual stress analysis from detail 3D models had not been done. 3D model studies offer the possibility of improving the efficiency and selection of thermal processing.

Besides residual stress, processing flaws could also be the primary cause of fracture. Quinn *et al.* (2011) and Lohbauer *et al.* (2010) did fractography studies on fractured crown for both porcelain and zirconia. Their work showed that if the flaws clustered together, two or three flaws with edges touch each other or one single flaw with an edge touching surface, they would very likely cause fracture. Flaws with the size as small as 35μm could cause local failure, even in zirconia.

This work studied cooling rate and porcelain CTE change effects on residual stress using a detailed 3D crown model. The 3D crown model was created from μCT tomography data of a real crown. The residual stress was also compared to residual stress formed only because of mismatch of constant CTE. Also this study examined cooling rate effect on microstructure by imaging three crowns cooled differently with SEM.

6.2 Materials and Methods

6.2.1 Finite Element Method

A detailed 3D crown model based on μCT data was used to simulate residual stress formed during the final cooling process in commercial finite element analysis software ABAQUS 6.9–1. A Y-TZP dental crown was scanned with a desktop 1172 μCT (Skyscan, Kontich, Belgium) scanner, then a solid 3D model and finite mesh was created in Amira 4.1 based on the scanned tomography. The original scan resolution was 9 μm, but because of computation capacity limitations, the originally scanned image had to be re-sampled to resolution of 18 μm when forming the 3D solid model. The flaws showed on the high resolution scan were lost during re-sampling. Therefore, the solid model was isotropic and contained no flaws. 3D model formed in Amira was imported to ABAQUS as an input. The detailed model is shown in Fig. 6-1. The zirconia core thickness ranges 0.5 to 0.7 mm and the porcelain thickness varied from 1 to 2.6 mm. There were 1008757 tetrahedral elements and 185429 nodes in the model. The element types were DC3D4 for heat transfer and C3D4 for stress analysis. The simulation required a sequential thermal-mechanical simulation procedure. First, a heat transfer analysis simulated the crown cooling process from the heat soak temperature of 600 °C to

heat sink temperature of 25 °C to obtain the temperature at each node at any time point. Then the temperature was used as a boundary condition in the sub-sequential stress analysis to obtain the final residual stress. Dental labs often used a tempering process to achieve a porcelain surface with more compressive residual stress than the inside to restrain crack growth. Two different cooling conditions, fast and slow, simulated the tempering and bench cooling process. The tempering process often achieved by blowing a stream of cold air. Anusavice *et al*. (1989) had measured the tempering heat transfer coefficient for a porcelain-porcelain system at 560 W/m^2-C and bench cooling with a heat transfer coefficient of 17 W/m^2-C. They were used as the film coefficient for the simulation. The CTE of porcelain often changed significantly below and above the glass transition region. Two porcelain CTE changing cases, $\Delta\alpha=5x\ 10^{-6}$ and $\Delta\alpha=20x\ 10^{-6}$ were used here. Residual stress formed due to only the mismatch of a constant CTE between zirconia and porcelain was also carried out as a comparison. For the boundary conditions, only some nodes in the bottom of the crown were restricted to movement in the normal direction of the surface where the crown would rest.

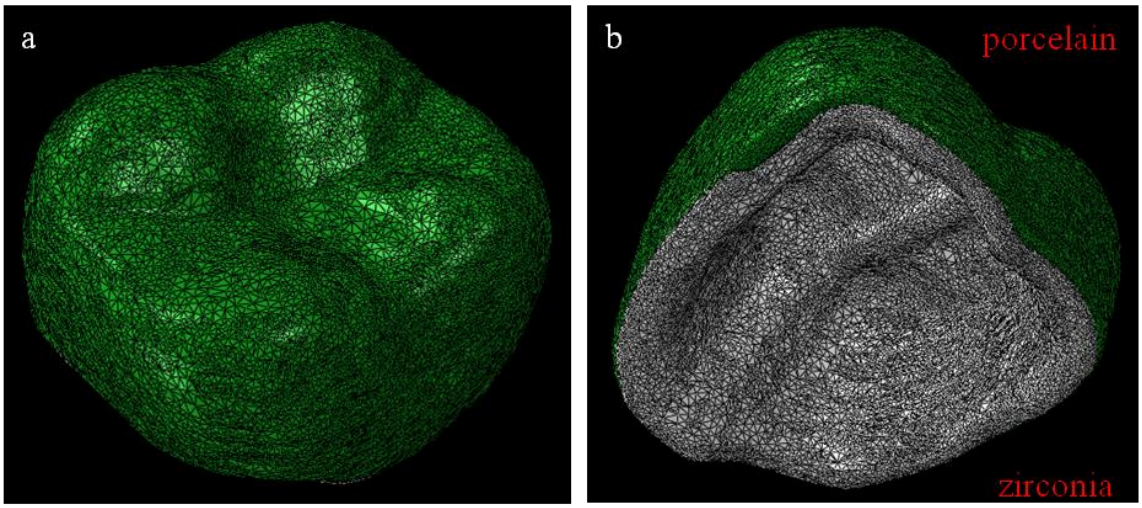

Fig. 6-1 Finite element model for zirconia-porcelain crown, material in green was veneered porcelain and material in gray was Y-TZP core (a) occlusal view (b) bottom view

Zirconia was assumed to behave elastically in all cases. In one case for comparison purposes porcelain was assumed to behave elastically and all the parameters including the CTE and Young's modulus were constant during cooling. In any other cases, the porcelain was assumed to be elastic perfectly plastic. Porcelain's CTE and Young's Modulus were assumed to be temperature dependent through the glass transition temperature, 500 to 600 ºC, and assumed linear with increase in temperature. The glass transition temperature was assumed to start at 500 ºC and end at 600 ºC. It was assumed the properties were constant below the glass transition temperature. All the material parameters used in the simulation are listed in Table 6-1(Swain, 2009; Dehoff *et al*., 2008). The simulation covers temperature ranges from a heat soak temperature of 600 ºC to the heat sink temperature of 25 ºC.

Table 6-1 Porcelain and zirconia thermal and mechanical properties.

	Young's Modulus (GPa)	Powasson's ratio	Yield stress (MPa)	CTE ($x10^{-6}$)	Thermal conductivity (W/m-K)	Specific heat (J/kg-K)	Density (g/cm^3)	Temperature (°C)
porcelain	70	0.25	200	10	2	840	2.4	25
	70	0.25	200	10	2	840	2.4	500
	7	0.25	20	15(30)*	2	840	2.4	600
zirconia	205	0.25		11	2	450	6	600~25

*****Two cases were simulated

6.2.2 SEM

Three ceramic crowns with a 3% Y-TZP core (3M LAVA, St. Paul, MN) and porcelain veneer (Noritake CZR, Japan) made at different cooling rates were used to image microstructure with SEM. All the manufacturing procedures were the same for the three crowns except the hold time at high temperature and furnace cool time in the final cooling step. The schedule for the final firing step is the same as those listed in Table 5-1. One crown was processed following the normal industry standard cooling procedure, while the other two crowns were made at slower and faster than the normal cooling rates. A Quanta ESEM 600 was used to image the microstructure. The commercial software Skyscan CTAn (Skyscan, Belgium) was used to measure the flaw size and pore distribution from SEM images.

6.3 Results

6.3.1 Finite element analysis

Temperature and stress at any part of the model at any time during the cooling process could be extracted, but only results related to this work's interest: temperature gradient, transient stress and residual stress, is presented. During the simulation, the temperature history was obtained during the heat transfer step for every node in the model during the whole cooling process from 600 to 25 °C. The temperature gradient in the cusp was of particular interest since that was where chipping typically occurs. Fig. 6-2 shows temperature history for five representative points along the thickness in the cusp area. These five represented points were at the outside surface of the porcelain, middle point of the porcelain, the porcelain and zirconia interface, and the middle point

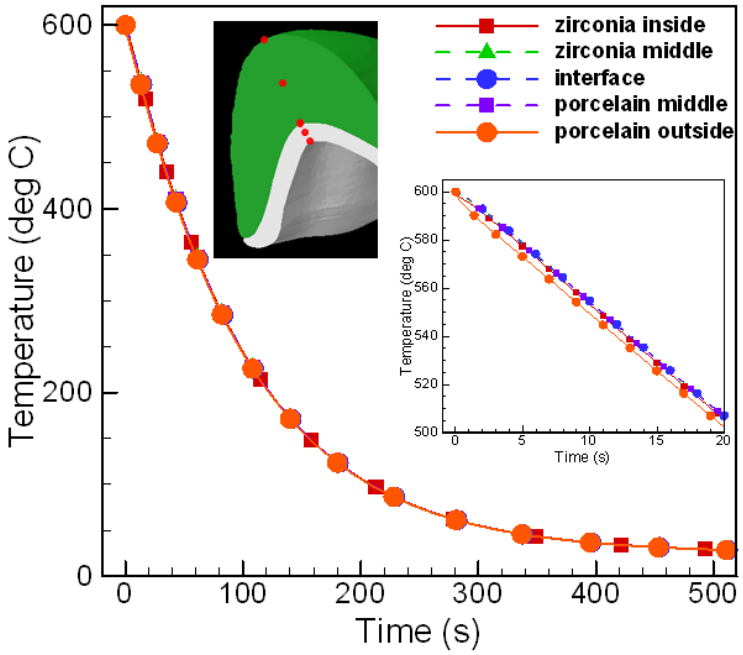

(a)

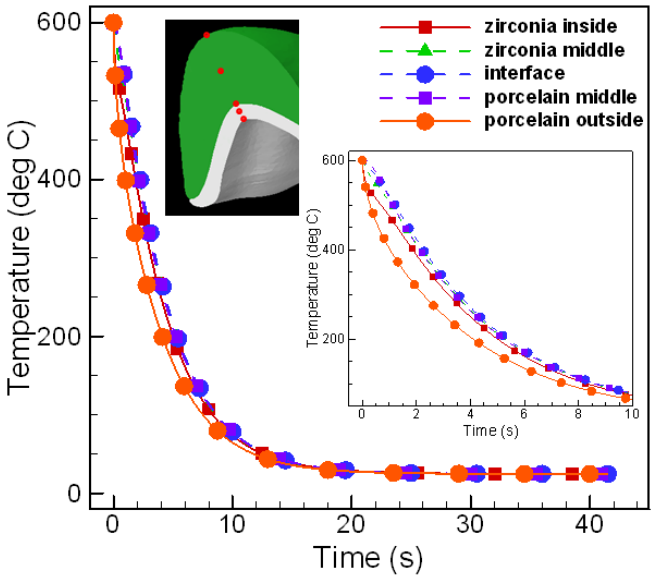

(b)

Fig. 6-2 Temperature history during cooling (a) slow cooling (b) fast cooling

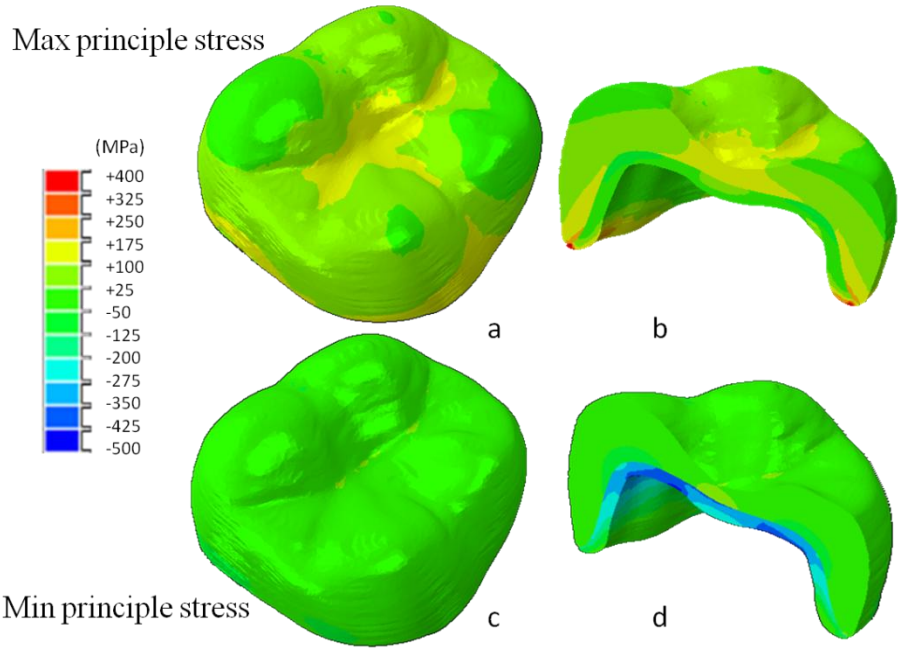

Fig. 6-3 Fast cooling (a) occlusal view of the maximum principle stress (b) cross section view of the maximum principle stress (c) occlusal view of the minimum principle stress (d) cross section view of the minimum principle stress.

of zirconia and inside surface of zirconia, as marked on the crown shown in the inset in the graph. Fig. 6-2a shows the slow cooling process. Fig. 6-2b represents for the fast cooling process. For both cases, the porcelain and zirconia outside the surface cooled faster than its inner surface. Also the porcelain outside surface was cooled faster than the zirconia inside surface. The biggest temperature gradient was between the porcelain outside surface and the zirconia-porcelain interface. The Temperature gradient was very large for fast cooling with a maximum difference of 118 °C. There were relatively small temperature gradients for the slow cooling which was at 6 °C. It took 20s for the whole crown to reach room temperature for fast cooling and 400s for slow cooling.

During cooling, stress formed due to the mismatch of coefficient of thermal expansion, and thermal temperature gradients. The resulting stress at room temperature was the residual stress. Fig. 6-3 plotted the maximum and minimum principle stress to show tensile and compressive residual stress in the composite crown formed during the fast cooling process with porcelain's CTE change of $\Delta\alpha=5x10^{-6}$. Fig. 6-3a shows the occlusal view of the maximum principle stress. Fig. 6-3b shows a cross section view of the maximum principle stress distribution and Fig. 6-3c is the occlusal view of the minimum principle stress. Fig. 6-3d shows cross sectional view of the minimum principle stress distribution. In general, porcelain had more tensile stress while zirconia had more compressive stress. There was a tensile stress zone beneath the more compressive porcelain surface and porcelain-zirconia interface in the cusp area. This could explain the unique chipping behavior associated with Y-TZP framework crowns, where chipping does not continue all the way through the interface, and presents a layer of porcelain left after chipping. The cusp area where the porcelain layer was thicker behaves differently

from other locations. From the occlusal and cross section view of maximum principle stress, the thicker the porcelain, the more compressive porcelain outside and the more tensile inside. The shape of the curvature also affected the residual stress. A curved in shape, like the cusp area, had more compressive stress in the porcelain surface. A curved out shape, like the area between the cusps, had more tensile in the porcelain surface. The case for slow cooling shows a similar trend as the results obtained from fast cooling, only the magnitude of the stresses were smaller. Fig. 6-4 shows stress map for the case of residual stress caused only by mismatch of a constant CTE. Fig. 6-4a shows the occlusal view of the maximum principle stress. Fig. 6-4b shows a cross section view of the maximum principle stress distribution and Fig. 6-4c is the occlusal view of the minimum principle stress. Fig. 6-4d shows cross section view of the minimum principle stress distribution. Because the CTE was treated as constant during the cooling process, and zirconia's CTE is $1x10^{-6}$ larger than porcelain's CTE, porcelain was more compressive while zirconia was more tensile.

To further quantify the cooling rate effect on residual stress, the magnitude of residual stress over a diagonal cross section of the crown at five different locations, as shown in the inset of Fig. 6-5 and Fig. 6-6, for the three simulated condition was compared and details are plotted in Fig. 6-5 and Fig. 6-6. Fig. 6-5 is for the maximum principle stress. Fig. 6-6 is for the minimum principle stress. Fig. 6-5a shows the case assuming both porcelain and zirconia have a constant CTE and behave elastically. Zirconia layer had tensile stress. The maximum principle stress in zirconia ranges from 76 to 106 MPa. Fig. 6-5b and Fig. 6-5c show the maximum principle stress for fast cooling and slow cooling, assuming a porcelain CTE change of $\Delta\alpha=5x10^{-6}$. Porcelain

layer had tensile stress. The maximum principle stress in porcelain ranges from 6 to 128 MPa for fast cooling, and from 7 to 127MPa for slow cooling. The stresses at these five locations were different, especially at the cusp area (path 2 and 4). Residual stress along thickness showed a tensile hump which showed the effect of tempering. The stress had an opposite trend across path 2, 4 and path 3, which showed curvature's impact on the residual stress. Fig. 6-5d compared the model with the elastic properties and a constant CTE with fast cooling and slow cooling models with a CTE change $\Delta\alpha=5x10^{-6}$ for the location along line 2, which lies in the cusp area. For the case with constant porcelain CTE, the maximum tensile stress occurred at the porcelain–zirconia interface with a magnitude of 26 MPa on porcelain. For the case with changing porcelain CTE and temperature dependent material properties, the results showed a tensile zone inside the porcelain layer. Different cooling rate affects magnitude and location of the tensile stress , for faster cooling rate the location with the maximum tensile more toward the interface with magnitude at 85 MPa. While for slow cooling the location was more toward the porcelain surface with a magnitude at 79 MPa. The magnitude of the residual stress for fast cooling was larger. Cooling rate had an effect on the residual stress. Fig. 6-5b shows that stress gradients at the cusp were especially high with an outside stress of 6MPa and inside tensile stress at 85MPa. Considering thermal tempering, temperature dependent material properties, especially the CTE, produced different results than using constant properties.

Fig. 6-6plots the minimum principle stress which shows the compressive stress in the composite dental crowns. Fig. 6-6a shows the case assuming both porcelain and zirconia have constant CTE and behave elastically. Porcelain had the maximum

compressive residual stress and its magnitude ranges from -36 to - 9 MPa. Fig. 6-6b and 6-6c show the minimum principle stress for fast cooling and slow cooling assuming porcelain's CTE changed $\Delta\alpha=5x10^{-6}$. Fig. 6-6b shows the results from fast cooling with the magnitude for minimum principle stress ranging from -364 to -263 MPa. Fig. 6-6c shows the results from slow cooling with the magnitude for minimum principle stress ranging from-361 to -262 MPa. Fig. 6-6d compares the minimum principle stress of the model with elastic properties and constant CTE with fast cooling and slow cooling models with a CTE change of $\Delta\alpha=5x10^{-6}$ for the location along path 2. For constant CTE, the minimum principle stress was in porcelain with a magnitude of -28 MPa. For slow

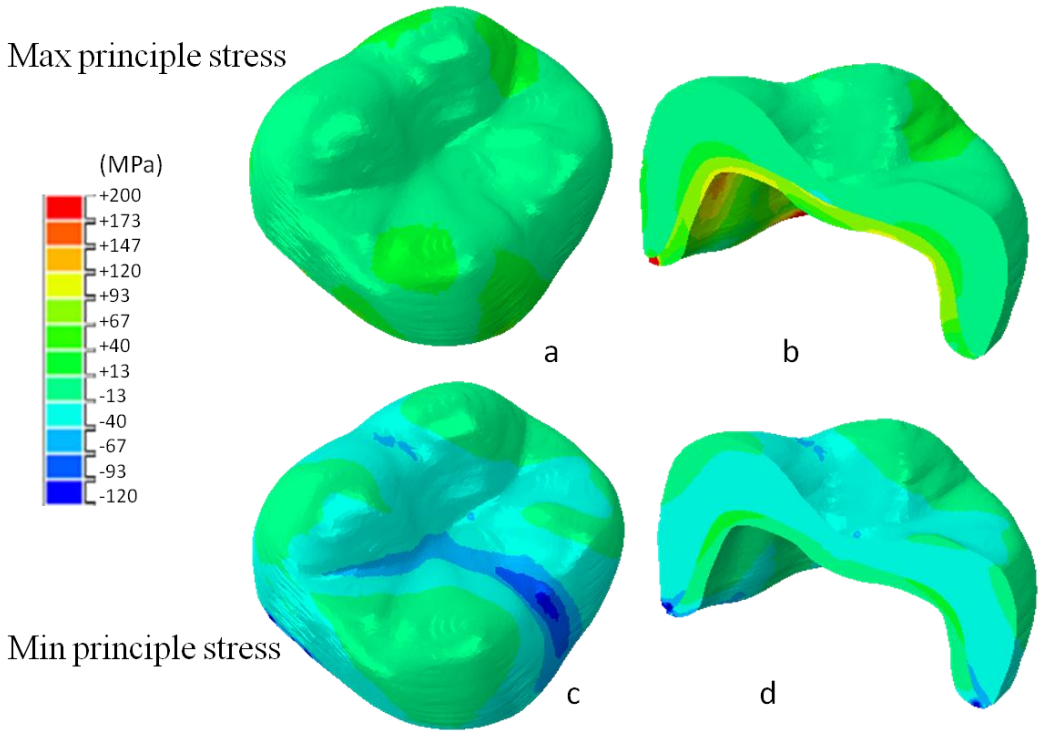

Fig. 6-4 Elastic, constant CTE (a) occlusal view of maximum principle stress (b) cross section view maximum principle stress (c) occlusal view of minimum principle stress (d) cross section view minimum principle stress.

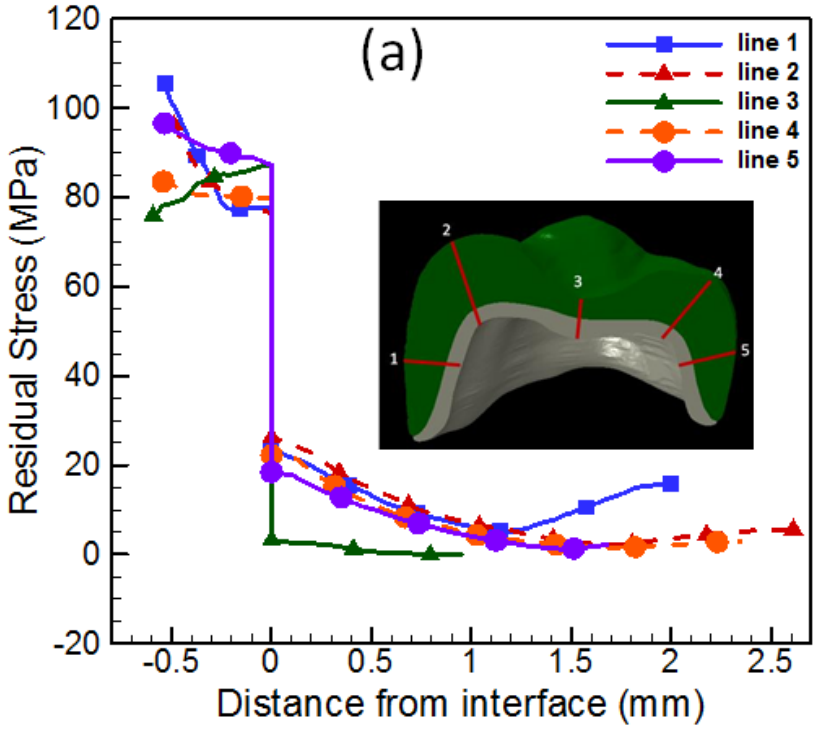
(a)
line 1
line 2
line 3
line 4
line 5
Residual Stress (MPa)
Distance from interface (mm)
120
100
80
60
40
20
0
-20
-0.5
0
0.5
1
1.5
2
2.5
1
2
3
4
5

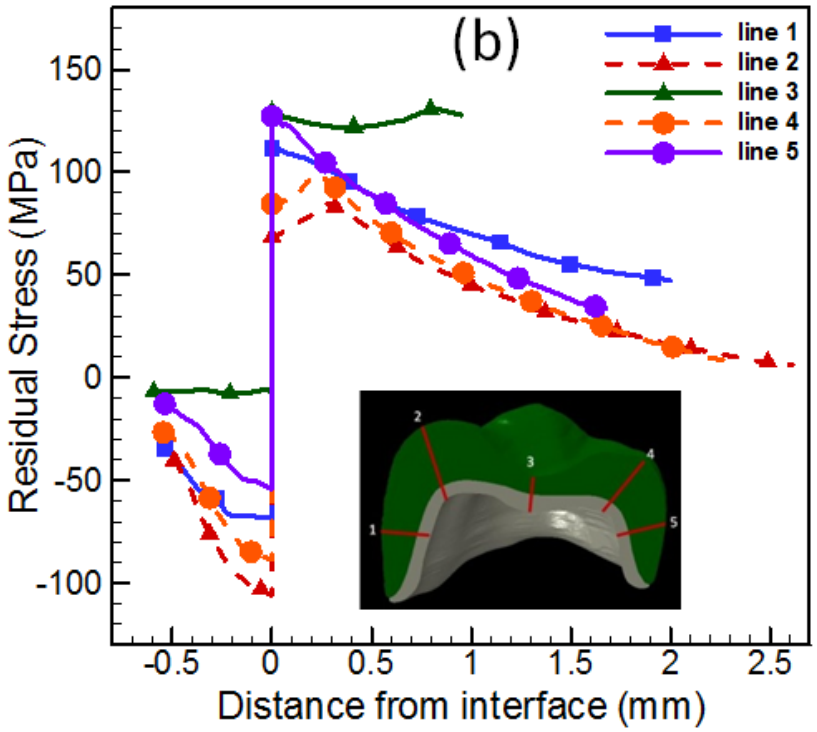
(b)
line 1
line 2
line 3
line 4
line 5
Residual Stress (MPa)
Distance from interface (mm)
150
100
50
0
-50
-100
-0.5
0
0.5
1
1.5
2
2.5
1
2
3
4
5

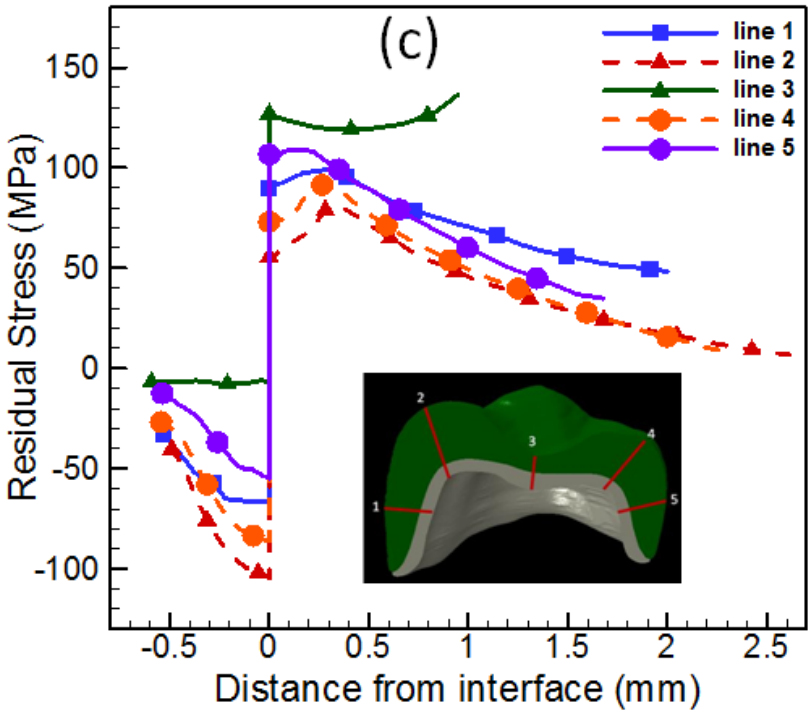

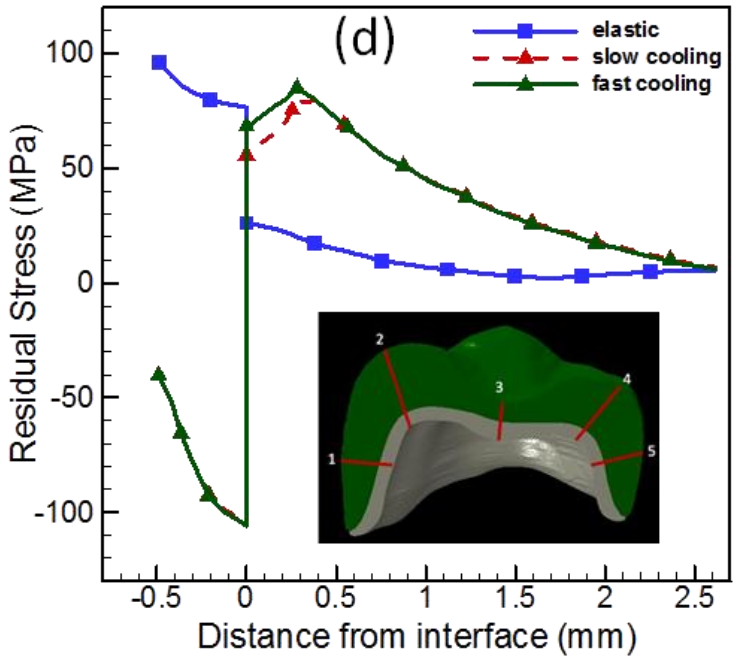

Fig. 6-5 Maximum principle stress along five locations (a) elastic constant CTE (b) fast cooling (c) slow cooling (d) along line 2

cooling and fast cooling, minimum principle stresses were at the zirconia inside surface with a magnitude of -285 MPa, and -293MPa, respectively.

If the CTE reached 30 x10^{-6} at 600 °C, the effect was much larger. Fig. 6-7 shows the maximum principle stress and the minimum principle stress. The places with the maximum tensile stress were both in porcelain with the magnitude for slow cooling and fast cooling at 146 and 220 MPa respectively. The maximum was in the middle of the porcelain thickness. The porcelain outside surface for slow and fast cooling were 15and -4 MPa, interface was -50 and 101 MPa for slow and fast cooled. Zirconia was more compressive and the minimum principle stress was in zirconia. The minimum principle stress was at the zirconia inside surface with slow cooled and fast cooled at -686, and -382 MPa.

Fig. 6-8 describes the transient stress during slow cooling at the surface of the porcelain, inside surface of zirconia, and the inside surface of porcelain in the cusp area.

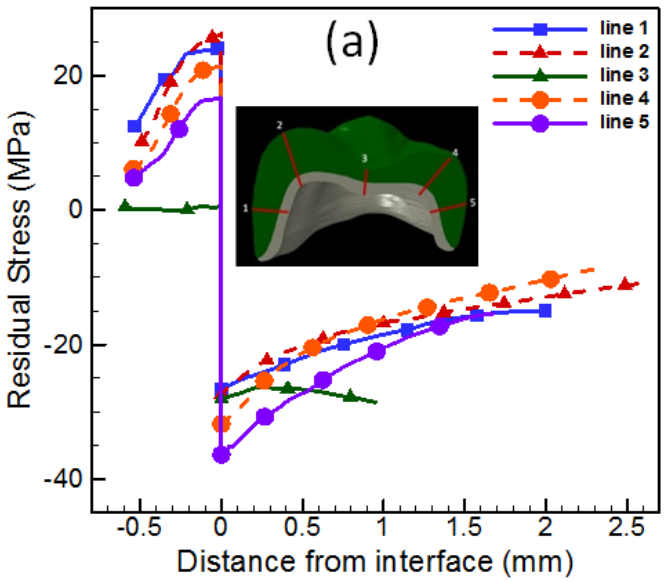

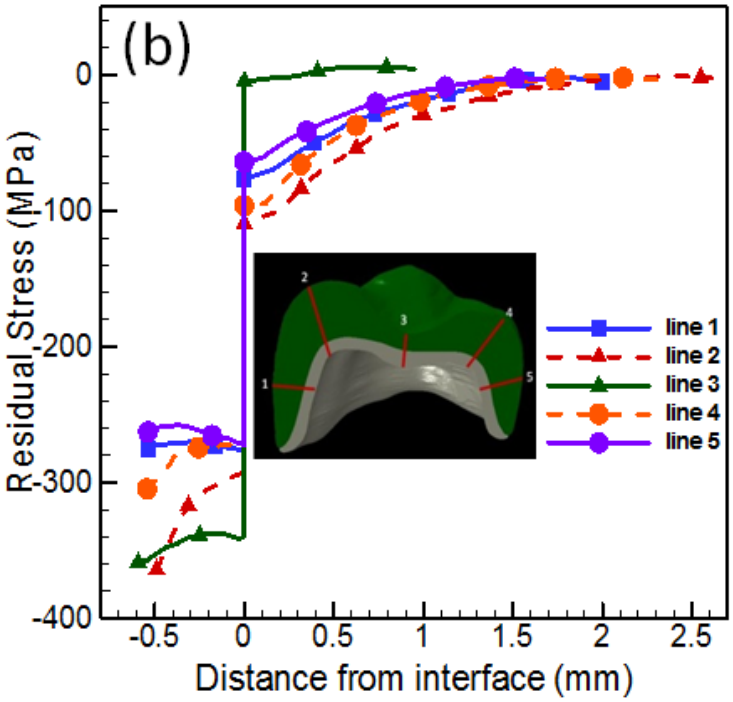
(b)
Residual Stress (MPa)
0
-100
-200
-300
-400
-0.5
0
0.5
1
1.5
2
2.5
Distance from interface (mm)
line 1
line 2
line 3
line 4
line 5
1
2
3
4
5

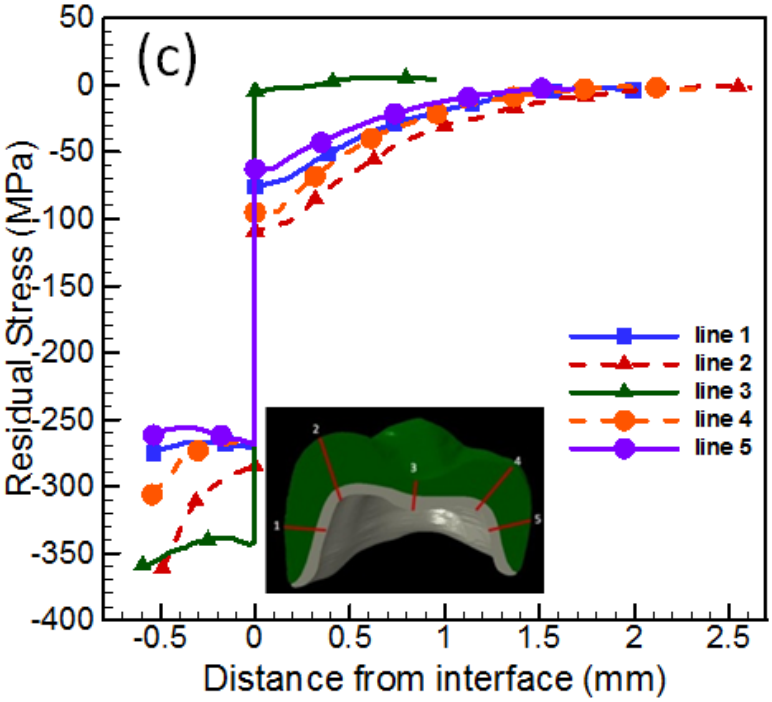
(c)
Residual Stress (MPa)
50
0
-50
-100
-150
-200
-250
-300
-350
-400
-0.5
0
0.5
1
1.5
2
2.5
Distance from interface (mm)
line 1
line 2
line 3
line 4
line 5
1
2
3
4
5

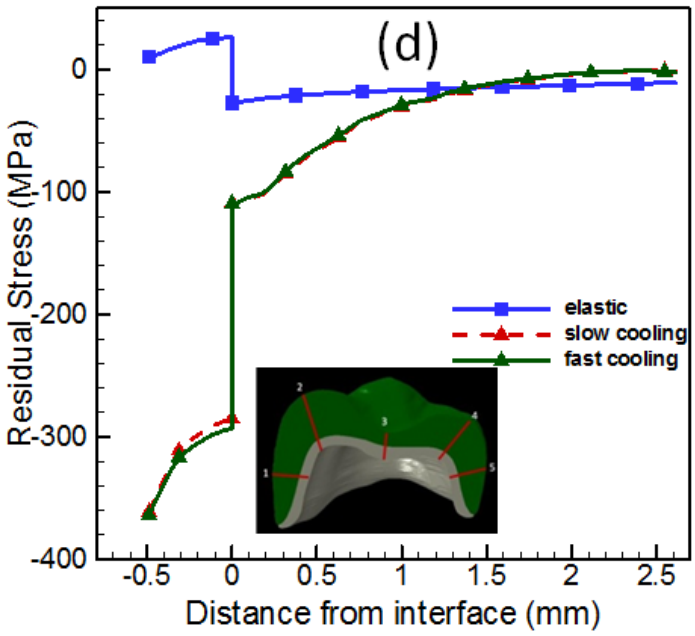

Fig. 6-6 Minimum principle stress along five locations (a) elastic, constant CTE (b) fast cooling (c) slow cooling (d) along line 2

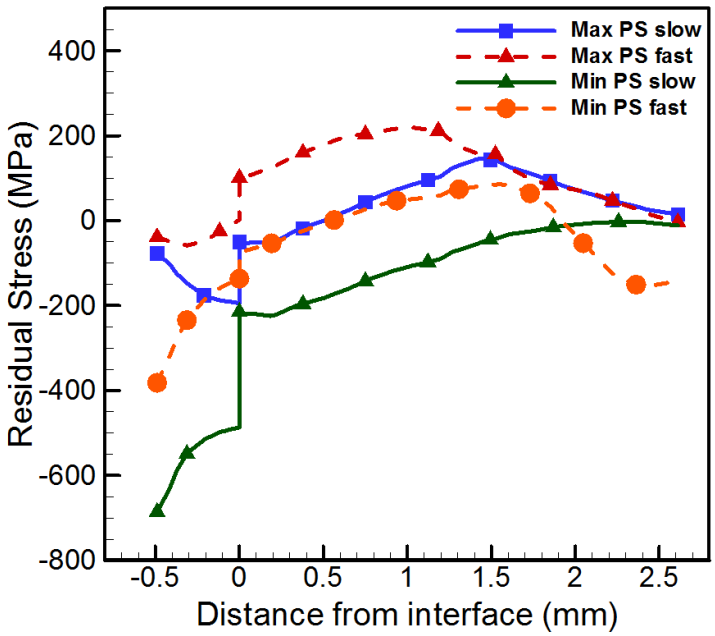

Fig. 6-7 Maximum and minimum principle stress formed during slow and fast cooling assuming the CTE=30x10^{-6} at t = 600^{o}C.

Stress forms and increases as it approaches the glass transition region and relaxes as it cools down. The maximum tensile stress is in the middle of the porcelain layer and its magnitude is at 48 MPa, while zirconia inside surface and porcelain's outside surface has a stress of -57 and 15 MPa, respectively.

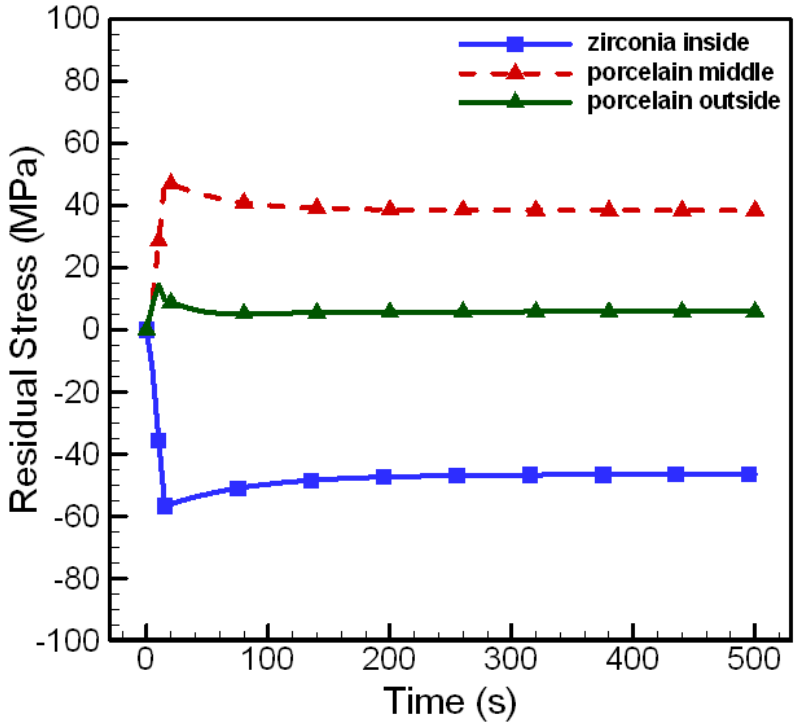

Fig. 6-8 Stress history during the slow cooling process for three locations on the crown in the cusp area

6.3.2 SEM

Microstructure of the three crown with different cooling rates was shown in Fig. 6-9. Pore analysis was shown in Fig. 6-10. A 7 μm x 7μm area as marked in Fig. 6-9 was used for pore analysis. Most pores were below 50nm. For pore size smaller than 50nm, fast cooled had less pores than normal and slow cooled. Normal cool had more than slow cooled. For pore sizes larger than 50 nm, the distribution was random. There were no

clear trends for how cooling rate affects the pore size, so the cooling rate must not significantly affect the pore size.

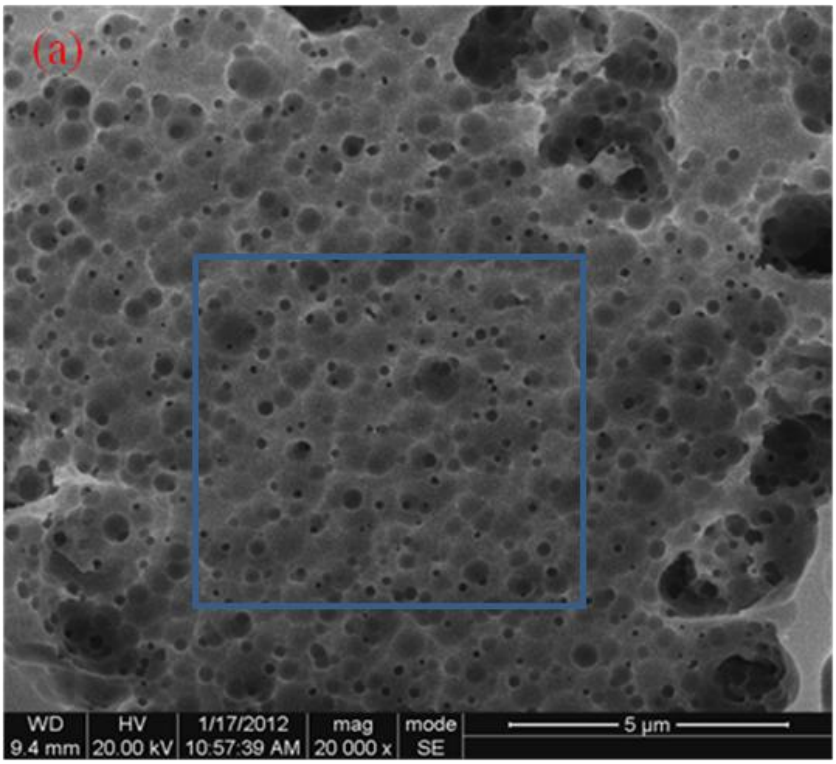

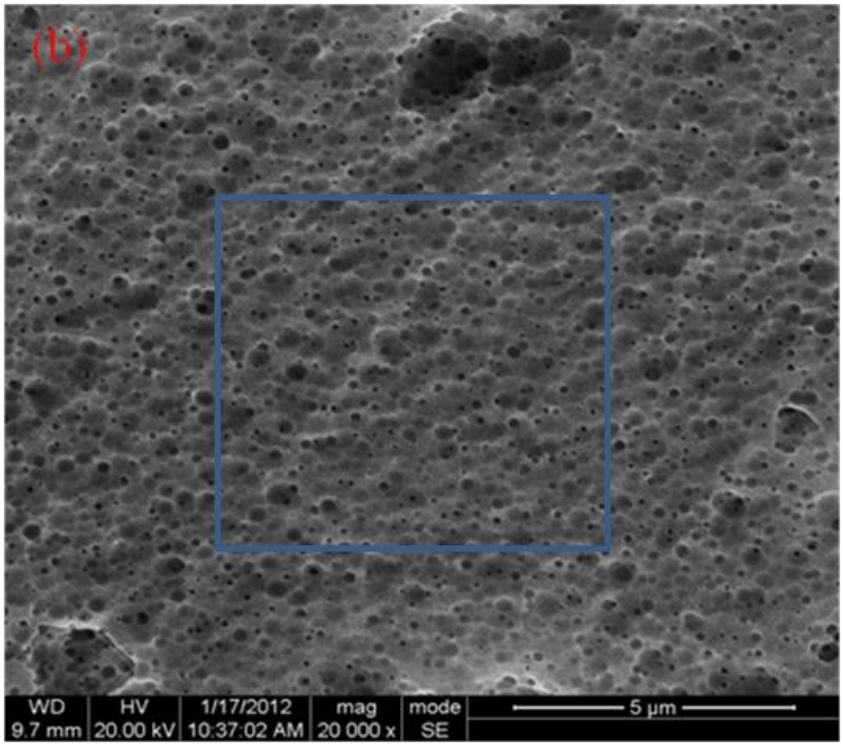

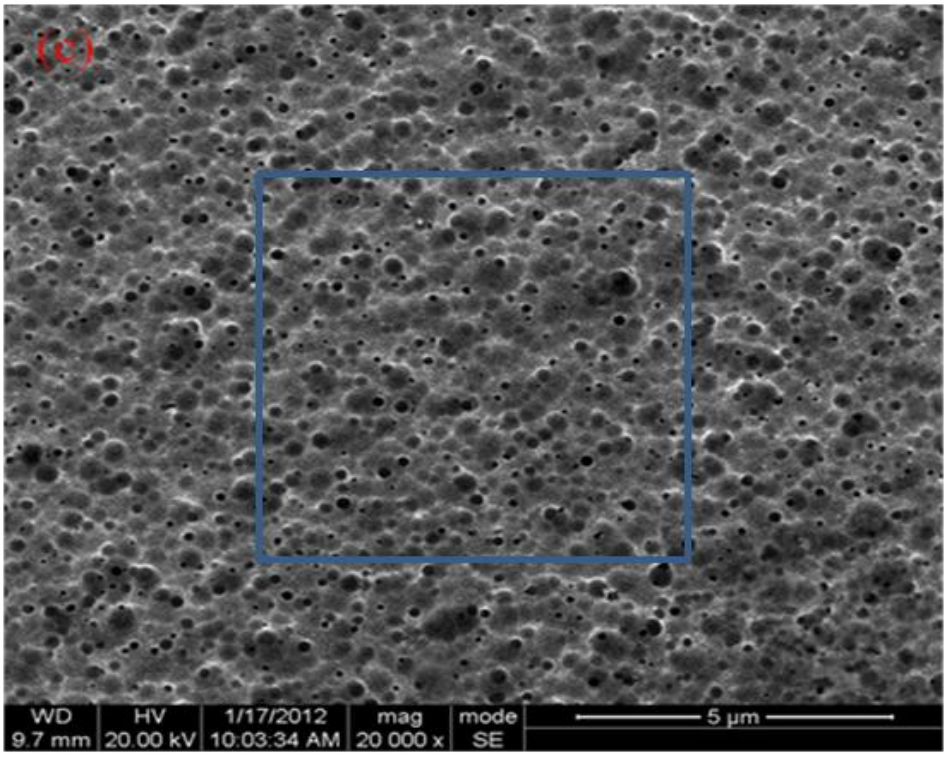

Fig. 6-9 Porcelain microstructure (a) slow cooling (b) regular cooling (c) fast cooling

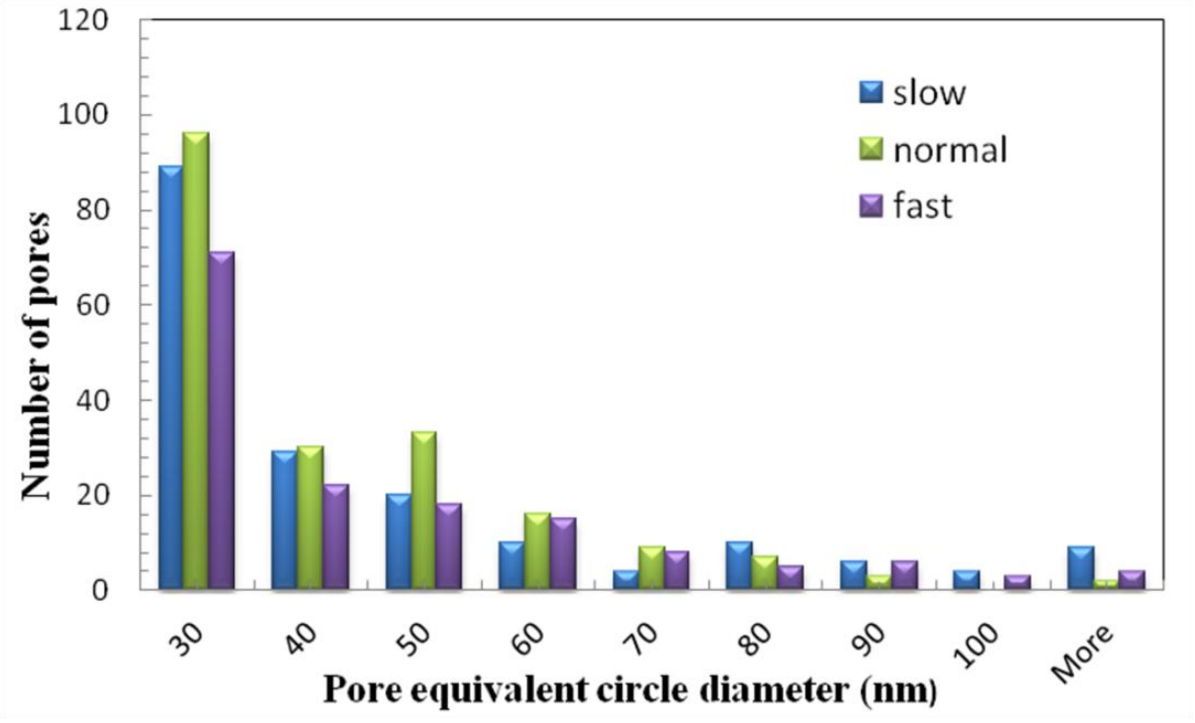

Fig. 6-10 Porcelain pore distribution from different cooling rates.

6.4 Discussion

Crown making involves several firing and cooling cycles. The very last cooling cycle principally affects the final residual stress. During cooling, the outside porcelain layer cools faster than the rest of the crown. As typical with tempering, when the outside surface becomes solid, some parts in the middle remain more viscous. This will result in relatively more compressive residual stress in the porcelain outside layer, and tensile stress in the middle to balance. This was especially apparent for the fast cooled crown and in the cusp region with thicker porcelain. Tholey *et al.* (2011) measured the temperature at different locations of the crown during cooling and confirmed the porcelain outside surface cooled the fastest. Simulated temperature data and stress data from this work clearly showed the same. For both cases, slow cooling and fast cooling, porcelain outside cools first and results in more compressive residual stress than the inside part. Faster cooling rates will result in bigger temperature differences and larger magnitudes of tensile residual stress in the cusp area. CTE was one of the most important factors to determine residual stress. If we assume the CTE reached 15 $x10^{-6}$ at 600 °C after glass transition, Fig. 6-5d and Fig. 6-6d show there were cooling rate effect but the effect was very small. If the CTE reached 30 $x10^{-6}$ at 600 °C, the effect is much larger as shown in Fig. 6-7. The maximum difference between the maximum principle is 74 MPa.

A simulation's reliability highly depends on the boundary conditions from experimental measurements. Many different of types of porcelain exists. This work only demonstrated a few material combinations. Thermal expansion data for both materials were extremely important. It was not clear how the material will behave in the glass transition region experimentally. However, if the CTE of porcelain becomes much larger

as the limited data (Fairhurst *et al*., 1989) shows, the cooling effect on the residual stress will be very large as shown in Fig. 6-7. Then there would be a tensile zone in the middle of the porcelain layer. This is especially true for the area with thicker porcelain. Once the crack crossed the surface compressive stress zone and into the tensile zone, the crown could be easily broken. This tensile zone inside the thicker portion could explain why porcelain normally chips in the cusp area, and that the chipping does not go all the way through the interface leaving a residue layer of porcelain on top of the zirconia.

Porcelain's CTE change during the glass transition was very important in determining the residual stress in zirconia-porcelain dental crowns. At present, dental labs are recommended to match zirconia and porcelain with a CTE difference $1x10^{-6}$ or less to reduce residual stress. Assuming the CTE of porcelain is always $1x10^{-6}$ smaller than the CTE of zirconia, all porcelain areas are more compressive than zirconia in crowns. This was the objective to resist crack growth. However, only limited experimental data suggested the CTE of porcelain increases during the glass transition region. If, assuming the porcelain CTE changed $5x10^{-6}$ during the glass transition temperature region, 600 to 500 ºC, and the CTE of porcelain was always $1x10^{-6}$ smaller than CTE of zirconia at 500 to 25 ºC, all porcelain locations in the crown were more tensile than zirconia. Considering porcelain's CTE change during glass transition would help more correctly determine residual stress in dental crowns. Even small CTE changes can change the sign of the residual stress in porcelain and zirconia. The measured residual stress in chapter IV shows similar value as results for the case with porcelain's CTE change at $\Delta\alpha=20x\ 10^{-6}$.

Recently, some researchers suggested processing flaws might be the cause of failure for crowns (Quinn *et al*., 2011; Lohbauer *et al*., 2010). Microstructure analysis from SEM in this chapter and flaw distribution analysis from μCT in chapter V shows that cooling rate did not significantly change the microstructure of the porcelain, but affected the number of flaws presented.

6.5 Conclusion

A detailed crown model was used to simulate residual stress and the effect of cooling rate, porcelain's CTE change, and the relationship with porcelain chipping. Results shows when porcelain's CTE change was large, the cooling rate effect on residual stress was large. There were tensile stress zone underneath the more compressive surface and interface, which could explain clinically observed chipping of porcelain in zirconia frame dental crowns. A higher cooling rate make the tensile zone larger and its magnitude higher, especially in the cusp area, so a slow cooling rate and porcelain with a small CTE change during glass transition are recommended regarding minimizing residual stress. A model with constant elastic materials properties does not capture the tensile zone beneath the surface. A transient simulation should be carried out for residual stress calculation. Further experimental data will help to produce and validate more representative results. Cooling rates showed no significant effect on the porcelain microstructure, but effected number of flaws presented. Slow cooling would reduce number of flaws formed.

CHAPTER VII

7 PARTIAL CROWN GEOMETRY TO EVALUATE DESIGN FACTOR EFFECTS ON RESIDUAL STRESS

Failure modes in zirconia porcelain dental crowns had mainly been chipping of porcelain in the cusp area. Residual stress was believed to have played a key role. A simple geometry similar to crown cusp was used to evaluate different design factors on residual stress. To make sure the simple geometry is representative of the crown cusp, first, the residual stress obtained from the simple geometry was compared with a detailed 3D crown model based on μCT data. The results agreed very well, except the area where the curvature was different. Small curvature will result in more stress concentration. The simple geometry behaved similarly to the crown cusp. Then three different designs with different porcelain thickness and curvature were analyzed for residual stress and performance under 50 MPa local biting pressure. Results showed uniform porcelain thickness with more zirconia support performed better than the other two cases with varying porcelain thickness. A porcelain layer with minimal thickness gradient is recommended. The residual stress difference between two different cusps measured by nanoindentation was 18 MPa, additionally shows that thickness and curvature affect residual stress.

7.1 Introduction

Over the past decade, all-ceramic crowns gained popularity over metal crowns due to aesthetics and biocompatibility. The strength of all-ceramic dental crowns improved with improvement on manufacture and material science technology. However, the failure rate of all-ceramic crowns is still in the range of 1 to 4% every year (Fradeani, 1998; Fradeani*et al.* , 2002; Fradeani*et al.* , 2005; Malament *et al.* ,2001). Clinical evaluation showed most all-ceramic crowns failed due to cohesive fracture in the porcelain veneered layer. The Y-TZP framework with porcelain veneer crown has a special failure phenomenon. Porcelain chipping was exclusively limited to the porcelain layer and had not appeared to run to the zirconia porcelain interface. The failed crown often had a thin porcelain layer beneath where the chipping occurred (Kim *et al*.,2007; Pjetursson *et al*., 2008). One hypothesis for this special behavior is that residual stress formed inside the crown during cooling because of the mismatch of coefficient of thermal expansion (CTE) and thermal gradients. This residual stress will superimpose on the biting force and potentially accelerate fatigue and fracture. Measuring residual stress is extremely challenging due to the sample size, stress magnitude, and complex geometry. Researchers (Swain, 2009; Mainjot *et al*., 2011) often use flat bilayer samples, but due to complexity of the crown shape, flat sample measurement does not represent well 3D crown behavior. Zhang *et al*. (Zhang *et al*., 2012) measured the residual stress of both porcelain and zirconia on a crown, but finding the zero strain reference samples was a challenge. Correctly finding the absolute magnitude of the residual stress is difficult. Comparing experiment, FEM is more time and cost efficient. Some researchers (Bonfante *et al*., 2010; Raffery *et al*.,2009) had used FEM to evaluate design parameters on the maximum principle stress. However, their main focus was stress under biting pressure, no residual stress was included.

Research had shown that the cusp area was subjected to the most loading and was the location of most failures. This work will evaluate design factor effects on residual stress based on a simple geometry similar to a crown cusp. To prove the simple geometry is representative the crown cusp, first residual stress from the simple geometry was compared to a detailed 3D model formed based on tomography from a clinically relevant crown. Once it was validated that the simple geometry represents the crown cusp behavior, three different designs with different porcelain thickness variation were compared based on the simple geometry. Stress under loading for the three different designs was also carried out to evaluate performance under a biting pressure. Residual stress differences between two cusps were also measured by nanoindentation.

7.2 Methods

7.2.1 Nanoindentation

A MTS Nanoindenter XP with a resolution of 0.2 nm in displacement and 50 nN in load was used to test the residual stress difference in porcelain at two cusps, as shown in Fig.7-1. The top of the cusps were polished and 8 indents were performed on each location. The load applied was 200 mN and loading time was 40 s. A cube corner tip was used. The crack length was measured with Secondary Electron Microscopy (Quanta ESEM 600). The examined ceramic crown has a yttria stabilized tetragonal zirconia polycrystal (Y-TZP) core (LAVA, 3M/ESPE, St. Paul, MN) and porcelain veneer (LAVA Ceram 3M/ESPE, St. Paul, MN). The zirconia core has a Young's modulus of 205 MPa and CTE of $11x10^{-6}$/ ºC. The veneered porcelain has a Young's modulus of 70 MPa and a CTE of approximately $10x10^{-6}$/ ºC (Raffery *et al*.,2009; Bale, 2010). They

were prepared in a dental lab following a typical procedure for zirconia core and porcelain veneer crowns. Several firing cycles are normally involved when making dental crowns, but the firing temperature at the final cycle has the greatest influence on residual stress. The crown was cooled down to room temperature from its final firing temperature of 840 ºC following the manufacture's recommended procedures.

The residual stress was extracted according to fracture theory (Tandon, 2007):

$$K_1 = m\frac{P}{c_1^{3/2}} \ (cusp1) \tag{1}$$

$$K_2 = m\frac{P}{c_2^{3/2}} - 2\,f\sigma_r(\frac{c_2}{\pi})^{1/2}\ (cusp2) \tag{2}$$

$$m = \varepsilon(\frac{E}{H})^{1/2} \tag{3}$$

Where K was stress intensity factor, P was load, c was crack length, f was factor associated with the crack geometry, assumed to be 1 for half-penny cracks. E and H were the elastic modulus and hardness, while ε was a constant determined by indenter geometry, it is 0.04 for cube corner. σ_r was the residual stress.

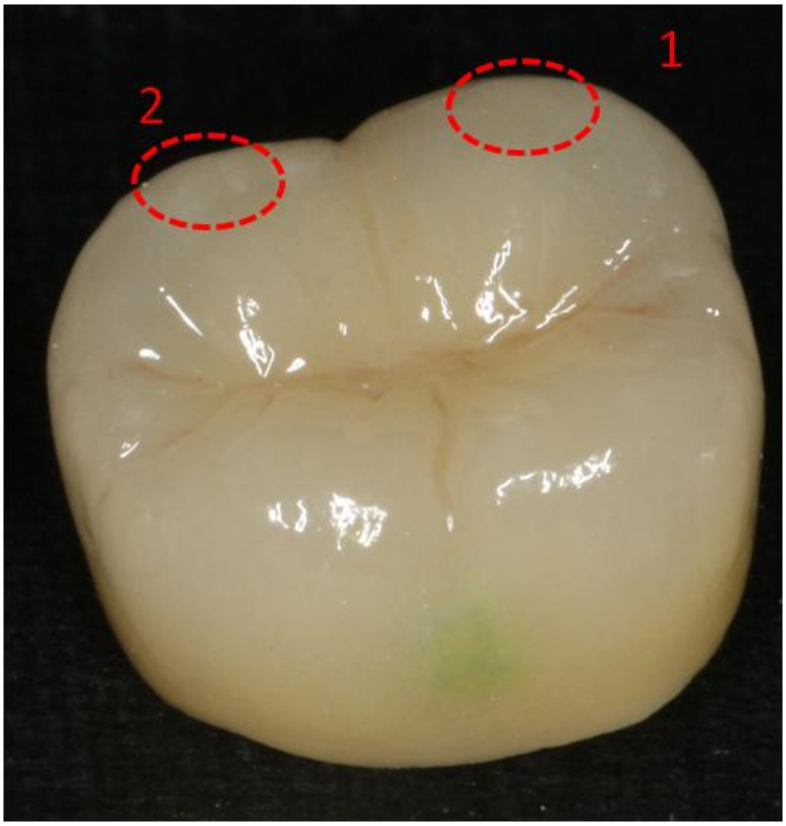

Fig.7-1 Nanoindentation were performed on the two cusp indicated to obtain residual stress difference

7.2.2 Finite element analysis

Commercial finite element analysis software ABAQUS 6.9-1was used to evaluate residual stress from different designs and loading conditions. Stress distribution in a detailed crown was obtained first (the detail procedure was shown in chapter VI). Then the stress distribution for a simple geometry to mimic the behavior of the cusp was obtained and compared with the detailed crown. Then the porcelain and zirconia thickness and shape in the cusp area was altered to find out the residual stress change because of mismatch of CTE. Also, the stress distribution under 50 MPa biting pressure was obtained for different designs.

Fig.7-2a and Fig.7-2b shows a detail model of the whole crown. There are 185429 nodes and 1008757 tetrahedral elements. Results from chapter VI showed porcelain shape and thickness played an important role in the forming of residual stress. A simple shape similar to the shape of the cusp, as shown in Fig.7-2c, was used to evaluate three different designs. The three different designs were: (1) uniform zirconia thickness of 0.5 mm, increasing porcelain thickness from 0.5 mm in the valley to 1.8 mm in the cusp area (2) uniform zirconia thickness at 0.5 mm, increasing porcelain thickness from 0.5 mm in the valley to 1.3 mm in the cusp area, and (3) uniform porcelain and zirconia thickness of 0.5 mm. Case 1 and 2 had the same basic shape except for the porcelain thickness reduction of about 28% in the cusp area, For case 3, the outside shape was the same as case 1 but the curvature of zirconia had changed. This case was to simulate the use of uniform thickness porcelain, but with a zirconia core which has a complex shape to match the real crown and provide more support for the porcelain. Fig.7-2c shows detail of the case 1 design, which was similar to the cusp design used in modern crown systems.

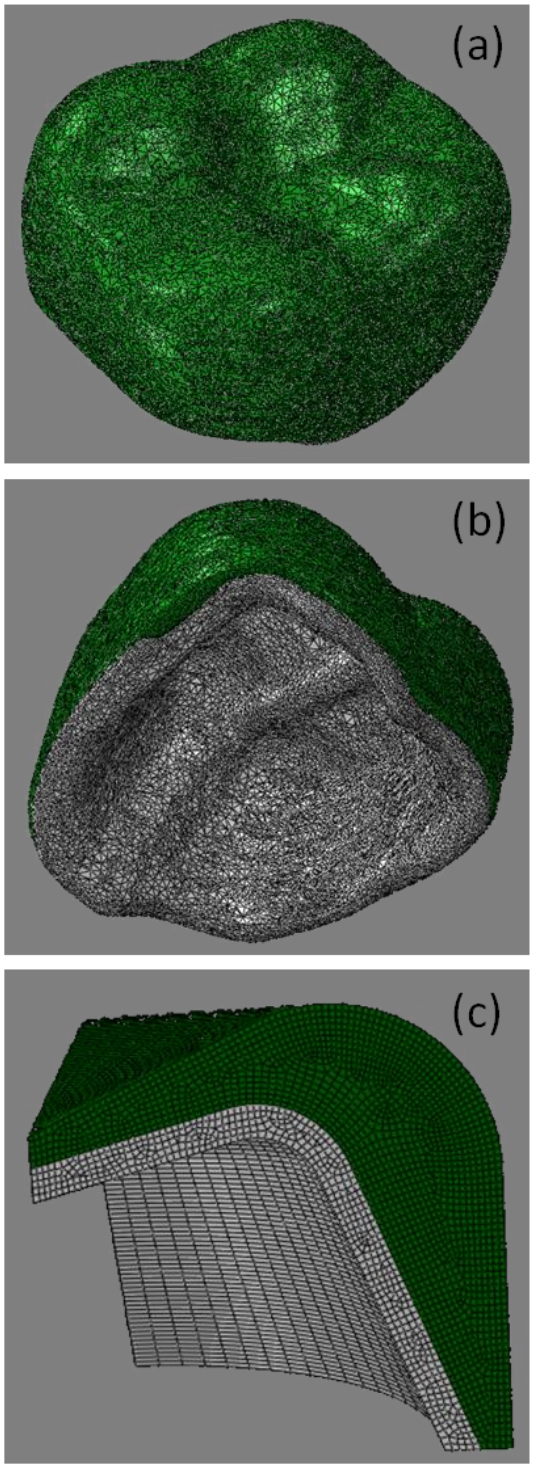

Fig.7-2 (a) Top view of detailed 3D crown model created from scanning tomography of real crown (b) bottom view(c) partial model similar to the cusp area used for different designs comparison.

In all the models, both porcelain and zirconia were assumed isotropic and to behave elastically. CTE mismatch was one of the most importance factors in forming residual stress. To achieve compressive stress in the porcelain layer, industry often uses zirconia with a CTE 1 ppm higher than that of porcelain. In this simulation, the CTE of zirconia was also assumed 1 ppm higher than that of porcelain so that porcelain veneer would have compressive stress and zirconia would have tensile stress. The main goal of this study was to compare stress distributions from different designs during cooling and under loading from a simple geometry. Porcelain is a viscoelastic material during glass transition. Only residual stress during cooling below the glass transition temperature to room temperature was considered, and the temperature range was 500 to 25 °C. The material data used is listed in Table 7 -1.

Table 7 -1 Zirconia and porcelain material properties (Swain, 2009; Raffery *et al.*, 2009)

	Young's Modulus (GPa)	Poisson's ratio	CTE ($x10^{-6}$)	Temperature (°C)
porcelain	70	0.25	10	500 ~ 25
zirconia	205	0.25	11	500 ~ 25

On top of residual stress, a 50 MPa biting pressure was applied in the three design cases. Stress distribution under the load will be extracted to compare their performance. For residual stress distribution simulation, only one degree of freedom was limited at the

bottom surface of the model. To simulate the stress distribution under load, all six degrees of freedom were fixed at the bottom surface of the model.

7.3 Results

7.3.1 Nanoindentation

A cube corner tip was used to probe the residual stress difference at two different cusps. The advantage of this tip is to be able to fracture the material at very low load. Comparing the crack length under the same load at the two cusps using fracture mechanics theory, as in equations 1-3, shows that cusp 1 had 18.26 MPa more compressive residual stress than cusp 2. Fig. 7-3 shows a typical cube corner indent impression.

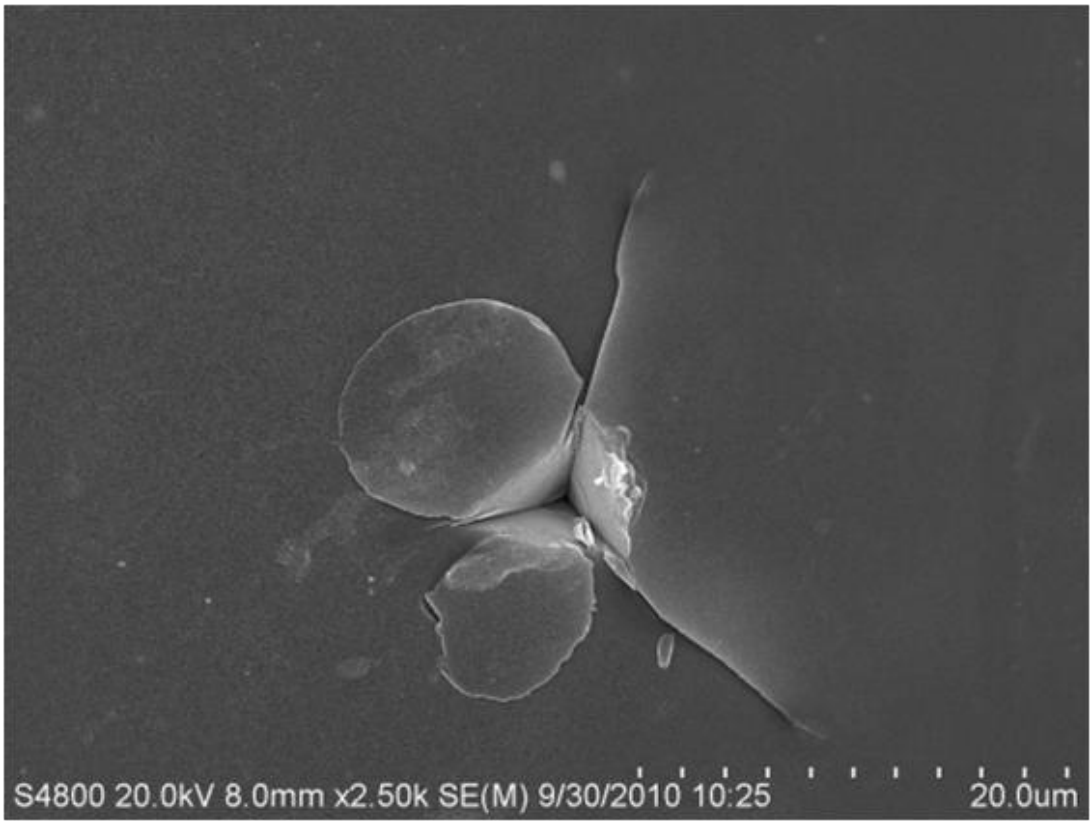

Fig. 7-3 A typical cube corner indent impression to show the crack length and shape.

7.3.2 Finite element analysis

Stress distribution in the detailed crown was obtained first and is shown in Fig. 7-4. Fig. 7-4a shows the maximum principle stress on the surface, Fig. 7-4b is a cross section view. Fig. 7-4a shows geometry had an effect on the residual stress distribution. The cusp area was more tensile on the surface and the valley between the cusps was more compressive. Fig. 7-4b represents the stress distribution across the zirconia porcelain thickness. In general, porcelain appears more compressive than zirconia. Fig. 7-4c and Fig. 7-4d are a top view and cross section view of the minimum principle stress. It confirms the trend from the maximum principle stress. The cusp was more tensile than the valley between the cusps. The detailed stress magnitude at three critical locations is plotted in Fig.7-5.

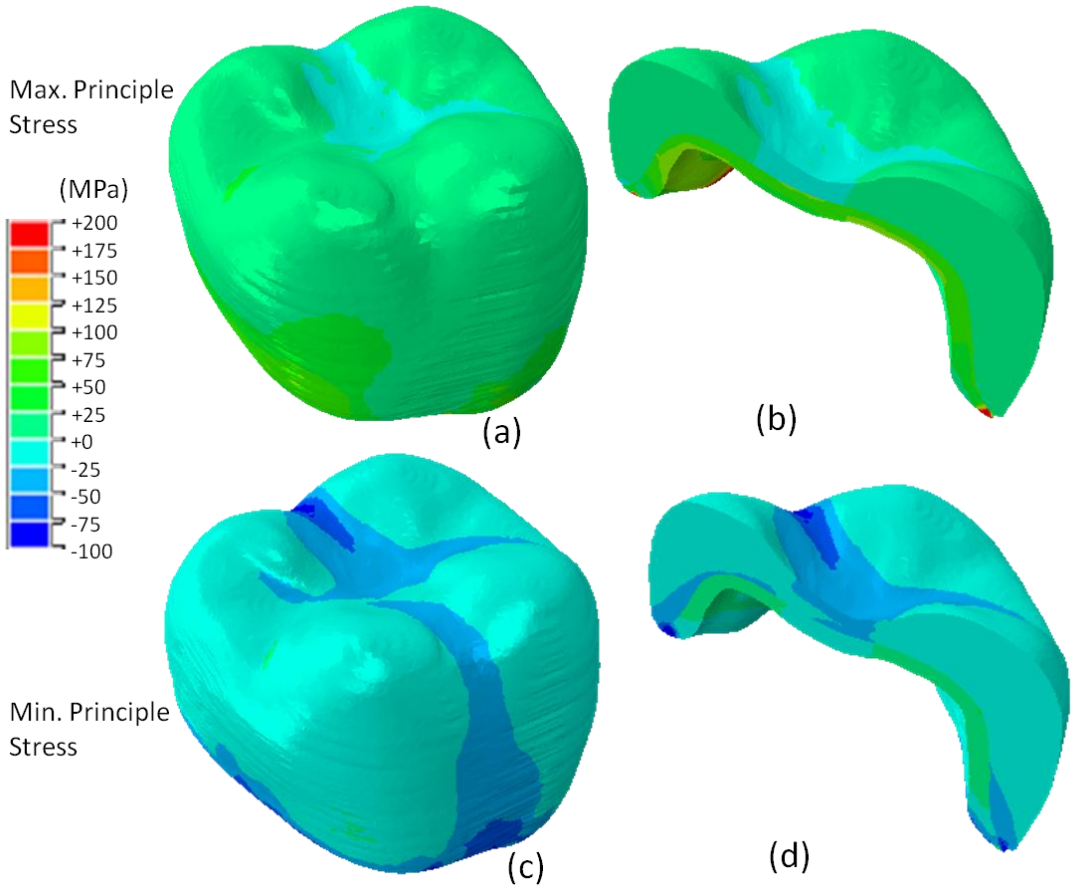

Fig. 7-4 principle stress in the crown (a) top view of maximum principle (b) cross section view of maximum principle (c) top view of minimum principle stress (d) cross section view of minimum principle stress

Fig.7-5 shows the maximum principle stress along the three lines. Line 1 and 3 are in different cusp and with different porcelain thickness. For line 1, the maximum principle stress at the porcelain surface and interface are 5 and 19 MPa respectively. The Maximum principle stress at the zirconia surface and interface is 81 and 64 MPa. For line 3, the maximum principle stress at the porcelain surface and interface is 9 and 15 MPa. The Maximum principle stress at the zirconia surface and interface are both 66 MPa. In line 2, the maximum principle stress at porcelain surface and interface is -0.4

and 10 MPa respectively, at the zirconia surface and the interface is 73 and 65 MPa. The porcelain veneer thickness affects the residual stress distribution, and the maximum principle stress at the interface for porcelain at the chosen location.

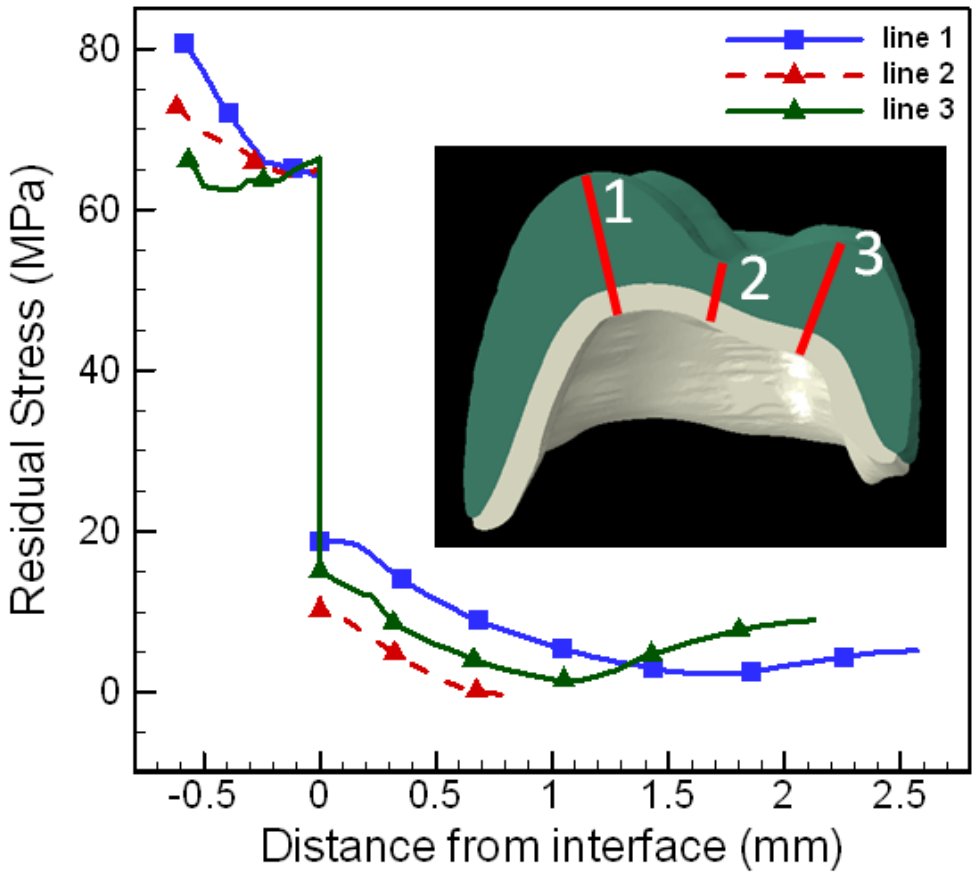

Fig.7-5 Maximum principle stress along three critical locations with different thickness.

The maximum principle stress from the simple geometry and detailed 3D crown is compared and shown in Fig. 7-6. The porcelain surface stress are zero and 5 MPa for the simple and detailed crown. However, at the interface, the residual stress is 22 and 19 MPa in the simple geometry and detailed crown, 63 and 64 MPa at the zirconia

interface. The residual stress is 68 and 81 MPa in the zirconia surface for the simple geometry and detailed crown. The residual stress obtained from the detailed 3D crown and simple geometry matchs very well with maximum principle stress within 100MPa, except the zirconia inside surface, the reason is the difference caused by stress concentration because of curvature of the crown.

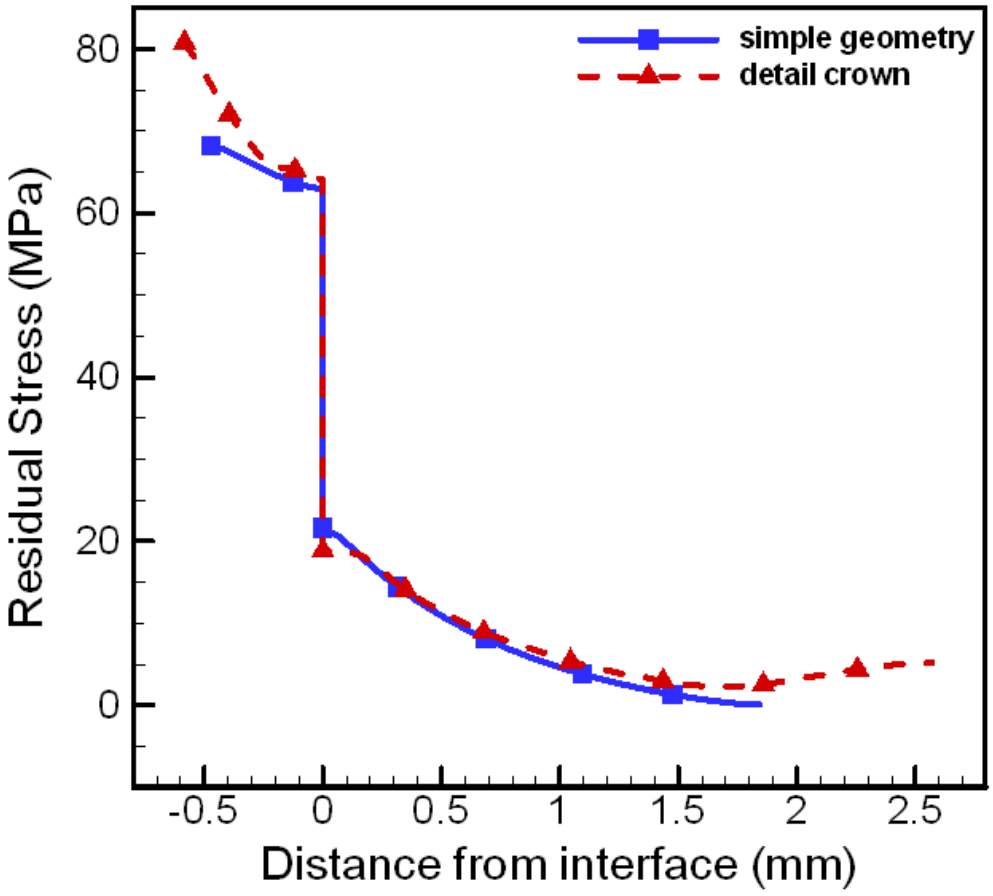

Fig. 7-6 Comparison between detail crown and simple geometry maximum principle stress

Since residual stress from the detailed crown and simplified geometry agreed well, the simple geometry was used to analyze and test design modifications to reduce cost and

computation time. Residual stress for the three different designs is shown in Fig.7-7. There is a tensile zone beneath the compressive porcelain, which doesn't show up in the uniform porcelain and zirconia shape. A detailed stress state is shown in Fig. 7-8a. Stress in the cusp area is compared and listed in Table 7-2. The maximum principle stress at the porcelain surface is 0.1, 0.2, and 0.6 MPa for designs 1, 2 and 3. The maximum principle stress at the porcelain interface is 22, 19 and 8 MPa respectively for designs 1, 2 and 3. The maximum principle stress at the zirconia interface is 63, 53 and 34 MPa for designs 1, 2, and 3. The maximum principle stress at the zirconia surface is 68, 59, and 34 MPa for designs 1, 2 and 3. Design three which has the thinnest porcelain and uniform porcelain and zirconia thickness has the least maximum principle stress.

Table 7-2 Residual maximum principle stress in the cusp area for the three different designs

			Maximum principle stress (MPa)			
design	zirconia thickness (mm)	Max porcelain thickness (mm)	porcelain surface	porcelain interface	zirconia interface	zirconia surface
1	0.5	1.8	0.1	22	63	68
2	0.5	1.3	0.2	19	53	59
3	0.5	0.5	0.6	8	34	34

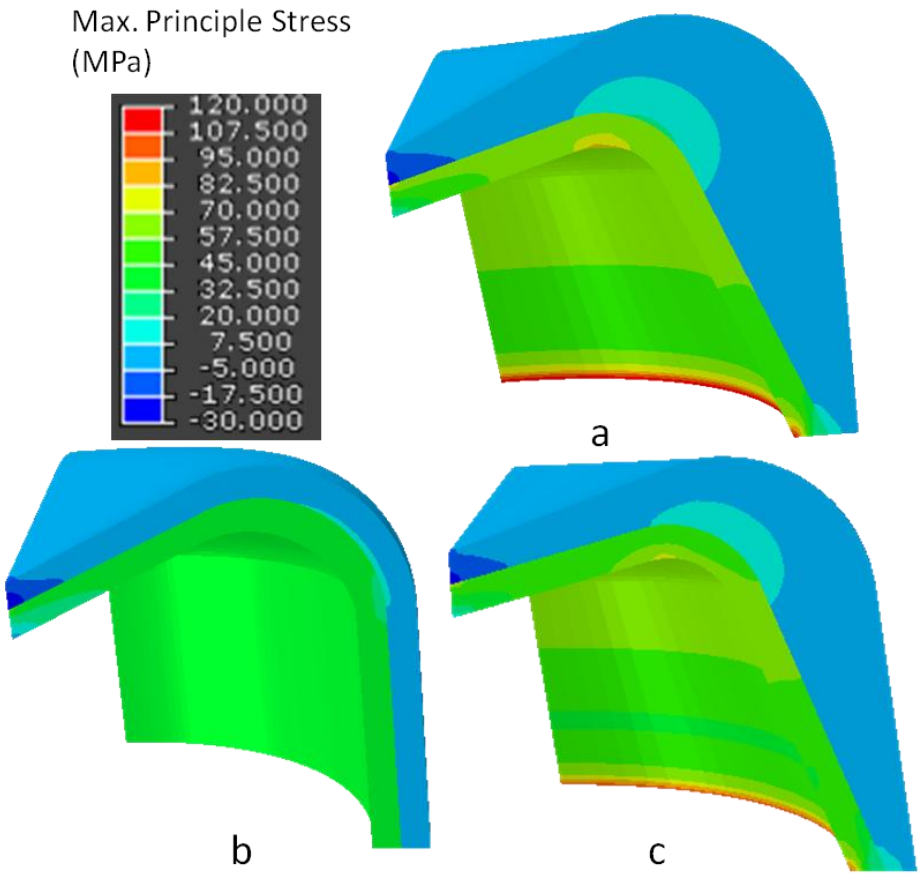

Fig.7-7 Maximum principle stress under load at different designs (a) zirconia thickness 0.5mm porcelain varies 0.5 ~1.8 (b) zirconia and porcelain at 0.5 mm (c) zirconia 0.5 mm porcelain varies 0.5mm ~ 1.3mm (28 % thickness reduction in the cusp area)

To understand how the different designs would perform, a 50 MPa biting pressure was applied on a 0.5 mm^2 area. The stress state directly below the bite area is plotted in Fig. 7-8b and listed in Table 7-3. The maximum principle stress at the porcelain surface was -47, -50 and -46 MPa for designs 1, 2, and 3. The maximum principle stress at the porcelain interface is 22, -1, and -15 MPa for designs 1, 2, and 3. The maximum principle stress at the zirconia interface is 36, 12, and 9 for designs 1, 2, and 3. The

maximum principle stress at the zirconia surface is 110, 88, and 20 for designs 1, 2, and 3. Design three has the least compressive stress.

Table 7-3 Maximum principle stress under 50MPa biting pressure for different crown designs

			Maximum principle stress (MPa)			
design	zirconia thickness (mm)	Max porcelain thickness (mm)	porcelain surface	porcelain interface	zirconia interface	zirconia surface
1	0.5	1.8	-47	22	36	110
2	0.5	1.3	-50	-1	12	88
3	0.5	0.5	-46	-15	9	20

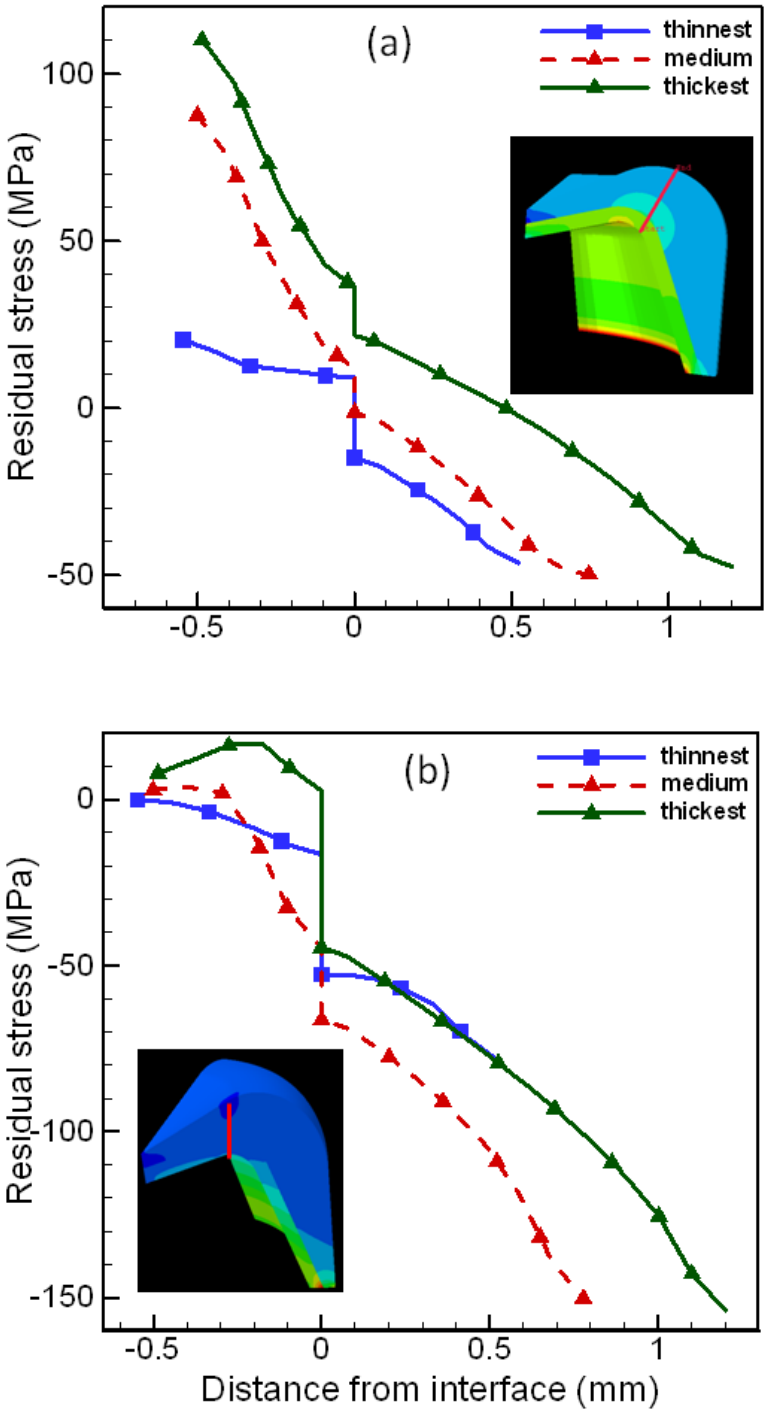

Fig. 7-8 (a) Maximum principle stress of three designs from mismatch of CTE (b) Minimum principle stress for three designs under biting pressure 50MPa.

7.4 Discussion

Residual stresses in dental crowns have been non-trivial to measure due to complex shapes and the lack of temperature dependent materials data. Both curvature and thickness affect residual stress. Finite element analysis was a useful tool to predict residual stress based on available data. Computation was expensive with a 3D detailed crown (with over 1 million elements). There are many factors that can affect the final stress. It would take many simulations to figure out the effect of different factors. Since most of the failures occur in the cusp area, it would significantly reduce the computation time and reduce design cycle if there was a simple geometry which could represent the cusp behavior of the crowns. A simple shape similar to a crown cusp was designed, and the residual stress was compared with that in the detailed 3D crown. Results were very close except at the zirconia interface, where the curvature was a little different. The smaller curvature showed more stress concentration. If the simple geometry has the same curvature on the porcelain and zirconia, the residual stress would be expected to be very close to the real crown.

Three different designs based on the simple geometry were carried out to evaluate its residual stress and performance under load. Results showed thicker porcelain causes larger tensile stress, less porcelain thickness and less thickness variation would have less residual stress. From the residual stress standpoint, less porcelain thickness would perform better. A 50 MPa biting pressure was applied to evaluate the three designs, it turned out a design with a 0.5 mm porcelain thickness showed less maximum compressive stress than the other two designs with thicker porcelain, which suggested a crown with uniform porcelain thickness and varying zirconia thickness would perform

better than crown with uniform zirconia core thickness and varying porcelain veneer thickness. This is in consistent with findings of Rekow *et al*. (2006) that layer thickness is one of the most important factors in determining residual stress.

The detailed crown used tetrahedral elements because complexity of the shape. The simple geometry used hexagonal elements. Results from tetrahedral element and hexagon element meshing are compared and plotted in Fig. 7. The results agreed very well (within 100 MPa).

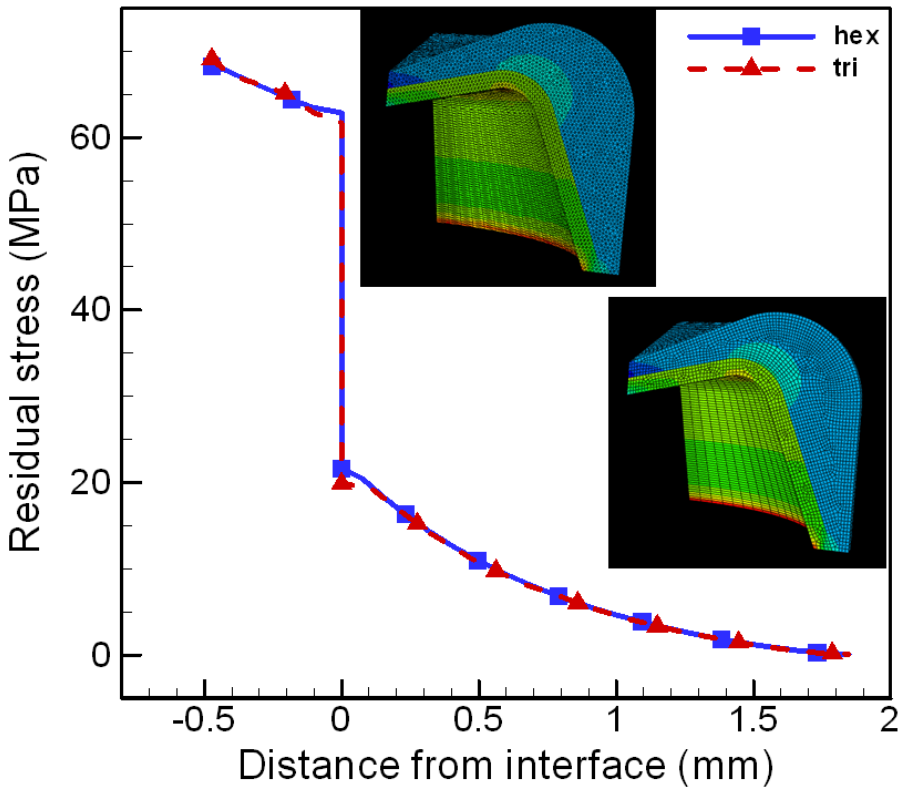

Fig. 7-9 Comparing results from models with hexagon and tetrahedral elements

This study assumed elastic material behavior and no thermal tempering for zirconia and porcelain. In dental lab practice, the CTE of zirconia is normally1 ppm higher than

that of the porcelain to produce favorable compressive residual stress in the porcelain layer for suppressing crack growth. Therefore in the simulation, the CTE of zirconia was assumed 1 ppm higher than that of porcelain and kept constant during the cooling process. Results showed a cusp with larger porcelain thickness would show more tensile stress in general. The maximum tensile stress was at the porcelain-zirconia interface for porcelain. It could not explain clinical observations of chipping in porcelain that normally had a small porcelain layer left on top of zirconia. The reason could be that thermal tempering. Both porcelain and zirconia have very poor thermal conductivity, thicker materials would have temperature differences across the layers. Also, porcelain is a viscoelastic material with temperature dependent material properties. Further studies considering the effect of tempering stress should carried out to have a further evaluation of different designs. The degree of freedom at the bottom layer of the detailed crown and the simple geometry had been limited. Therefore, the bottom layer had shown some stress concentration. This did not affect the cusp area, the focus of the above analysis as has been reported elsewhere (Coelho *et al.* 2009).

7.5 Conclusion

Clinical study had shown that the failure mode of zirconia porcelain dental restorations had been chipping of porcelain in the cusp area. Residual stress at the different cusps was different. Nanoindentation and finite element analysis from a detailed crown model had shown this, as you see from chapter IV and VI. A simple geometry was built to behave similar to the crown cusp and could be used to evaluate design factors such as thickness and curvature. Three designs with different porcelain

thickness and curvature were evaluated and the results showed, less porcelain thickness change would produce less residual stress and have less stress under biting pressure.

CHAPTER VIII

8 CONCLUSION AND FUTURE WORK

Overall, it is clear residual stress plays a much bigger role in failure of all ceramic zirconia-porcelain dental crowns than metal-porcelain dental crowns. Why zirconia-porcelain dental crowns behave differently than metal-ceramic crowns had not been fully understood. This work involved the development of several new methods principally for measuring the residual stress in zirconia-porcelain dental crowns using nanoindentation. It also predicted the residual stress using the finite element method, analyzed the factors contributing to residual stress, and explored designs to reduce residual stress.

First, a bilayer system was used to analyze residual stress caused by mismatch of CTE and thermal tempering. Two porcelain zirconia dental frames with different thickness underwent two different tempering processes. Results showed that tempering rate and porcelain zirconia thickness have effects on residual stress and are interrelated. Tempering effects on residual stress for locations with smaller thickness are less relatively to locations with larger thickness. The higher the tempering rate, the more tensile stress will develop in porcelain and the more compressive stress in zirconia, and this is more apparent in thicker locations.

Second, Residual stress can be extracted by comparing the hardness of stressed and reference samples. Residual stress along four critical locations in a crown across the

thickness for both zirconia and porcelain was obtained by nanoindentation. Results showed large residual stresses existed in the dental crown, and the magnitudes differ from location to location, as might be expected from the geometry. Both geometry and thickness have an effect on the residual stress distribution. The cusp area in porcelain has the biggest tensile stress. Results by XRD and nanoindentation were compared and showed agreement in trend, but given the references used here, the magnitudes did not agree. Some of this can be due to sampling volume differences or reference determination, but clearly for unambiguous application, where absolute values are important, the new technique needs further refinement. Finite element analysis was also used to simulate the material response at different residual stress and compared with experimental data, results agreed very well, building confidence in these measurements. An examination of the 3D stress state either by FEM or a biaxial XRD analysis would further aid in comparison of the techniques. At this stage, nanoindentation was shown a useful tool to explore the otherwise unseen residual stresses.

Third microtomography was used to evaluate the number and size of flaws in three crowns made at different cooling rates. The flaws were clearly observed in the tomographs, with the biggest flaw observed at 220 μm. A simplified view from a fracture standpoint suggests such crowns can fail at a stress of 42 MPa, if the flaw size was the dominant factor. The cooling rate seemed to affect the number and size of flaws, with slow cooling produced less flaws. Additional research on a larger number of samples is needed to draw conclusion.

Fourth, a detailed crown model formed from μCT scanned data was used to simulate residual stress and effect of cooling rate, porcelain CTE change, and the

relationship with porcelain chipping. Results show, when porcelain CTE change was large, the cooling rate effect on residual stress was large. There were tensile stress zones underneath the more compressive surface and interface, which could explain chipping of porcelain in zirconia frame dental crowns. A higher cooling rate makes the tensile zone larger, and a magnitude higher especially in the cusp area, so slow cooling rate and porcelain with a small CTE change during glass transition were recommended regarding managing residual stress. A model with elastic, constant material properties will not be able to capture the tensile zone beneath the surface. Transient simulations should be carried out for residual stress calculation. Further experimental data will help to produce more validated results. Cooling rates showed not to significantly affect the porcelain microstructure, but affected the number of flaws formed. Slow cooling would reduce flaws.

Finally, Clinical study had shown that the failure mode of zirconia porcelain dental restorations had been chipping of porcelain in the cusp area. Residual stress at the different cusps was different. Nanoindentation and finite element analysis from detailed crown models had shown that. A simple geometry, similar to a crown cusp behaved similar to the crown cusp and could be used to evaluate design factors such as thickness variation and curvature. Three designs with different porcelain thickness variation and curvature were evaluated and results showed, less porcelain thickness variation would produce less residual stress and have less stress under biting pressure.

Predicted residual stress in dental crowns highly depends on the experiment data, especially coefficient of thermal expansion of porcelain and zirconia. Porcelain has temperature dependent material properties, but temperature dependent coefficient of

thermal expansion has not been well published, especially from the temperature it starts at near the glass transition temperature. Material properties during that range are extremely important to model residual stress.

Future work should consider measuring and documenting temperature dependent CTE and Young's modulus for the different types of porcelain used as dental materials. Making these material data readily available would be a big step forward in improving reliability of 3D crown stress simulation. With improvement in computing capacity and scan resolution, 3D simulation could incorporate flaws effect on stress. The crack propagation can also be studied using the 3D model formed from tomography data.

REFERENCES

1. Aboushelib MN, Feilzer AJ, de Jager N, Kleverlaan CJ. Prestresses in bilayered all-ceramic restorations. *J Biomed Mater Res B Appl Biomater* 87:139-145, 2008.

2. Allahkarami M, Hanan JC. Mapping the tetragonal to monoclinic phase transformation in zirconia core dental crowns. *Dent Mater* 27:1279-1284, 2011.

3. Allahkarami M, Bale HA, Hanan JC. Analytical model for prediction of residual stress in zirconia porcelain bi-layer. *Advances in bioceramics and porous ceramics III: Ceramic Engr. and Sci. Proc. John Wiley & Sons*, Vol. 31: 19-26, 2010.

4. Anusavice KJ, and Dehoff PH, Hojjatie B, Gray A. Influence of tempering and contraction mismatch on crack development in ceramic surface. *J Dent Res* 68: 1182-1187, 1989.

5. Asaoka K, Kuwayama N, Tesk JA. Influence of tempering method on residual stress in dental porcelain. *J Dent Res* 71(9): 1623-1627, 1992.

6. Asaoka K, and Tesk JA. 1989, Transient and residual stresses in dental porcelains as affected by cooling rates. *Dent mater* 8(1): 9-25, 1989.

7. Bale HA, Allahkarami M, Tamura N, Hanan JC. Microbeam X-ray grain averaged residual stress in dental ceramics. *35th international conference on advanced ceramics & composites (ICACC)*, FL, USA, 2011.

8. Bale HA Measurement and analysis of residual stresses in zirconia dental composites using micro x-ray. *Dissertation, Oklahoma State University*, 2010.

9. Bale HA, Hanan JC. Interface residual stresses in dental zirconia using laue micro diffraction. *8th International Conference on Residual Stresses, Denver, CO*. 2008.

10. Bertolotti RL. Calculation of interfacial stress in porcelain-fused-to metal systems. *J Dent Res* 59 (11): 1972-1977, 1980.

11. Bolshakov A, Oliver WC, Pharr GM. Influence of stress on the measurement of mechanical properties using nanoindentation: part II. finite element simulations. *J. Mater. Res.* 11(3): 760-768, 1996.

12. Bonfante EA, Rafferty BT, Zavanelli RA, Silva NRFA, Rekow ED, Thompson VP, Coelho PG. Thermal/Mechanical simulation andlaboratory fatigure testing of an alternative yttria tetragonal zirconia polycrystal core-veneer all-ceramic layered crown design. *Eur J Oral Sci* 118: 202-209:2010.

13. Bottino MA, Salazar-Marocho SM, Leite FP, Vasquez VC, Valandro LF, Flexural strength of glass-infiltrated zirconia/alumina-based ceramics and feldspathic veneering porcelains. *J Prosthodont* 18: 417-420, 2009.

14. Burke FJ, Lucarotti PS. Ten year outcome of crowns placed within the General Dental Services in England and Wales. *J Dent* 37:12-24, 2009.

15. Carlsson S, Larsson PL. On the determination of residual stress and strain fields by sharp indentation testing part II: experimental investigation. *Acta Mater* 49: 2193-2203, 2001.

16. Cehreli PFMC, Kokat AM, Akca K. CAD/CAM Zirconia vs. slip-cast glass-infiltrated Alumina/zirconia all-ceramic crowns: 2-year results of a randomized controlled clinical trial. *J Appl Oral SCi* 17: 49-55. 2009.

17. Chintapalli RK, Jimenez-Pique E, Marro FG, Yan H, Reece M, and Anglada M. Spherical instrumented indentation of porous nanocrystalline zirconia. *J Eur Ceram Soc* 32: 123-132, 2012.

18. Choi Y, Lee HS, Kwon D. Analysis of sharp-tip-indentation load-depth curve for contact area determination taking account pile-up and sink-in effects. *J Mater Res* 19 (11): 3307-3315, 2004.

19. Christel P, Munier A, Heller M, Torre J P, Peille CN. Mechanical properties and short-term in-vivo evaluation of yttrium-oxide-partially-stablized zirconia. *J Biomed Mater Res* 23(1): 45-61, 1989.

20. Cnudde V, Cnudde JP, Dupuis C, Jacobs PJS. X-ray micro-CT used for the localization of water repellents and consolidants inside natural building stones. *Mater Charact* 53: 259– 271, 2004.

21. Coelho PG, Bonfante EA, Silva NRF, Rekow ED, Thompson VP. Laboratory simulation of Y-TZP all-ceramic crown clinical failures. *J Dent Res* 88(4): 382-386, 2009.

22. Coelho PG, Silva NRF, Bonfante EA, Guess PC, Rekow ED, Thompson VP. Fatigue testing of two porcelain-zirconia all-ceramic crown systems. *Dent Mater* 25: 1122-1127, 2009.

23. Cottom BA, Mayo MJ. Fracture toughness of nanocrystalline zro2-3mol% Y2O3 determined by Vickers indentation. *Scripta Mater* 34:809-814, 1996.

24. Dehoff PH, Barrett AA, Lee RB, Anusavice KJ. Thermal compatibility of dental ceramic systems using cylindrical and spherical geometries. *Dent Mater* 24: 744-752, 2008.

25. Dehoff PH, Anusavice KJ, Gotzen N. Viscoelastic finite element analysis of all-ceramic fixed partial denture. *J of Biomechanics* 39: 40-48, 2006.

26. Dehoff PH, Anusavice KJ, Vontivillu SB. Analysis of tempering stresses in metal-ceramic disks. *J dent Res* 75(2): 743-751, 1996.

27. Dehoff PH and Anusavice KJ. Analysis of tempering stresses in bilayered porcelain discs. *J Dent Res* 71 (5): 1139-1144, 1991.

28. Denry I, Kelly JR. State of the art of zircionia for dental application. *Dent Mater* 24: 299-307, 2008.

29. Edelhoff D, Florian B, Florian W, Johnen C. HIP zirconia fixed partial dentures-clinical results after 3 years of clinical service. *Quintessence Int* 39:459-471, 2008.

30. Fairhurst CW, Hashinger DT, Twiggs SW. The effect of thermal history on porcelain expansion behavior, *J Dent Res* 68(9):1313-1315, 1989.

31. Fernandes CP, Glantz PJ, Svensson SA, Bergmark A. A novel sensor for bite force determination. *Dent Mater* 19: 118-126, 2003.

32. Ferreira de Paiva R. De´veloppement d'un microtomographe X et application a` la characte´risation des roches re´servoirs", *The`se de doctorat de l'Universite´ de Paris* VI: 170, 1995.

33. Fischer J, Stawarczyk B, Hämmerle CH. Flexural strength of veneering ceramics for zirconia. *J Dent* 36:316-321, 2008.

34. Fischer H, Hemelik M, Telle R, Mark, R, Influence of annealing temperature on the strength of dental glass ceramic materials. *Dent Mater* 21: 671-677, 2005.

35. Fischer J, Stawarczyk B, Hammerle CHF. Flexural strength of veneering ceramics for zirconia. *J Dent* 36: 316-321, 2008.

36. Fradeani M. Six-year follow-up with express veneers. *Int J Periodont Restor Dent*18:216, 1998.

37. Fradeani M, Aquilano A, Corrado M. Clinical experience with in-ceram Spinell crowns: 5-year follow up. *Int J Periodont Restor Dent* 22:525, 2002.

38. Fradeani M, D'Ameio M, Redemagni M, Corrado M. Five-year followup with Procera all-ceramic crowns. *Quintessence Int* 36:105, 2005.

39. Fradeani M, Redemagni M, Corrado M. Porcelain laminate veneers: 6 to 12 years clinical evaluation– a retrospective study. *Int J Periodont Restor Dent* 25:9, 2005.

40. Freese AS. Porcelain fused to iridio-platinium crowns. *J Prosthet Dent* 9:847-850, 1959.

41. Gaillard Y, Anglada M., and Jimenez-Pique E. Nanoindentation of yttria dopped zirconia: effect of crystallographic structure on deformation mechanisms. *J Mater Res* 24(3): 719-727, 2009.

42. Garvie RC, Nicholson PS. Phase analysis in zirconia systems. *J Am Ceram Soc* 55: 303-305, 1972.

43. Garvie RC, Hannink RH, Pascoe RT. Ceramic Steel? *Nature* 258:703-704, 1975.

44. Gogotsi GA, Dub SN, Lomonova EE, and Ozersky BI. 1995. Vickers and knoop indentation behavior of cubic and partially stabilized zirconia crystals. *J Eur Ceram Soc* 15: 405-413, 1995.

45. Gong J, Miao H, Peng Z. Analysis of the nanoindentation data measured with a berkovich indenter for brittle materials: effect of the residual contact stress. *Acta Mater* 52, 785-793, 2004

46. Gonzaga CC, Cesar PF, Miranda Jr. WG, Yoshimura HN. Slow crack growth and reliability of dental ceramics. *Dent Mater* 27: 394-406, 2011.

47. Guazzato M, Albakry M, Ringer SP, Swain MV. Strength, fracture toughness and microstructure of a selection of all ceramic materials. Part II. Zirconia based dental ceramics. *Dent Mater* 20:449-56, 2004.

48. Hanan JC, Veazey C, Demetriou MD, DeCarlo F, Thompson JS. Microtomography of amorphous metal during thermo-plastic foaming. *Adv X-Ray Anal* 49, 85-91: 2006.

49. Heuer AH, Lange FF, Swain MV, Evans AG. Transformation toughening: an overview. *J Am Ceram Soc* 69: i-iv, 1986.

50. Heuer AH, Claussen N, Kriven WM, Ruhle M. Stability of tetragonal ZrO2 particles in ceramic matrices. *J Am Ceram Soc* 65:642-650 1982.

51. Ho CJ, Liu HC, Tuan WHM. Effect of abrasive grinding on the strength of Y-TZP. *J Eur Ceram Soc* 29: 2665-2669, 2009.

52. Hounsfield GN. Computerized transverse axial scanning (tomography): Part 1, Description of system. *The British Journal of Radiology* 46 (552): 1016–1022, 1973.

53. Hsueh CH, Thompson GA, Jadaan OM, Wereszczak AA, Becher PF. Analysis of layer-thickness effects in bilayer dental ceramics subjected to thermal stresses and ring on ring tests. *Dental Mater* 24: 9-19, 2008.

54. Hsueh CH, Luttrelll CR, Becher PF. Analysis of multilayered dental ceramics subjected to biaxial flexure tests. *Dent Mater* 22: 460-9, 2006.

55. Hsueh CH, Luttrelll CR, Becher PF. Modeling of multilayered disks subjected to biaxial flexure tests. *Int J Solids Struct* 43: 6014-25, 2006.

56. Hsueh CH, Lance MJ, Ferber MK. Stress distribution in thin bilayer discs subjected to ball-on-ring tests. *J Am Ceram Soc* 88: 1687-90, 2005

57. Jager ND, Kler MD, Zel JMV. The influence of different core material on the FEA-determined stress distribution in dental crowns. *Dent mater* 22: 234-242, 2006

58. Johnson KL. Contact Mechanics, *Cambridge University Press, Cambridge*, 1985.

59. Jones DW. Development of dental ceramics. *Dent Clin North Am* 29:621-644, 1985.

60. Juy A, Anglada M. Strength and grinding residual stresses of Y-TZP with duplex microstructures. *Engr Failure Anal* 16: 2586-2597, 2009

61. Kelly JR, Denry I. Stabilized zirconia as a structural ceramic: An overview. *Dent Mater* 24: 289-298, 2008.

62. Kelly JR, Nishimura I, Campbell SD. Ceramics in dentistry: historical roots and current prospective. J Pros Dent 75(1):18-32, 1996.

63. Kim JW, Kim JH, Tompson VP, Zhang Y. Sliding contact fatigue damage in layered ceramic structures. *J Dent Res* 86:1046, 2007.

64. Kon M, O'Brian WJ, Rasmussen ST, Asaoka K. Mechanical properties of glass-only porcelains prepared by the use of two feldspathic frits with different thermal properties. *J Dent Res* 80(8): 1758-1763, 2001.

65. Krawitz AD. Introduction to Diffraction in Materials, Science, and Engineering. *John Wiley*, 2001

66. Larsson C, Von SP, Sunzel B, Nilner K. All-ceramic two and five-unit implant-supported reconstructions, A randomized, prospective clinical trial. *J Swed Dent* 30: 45-53, 2006.

67. Lawn BR, Deng Y, Lloyd IK, Jananl MN, Rekow ED, Thompson VP. Materials design of ceramic-based layer structures for crowns. *J Dent Res* 81: 433-438, 2002

68. Lawn BR. Fracture of Brittle Solids, 2nd edition. *Cambridge University Press*, 1993.

69. Long H, Swennen R, Foubert A, Dierick M, Jacobs P. 3D quantification of mineral components and porosity distribution in Westphalian C sandstone by microfocus X-ray computed tomography. *Sedimentary Geo* 220: 116–125, 2009.

70. Lenz J, Thies M, Schweizerhof K, Rong Q. Thermal Stresses in ceramometallic crowns: firing in layers. *Chin J Dent Res* 5(3): 5-24, 2002.

71. Lohbauer U, Amberger G, Quinn GD, Scherrer SS. Fractographic analysis of a dental zirconia framework: a case study on design issues. *J Mech Behav Biomed Mater* 3: 623-629, 2009.

72. Lorenzoni FC, Martins LM, Silva NRFA, Coelho PG, Guess PC, Bonfante EA, Thompsaon VP, Bonfante G. Fatigure life and failure modes of crowns systems with a modified framework design. *J Dent* 38: 626-634, 2010.

73. Mainjot AK, Schajer GS, Vanheusden AJ, Sadoun MJ. Residual stress measurement in veneering ceramic by hole-drilling. *Dent Mater* 27: 439-444, 2011.

74. Malament KA, Socransky SS. Survival of Dicor glass-ceramic dental restorations over 20 years: part IV. The effects of combination of variables. *Int J Prosthodont* 23: 134-140 2010.

75. Malament KA, Socransky SS. Survial of Dicor glass-ceramic dental restorations over 16 years. PartIII. Effect of Luting agent and tooth ortooth-substitute core structures. *J Prosthet Dent* 86:511, 2001.

76. McLean JW. The alumina reinforced porcelain jacket crown. *J Am Dent Assoc* 75:621-628,1967.

77. Miranda P, Pajares A, Guiberteau F, Cumbrera FL, Lawn BR. Role of flaw statistics in contact fracture of brittle coatings. *Acta Mater* 49: 3719-3726, 2001.

78. Molin MK, Karlsson SL. Five-year clinical prospective evaluation of zirconia-based Denzir 3-unit FPDs. *Int J Prosthodont* 21:223-227, 2008.

79. Morena R, Lockwood PE, Fairhurst CW. Fracture toughness of commercial dental porcelain. *Dent Mater* 2: 58-62, 1986.

80. Oliver WC, Pharr GM. An improved technique for determining hardness and elastic modulus using load and displacement sensing indentation experiments. *J Mater Res* **7**: 1564-1583, 1992.

81. Olsson KG, Furst B, Andersson B, Carlsson GE. A long-term retrospective and clinical follow-up study of In-Ceram Aluminam FPDs. *Int J Prothodont* 16: 150-156, 2003.

82. Ortorp A, Kihl ML, Carlsson GE. A 3-year retrospective and clinical follow-up study of In-Ceram Alumina FPDs. *Int J Prothodont* 16:150-156 2009.

83. Paphangkorakit J, Osborn JW. Effects on human maximum bite force of bitting on a softer or harder object. *Archives of Oral Bio* 43: 833-839, 1998.

84. Pjetursson BE, Sailer I, Zwahlen M, Hammerle CH. A systematic review of the survival and complication rates of all-ceramic and metal-ceramic reconstructions after an observation period of at least 3 years. part I: single crowns. *Clin Oral Inpl Res* 18 (Suppl 3): 73-85, 2007.

85. Quinn GD, Hoffman K, Quinn, JB. Strength and fracture origins of a feldspathic porcelain. Dent Mater (2011) doi: 10.1016/j.dental.2011.12.005

86. Quinn JB, Sundar V, Parry EE, Quinn GD. Comarison of edge chipping resistance of PFM and veneered zirconia specimens. *Dent Mater* 26: 13-20, 2010.

87. Rafferty BT, Janal MN, Zavanelli RA, Silva NRFA, Rekow ED, Thompson VP, Coelho PG. Design features of a three dimensional molar crown and related maximum principle stress. A finite element model study. *Dent mater* 26: 156-163, 2010.

88. Raigrodski AJ, Chiche GJ, Potiket N, Hochstedler JL, Mohamed SE, Billot S. The efficacy of posterior three-unit zirconium-oxide-based ceramic fixed partial denture prostheses: a prospective clinical pilot study. *J Prosthet Dent* 96: 237-244, 2006.

89. Raigrodski AJ. Contemporary materials and technologies for all-ceramic fixed partial dentures: a review of the literature. *J Prosthet Dent* 92(6): 557-62, 2004

90. Rekow ED, Silva NRFA, Coelho PG, ZhangY, Guess P, Thompson VP. Perfromance of dental ceramics: chanllenges for improvements. *J Dent Res* 90(8): 937-952, 2011.

91. Rekow ED, Harsono M, Janal M, Thompson VP, Zhang G. Factorial analysis of variables influencing stress in all-ceramic crowns, *Dent Mater* 22:125, 2006.

92. Ring ME. Dentistry, an illustrated history. *New York HN Abrams*,160-181, 193-211, 1985

93. Roark RJ, Young WC. Formulas for stress and strain, 5th ed. *New York*, *McGrow-Hill*, 1986

94. Salazar Marocho SM, Studart AR, Bottino MA, Bona AD. Mechanical strength and subcritical crack growth under wet cyclic loading of glass-infiltrated dental ceramics. *Dent Mater* 25:892-898, 2010.

95. Silva NR, Sailer I, Zhang Y, Coelho P, Guess PD, Zembic A. Performance of zirconia for dental healthcare. *Mater* 3: 863-896, 2010a.

96. Sorrentino, R, Aversa, R, Ferro, V, Auriemma, T, Zarone, F, Ferrari, M, Apicella, A. Three-dimensional finite element analysis of strain and stress distributions in endodontically treated maxillary central incisos restored with different post, core and crown materials. *Dent Mater* 23: 983-993, 2007.

97. Sproull RC. A history of porcelain in dentistry. *Bull Hist Dent* 26:3-10, 1978.

98. Suresh S, Giannakopoulos AE. A new method estimating residual stress by instrumented sharp indentation. *Acta Mater* 46(16): 5755-5767, 1998.

99. Swadner JG, Taljat B, Pharr GM. Measurement of residual stress by load and depth sensing indentation with spherical indenters. *J Mater Res* 16(17): 2091-2102, 2001

100. Swain MV, Unstable cracking (chipping) of veneering porcelain on all-ceramic dental crowns and fixed partial dentures. *Acta Biomater* 5: 1668-1677, 2009

101. Tabor D. Hardness of Metals, *Cambridge University Press, Cambridge*, 1951.

102. Tanaka K, Kanari M, Matsui N. Acontinuum dislocation model of vickers indentation on zirconia. *Acta Mater* 47; 2243-2257, 1999.

103. Taskonak B, Griggs JA, Mecholsky JJ Jr, Yan J. Analysis of subcritical growth in dental ceramics using fracture mechanics and fractography. *Dent Mater* 24: 700-707, 2008.

104. Tholey MJ, Swain MV, Thiel N. Thermal gradients and residual stresses in veneered Y-TZP frameworks. *Dent Mater* 27(11): 1102-1110, 2011.

105. Thompson VP, Rekow ED. Dental Ceramics. In: Bioceramics and their clinical applications. *Kokubo T, editor. London, UK:CRC Press*, 518-547, 2008.

106. Timoshenko S. Analysis of bi-metal thermostats. *J Opt Soc Am Rev Sci Instrun* 11(3): 233-55, 1925.

107. Tinscherty J, Schulze KA, NAtt G, Latzke P, Heussen N, Spiekermann H. Clinical behavior of zirconia based fixed partial dentures made of DC-Zirkon: 3-year results. *Int J Prosthodont* 21:217-222, 2008.

108. Tandon R. Atechnique for measuring stress in small spatial regions using cube-corner indentation: application to tempered glass plates. *J Eur Ceram Soc* 27: 2407-2414, 2007.

109. Tsalouchou E, Cattell MJ, Knoeles JC, Pittayachawan P, McDonald A. 2008. Fatigue and fracture properties of yttria partially stabilized zirconia crown systems. *Dent Mater* 24: 308-318, 2008.

110. Tsui TY, Oliver WC, Pharr GM. Influence of stress on the measurement of mechanical properties using nanoindentation: part I. experimental studies in an aluminum alloy. *J Mater Res* 11(3): 752-759, 1996.

111. Van Geet M, Swennen R, Wevers M. Quantitative analysis of reservoir rocks by microfocus X-ray computerised tomography. *Sedimentary Geo* 132: 25–36, 2000.

112. Von SP. All-ceramic fixed partial dentures, studies on aluminum oxide- and zirconium dioxide based ceramic systems. *Swed Dent J Suppl* 173: 1-69, 2005.

113. Von SP, Calson P, Nilner K. All-ceramic fixed partial denture designed according to DC-Zircon® a two year clinical study. *J Oral Rehab* 32: 180-187, 2005.

114. Vult Von Steyern P, Jonsson O, Nilner K. Five-year evaluation of posterior all-ceramic three-unit (In-Ceram) FPDs. *Int J Prothodont* 14:379-384, 2001.

115. Williamson ED and Adam LH. Temperature distribution in solids during heating or cooling. *Phy Rev* 14 (2): 99-114, 1919.

116. Wittneben JG, Wright RF, Weber HP, Gallucci GO. A systematic review of the clinical performance of CAD/CAM single-tooth restorations. *Int J Prosthodont* 22:466-471, 2009.

117. Yao Y, Liu D, Che Y, Tang D, Tang S, Huang W. Non-destructive characterization of coal samples from China using microfocus X-ray computed tomography. *Int J Coal Geo* 80: 113–123, 2009.

118. Zarone F, Russo S, Sorrentino R. From porcelain-fused-to-metal to zirconia: clinical and experimental considerations. *Dent mater* 27:83-96, 2011.

119. Zhang Y, Hanan JC. Residual stress in ceramic zirconia-porcelain crowns by nanoindentation. Mechanical Properties and Performance of Engineering Ceramics and Composites VI: Ceramic Engineering and Science Proceedings, Volume 32, *John Wiley & Sons, Inc.*, Hoboken, NJ, USA, 2011.

120. Zhang Y, Allahkarami M, Hanan JC. Measuring residual stresss in ceramic zirconia-porcelain dental crowns by nanoindentation. *J Mech Behav Biomed Mater* 6: 120-127, 2012.

VITA

Yanli Zhang

Candidate for the Degree of

Doctor of Philosophy

Thesis: RESIDUAL STRESS IN ALL CERAMIC ZIRCONIA-PORCELAIN DENTAL SYSTEM BY SIMULATION AND NANOINDENTATION

Major Field: Mechanical Engineering

Biographical:

Education:

Completed the requirements for the Doctor of Philosophy in Mechanical Engineering at Oklahoma State University, Stillwater, Oklahoma in August, 2012.

Completed the requirements for the Master of Science in Mechanical Engineering at Oklahoma State University, Stillwater, Oklahoma in May, 2007.

Completed the requirements for the Bachelor of Science in Mechanical Engineering Technology at Oklahoma State University, Stillwater, Oklahoma, in December, 2004.

Completed the requirements for the Associate degree in Mechanical Engineering at Luoyang Institute of Science and Technology, Luoyang, Henan Province, China, in July, 1994.

Experience:

Employed by Oklahoma State University, School of Mechanical and Aerospace Engineering as a graduate research assistant from January 2006~December 2007, January 2009 ~ present.

Employed by Chenchang Building Materials Company in Beijing China as full-time engineer from November 1997 ~ January 1999.

Employed by Nankou Building Materials Company in Beijing China as a full-time engineer from July 1994 ~ November 1997.

Name: Yanli Zhang Date of Degree: July, 2012

Institution: Oklahoma State University Location: Stillwater, Oklahoma

Title of Study: RESIDUAL STRESS IN ALL CERAMIC ZIRCONIA-PORCELAIN DENTAL SYSTEM BY SIMULATION AND NANOINDENTATION

Pages in Study: 107 Candidate for the Degree of Doctor of Philosophy

Major Field: Mechanical Engineering

Scope and Method of Study:

All ceramic zirconia-porcelain dental crowns become more popular due to biocompatibility and esthetics. However, zirconia-porcelain dental crowns exhibits a unique failure behavior and fail at a faster rate than metal- ceramic crowns even under the same manufacturing procedures and thermal treatment guidelines. This unique failure behavior has not been fully understood. Residual stress was believed to have played an important role due to the poor thermal diffusivity of zirconia. The magnitude of residual stress in crown, especially in porcelain veneer layer, has not been thoroughly studied experimentally before. Interaction of cooling rate, mismatch of coefficient of thermal expansion between core and veneer material, and geometry effect on residual stress has not been thoroughly studied, especially for the three-dimensional geometry. Nanoindetation was used to measure the residual stress in a clinical relevant zirconia-porcelain dental crown. Finite element method was used to evaluate effects of different factors on residual stress and to improve crown designs to reduce residual stress.

Findings and Conclusions:

Nanoindention measurement showed that there are large amount of residual stress existed both in zirconia and porcelain layer in dental crowns. The average residual stress reading is -637 MPa and 323 MPa for zirconia and porcelain respectively. It is a challenge to find a stress free sample. Finite element method study showed that mismatch of CTE, cooling rate, crown geometry all have effect on residual stress. When the mismatch of coefficient of thermal expansion is 5 ppm difference during the porcelain glass transition region, the cooling rate effect on residual stress is small. When the mismatch of coefficient of thermal expansion is 20 ppm difference during the porcelain glass transition region, the cooling rate effect on residual stress are very big, with the maximum difference of maximum principle stress at 74 MPa. Different designs were compared and showed that more zirconia support and less porcelain thickness gradient would decrease the residual stress in design crowns. Slow cooling is recommended; also crown design should consider porcelain's CTE value during glass transition.

ADVISER'S APPROVAL: Dr. Jay C. Hanan